Université de Montréal

Phosphoproteome profiling approaches for comprehensive monitoring of cell signaling events in interferon-γ stimulated macrophages

par
Maria Marcantonio

Département de Biochimie, Université de Montréal
Faculté de Médecine

Mémoire présenté à la Faculté des études supérieures
en vue de l'obtention du grade de Maîtrise ès sciences (M.Sc.)
en Biochimie

Avril 2008

Université de Montréal
Faculté des études supérieures

Ce mémoire intitulé:

Phosphoproteome profiling approaches for comprehensive monitoring of cell signaling events in interferon-γ stimulated macrophages

présenté par :
Maria Marcantonio

a été évalué par un jury composé de personnes suivantes :

Dr. Michel Bouvier
président-rapporteur

Dr. Pierre Thibault
directeur de recherche

Dr. Sylvain Meloche
membre du jury

Résumé

La phosphorylation des protéines joue un role primordial dans les voies de signalisation cellulaire. De récents progrès en spectrométrie de masse (MS) permettent l'identification de milliers de sites de phosphorylation. Cependant, l'inefficacité d'ionisation des phosphopeptides limite leur détection. Ce travail présente une méthode d'identification des phosphopeptides à partir d'extraits cellulaires enrichis avec TiO_2 et déphosphorylés par la phosphatase alcaline. La corrélation des temps de rétention de plus de 750 paires de phospho- et déphosphopeptides indique que les changements d'hydrophobicité sont partiellement expliqués par l'interaction électrostatique avec des acides aminés basiques. Une augmentation d'au moins un facteur de 2 dans le nombre de phosphopeptide détectables a été observée suite à la déphosphorylation. Cette méthodologie a été appliquée à des extraits cellulaires de macrophage J774 traités ou non à l'interféron-gamma (IFN-γ) et a permis l'identification de phosphoprotéines impliquées dans différentes voies de signalisation.

Le profil cinétique du phosphoprotéome des cellules J774 stimulées par IFN-γ (jusqu'à 180 min) et enrichis avec TiO_2 a été obtenu pour mieux comprendre l'effet biologique de l'IFN-γ sur les macrophages. Des changements significatifs de phosphorylation ont été observés à 5 et 30 min après stimulation. L'analyse par 2D-LC-MS/MS des macrophages stimulés pendant 5 et 30 min par l'IFN-γ a permis l'identification de 2831 phosphopeptides incluant 1673 nouveaux sites de phosphorylation. L'analyse du réseau d'intéraction des phosphoprotéines a permis d'identifier des protéines impliquées dans les voies de signalisation du complexe NADPH oxydase ($p67^{phox}$), des phospholipides (SHIP-2), de la traduction de ARNm (eIF4B) et de l'apoptose (PEA-15, NF-κB).

Mots-clés: Phosphorylation, spectromètre de masse, profil d'expression, enrichissement par TiO_2, IFN-γ, macrophages, phosphatase alcaline, réseau d'interactions protéine-protéine, voies de signalisation, prédiction de kinases.

Abstract

In biological systems, signal transduction pathways are primarily guided through various protein phosphorylation and dephosphorylation events. Major analytical advances in mass spectrometry have enabled the direct identification of protein phosphorylation sites in complex mixtures. Yet, phosphoproteome analyses are still quite challenging due to the poor ionization efficiency of phosphopeptides. This work presents a combined enzymatic and data mining approach enabling more than 2-fold increase of phosphopeptides detection following alkaline phosphatase digestion of TiO_2-enriched J774 cell extracts. The retention time of more than 750 phosphopeptides was shifted toward higher and lower values compared to their dephosphorylated counterpart. The loss in hydrophobicity is partially explained by the electrostatic interaction of the phosphate group with basic amino groups. This approach was applied to 5 min interferon-gamma (IFN-γ) treated mouse macrophage cells and led to the identification of key IFN-γ signaling events.

Furthermore, activated signaling transductions were more clearly defined to understand IFN-γ biological effects on macrophages. We compared the temporal changes in the phosphoproteome of TiO_2-enriched J774 macrophages following IFN-γ stimulation (up to 180 min). Amongst the different trends observed, most significant changes in phosphorylation occurred to the same extent 5 and 30 min after IFN-γ induction. The 2D-LC-MS/MS analysis on TiO_2-enriched 5 and 30 min IFN-γ treated macrophages identified a total of 2831 phosphopeptides including 1673 novel phosphorylation sites. Network analyses of differentially regulated phosphopeptides led to the identification of early signaling and regulatory events including members of the NADPH complex ($p67^{phox}$), phospholipids (SHIP-2), protein synthesis (eIF4B) and apoptotic (PEA-15, NFκB) pathways.

Key words: Phosphorylation, mass spectrometry, expression profiling, TiO_2 enrichment, IFN-γ, macrophages, alkaline phosphatase, protein network, signaling pathways, kinase prediction.

Table of Contents

List of Tables

List of Figures

List of Abbreviations

AA	Arachidonic Acid
ACN	Acetonitrile
AP	Alkaline Phosphatase
ATP	Adenosine Triphosphate
$Ba(OH)_2$	Barium hydroxide
BCA	Bicinchoninic Acid
CDK2	Cell Division Protein Kinase 2
CE	Capillary Electrophoresis
CIS	Cytokine-Inducible SH2 protein
CK2	Casein Kinase 2
$cPLA_2$	Cytosolic Phospholipase A_2
C-trap	C-shaped storage trap
CV	Coefficient of Variation
2D	Two-Dimensional
DHB	2,5-Dihydroxybenzoic Acid
DMEM	Dulbecco's Modified Eagle's Medium
DTT	DL-Dithiolthreitol
4EBP1	eIF4E-Binding Protein 1
EDT	1,2-Ethanedithiol
eEF	eukaryotic Elongation Factor
eIF	eukaryotic Translation Initiation Factor
ERK1/2	Extracellular signal-Regulated Kinases 1/2
ESI	Electrospray Ionization
FA	Formic Acid
FADD	Fas-Associated Death Domain Protein

FBS	Fetal Bovine Serum
FMC	Fuzzy c-Means Clustering
FTIRC	Fourier Transform Ion Cyclotron Resonance
GSK-3	Glycogen Synthase Kinase-3
GTP	Guanosine-5'-Triphosphate
HPLC	High Performance Liquid Chromatography
IFN-γ	Interferon-gamma
IFNGR 1/2	IFN-γ Receptor 1/2
IKK	IκB Kinase
IL	Interleukin
IMAC	Immobilized Metal Ion Chromatography
IPI	International Protein Index
IRFs	IFN Regulatory Factors
JAK1/2	Janus Activated Kinase 1/2
LC-MS	Liquid Chromatographic-Mass Spectrometry
LC-MS/MS	Liquid Chromatography-Tandem Mass Spectrometry
LiOH	Lithium hydroxide
LPS	Lipopolysaccharide
LTQ	Linear Trap Quadrupole
MALDI-TOF	Matrix Assisted Laser Desorption Ionization-Time-of-Flight
MAPK14	Mitogen-Activated Protein Kinase 14
MHC	Major Histocompatibility Complex
MNK1/2	MAP Kinase Signal-Interacting Kinase 1/2
MS	Mass Spectrometer
MSK1	Mitogen- and Stress-Activated Protein Kinase 1
mTOR	Mammalian Target of Rapamycin

m/z	mass-to-charge ratio
NF-κB	Nuclear Factor-Kappa B
NO	Nitric Oxide
O_2^-	Superoxide
PBS	Phosphate Buffer Saline
PDK1	Pyruvate Dehydrogenase Kinase isozyme 1
PI3K	Phosphatidylinositol 3-Kinase
PIM2	Serine/Threonine-Protein Kinase Pim-2
$PI(4,5)P_2$	Phosphatidylinositol 4,5-biphosphate
PMSF	Phenylmethyl Sulphonyl Fluoride
PPSP	Prediction of PK-Specific Phosphorylation Site
p70 S6K	Ribosomal protein S6 kinase beta-1
PTEN	Phosphatase and Tensin Homologue Deleted on Chromosome Ten
PTMs	Post-Translational Modifications
Q-TOF	Hybrid Quadrupole-Time-of-Flight Hybrid
RAP1	Repressor Activator Protein 1
RF	Radio Frequency
RIP	Receptor-Interacting Protein
RNS	Reactive Nitrogen Species
ROS	Reactive Oxygen Species
RSD	Relative Standard Deviation
RSK-2	Ribosomal Protein S6 Kinase alpha-3
RT	Retention Time
SCX	Strong Cation Exchange
SDS-PAGE	Sodium Dodecyl Sulfate Polyacrylamide Gel Electrophoresis
SHIP-2	SH2 domain containing Inositol 5-Phosphatase

SOCS	Suppressors of Cytokine Signalling
SODD	Silencer of Death Domain
STAT1/2	Signal Transducers and Activators of Transcription 1/2
STRING	Search Tool for the Retrieval of Interacting Genes/Proteins
TCEP	Tris(2-carboxyethyl)Phosphine
TFA	Trifluoroacetic Acid
TGFBR2	TGF-Beta Receptor type-2
TiO_2	Titanium Dioxide
TLRs	Toll-Like Receptors
TNF-α	Tumor Necrosis Factor-alpha
TNFR1	Tumour Necrosis Factor Receptor 1
TPCK	$_L$-1-Tosylamido-2-Phenylethyl Chloromethyl Ketone
TRADD	TNF-R-Associated Death Domain Protein
TRAF2	TNF-Receptor-Associated Factor 2
z	Charge

Acknowledgements

First, I would like to thank my research director, Dr. Pierre Thibault, for giving me the opportunity to conduct my graduate studies in his laboratory. I realize that my Master's experience would not have been so successful and rewarding without his continuing assistance in every aspect of my project. His superior teaching abilities and knowledge in mass spectrometry broadened my horizons in the field of phosphoproteomics. I really appreciate his immense help and effort he gave me despite his very busy schedule and demanding role. I will always be grateful for the great opportunities he has given me to advance in my field.

I would also like to acknowledge Dr. Matthias Trost, who was always able to provide me with valuable information concerning my project. I thank him for playing such an important role in the completion of my thesis. His friendship and guidance has been very helpful throughout my years of study.

A special thanks to Dr. Eric Bonneil, whose excellent expertise in mass spectrometry helped immensely in the success of my experiments. Furthermore, I would like to thank Gagandeep Jaitly and Kevin Eng for their great assistance in data mining analyses. I also wish to express my appreciation to Mathieu Courcelles for the great input that he provided regarding the different bioinformatics' applications used in phosphoproteomics. I would also like to acknowledge Christelle Pomiès for her technical assistance. Given that their aid was needed quite frequently, I very much appreciate their patience and genuine willingness to devote time for my project.

Thanks to all Dr. Thibault's research team for their friendship, constant moral support and assistance. Whenever Pierre was not available, they took it upon themselves to show me the ropes. I am especially grateful to Gaëlle Bridon for her contribution in the second part of my thesis.

As well, the generous graduate scholarship from Natural Sciences and engineering research Council (NSERC) is greatly acknowledged.

Finally, this work would have never been possible without the support and patience from my husband, family and friends, who always encouraged me to strive and reach my goals in life.

1. General Introduction

1.1 Project's goal

Upon IFN-γ stimulation, macrophages are primed to protect the organism against infectious diseases [1]. With the exception of the classical anti-inflammatory JAK-STAT pathway [2], no other important IFN-γ stimulated pathways are completely characterized to fully understand the cell defence mechanism against invading pathogens [3]. The JAK-STAT pathway was also one of the first pathways demonstrating that phosphorylation plays a central role during IFN-γ activated cell signaling. Since only a small fraction of phosphoproteins is phosphorylated at any given time, powerful and sensitive tools like mass spectrometry are required for their detection [4].

In this context, the goal of this thesis consists of evaluating the phosphoproteome of intracellular signaling pathways in IFN-γ treated macrophages using mass spectrometry approaches. Phosphopeptide analysis by mass spectrometry is still limited since phosphorylated peptides do not efficiently ionize in positive ion mode due to their negative charge contribution [5]. Hence, the first part of this project will focus on the development and optimization of a novel technique for a higher phosphopeptide identification level. The method consists of treating half of the TiO_2-enriched phosphopeptide samples with alkaline phosphatase. The treated and non-treated chromatograms will be subsequently compared using in-house bioinformatic tools. Removal of the phosphate group is expected to not only enhance phosphopeptides detection but may also provide interesting feedback on phosphopeptide behaviour in MS. Following validation of the enzymatic approach, the method will be applied on J774 mouse macrophages to determine changes in phosphorylation occurring upon IFN-γ stimulation.

The second part of the study covers the evaluation of the phosphoproteome dynamics of IFN-γ treated macrophages. High-throughput phosphoproteomic strategies such as strong-cation exchange (SCX) chromatography combined with TiO_2 enrichment will be used to analyse the phosphoproteome changes of macrophages treated with the optimal cytokine incubation time. Furthermore, differentially expressed phosphoproteins will be identified using in-house softwares such as Mass Sense and peptide clustering. The last part of the analysis will combine kinase and motif prediction assays with protein networking to determine activated signaling pathways mediating important IFN-γ biological effects.

1.2 Innate immunity

Infectious diseases are the major cause of death and health problems in our society [6]. Innate and adaptive immune systems evolved to prevent and control the formation of inflammation diseases [7]. The innate immune system is the first line of defence against invading organisms with receptors recognizing the molecular structure of pathogens. For instance, Toll-like receptors (TLRs) identify the bacterial cell wall components and pathogen nucleic acids to subsequently activate intracellular signaling [8]. The innate immune system will also trigger the adaptive immune system by inducing pro-inflammatory cytokines, which will activate specialized cells and antibody production [8].

Macrophages are specialized cells responsible for the elimination of pathogens and cell debris from the system. The presence of inflammatory signals warn macrophages of viral and microbial infection [9]. The most important cytokine activation signal is interferon-gamma (IFN-γ). IFN-γ induces transcriptional regulation and activates signal transduction pathways involved in cytoskeletal reorganization, phospholipids composition, cell viability and protein synthesis, enabling the cell to fight invading micro-organisms [3, 10, 11].

1.2.1 Macrophages and inflammation

Inflammation response consists of the release of cytokines by T cells upon detection of micro-organisms and the recruitment of specialized cells such as macrophages that will in turn also further release mediators [10]. The name "macrophage" actually relates to "large eater" entailing that these cells clear invading micro-organisms. Macrophages can be stimulated by different types of innate and acquired immune activation systems such as the tumor necrosis factor-alpha (TNF-α) and IFN-γ. The classical activation of macrophages is mediated by IFN-γ and can be enhanced by a microbial trigger such as bacterial lipopolysaccharide (LPS) [12]. Binding of microbial ligands to phagocytic receptors on the macrophage activates and promotes changes in gene transcription and protein expression [2]. On the other hand, suppressors of cytokine signaling (SOCS) and cytokine-inducible

SH2 protein (CIS) negatively regulate cytokine activation to prevent over reaction of cytokines [13].

During inflammation, primed macrophages are versatile cells that play three important roles. Initially, these activated cells will engulf the foreign particle and form organelles called phagosomes. In these phagosomes, macrophages kill microbes by the production of nitric oxide and superoxide, the reduction of pH by the v-ATPase and the acquisition of hydrolases and proteases by fusion with endosomes and lysosomes [12]. IFN-γ also enhances the transcription of major histocompatibility complex (MHC) class I and II molecules, that will present microbial peptides, sugars and lipids to the cell surface [14]. Finally, several pro-inflammatory cytokines, enzymes and regulatory factors including IL-1 and IL-6 are secreted by activated macrophages to regulate the immune response and the development of inflammation [12]. This whole process results into activation of the adaptive and innate immune response [7].

Due to their major role in defending the organism by phagocytosis, macrophages are implicated in many infectious diseases of the immune system. For instance, macrophages are involved in atherosclerosis and targets of specific pathogens such as Mycobacterium tuberculosis or trypanosomes of the Leishmania genus [14-16]. Since cytokines are responsible to form the network of communication signals between the cells of the immune system, these molecules are often used as therapeutic agents [16, 17].

1.2.2 IFN-γ signaling pathways

IFNs are widely expressed pleiotropic cytokines classified into two categories, type I and II. IFN-γ is the only type II IFN and is structurally unrelated to type I. IFN-γ is mostly produced by CD4+ T cells and has a strong anti-viral effect [9, 18]. Macrophages are capable to overcome inflammation through a multitude of activated signaling pathways responsible to mediate the IFN-γ biological effects.

1.2.2.1 Transcriptional regulation

The first signaling pathway shown to be activated by IFNs was the JAK-STAT pathway. IFN-γ receptor 1/2 (IFNGR1/2) binds to IFN-γ molecules which then triggers the recruitment of Janus activated kinase 1/2 (Jak1/2) for the initiation of signal transduction [2]. Activated Jak1 phosphorylates signal transducers and activators of transcription 1 (Stat1) proteins which will in turn dimerize and translocate to the nucleus (Fig. 1.1) [19]. Stat1 phosphorylation is necessary for full transcriptional activation [3]. This cascade of tyrosine and serine phosphorylation is known to occur very promptly, in less than 1 min [9].

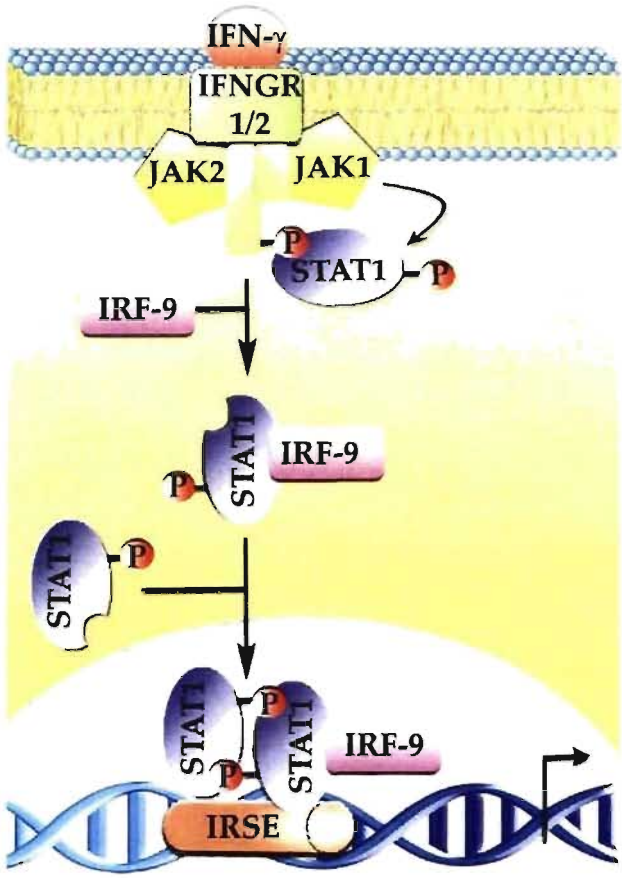

Figure 1.1: **The classical JAK-STAT pathway following IFN-γ stimulation of macrophages.** Ligand binding induces conformational changes of IFNGR1/2, which will translocate Jak1/2 to the membrane. Stimulated Jak1 will phosphorylate tyrosine residues on the IFNGR1/2 receptor to allow recruitment of Stat1. Following tyrosine phosphorylation and IRF-9 binding in the cytoplasm, Stat1 forms a homodimer. Dimerized Stat1 translocates to the nucleus and binds the IFN-stimulated response element (ISRE) to initiate or suppress transcription of IFN-γ-regulated genes.

Stat1 can even function with IFN regulatory factors (IRFs) to establish the delayed response entailing the assurance of proper transcription control for the antiviral state (Fig. 1.1) [20]. On the other hand, Jak kinase activity is negatively regulated by SOCS-1 and SOCS-3 proteins [9]. These Jak kinase inhibitor proteins bind to the phosphorylated tyrosine residue on IFNGR1 and mask Stat1 docking site [10].

In addition to Jak-Stat pathway, other IFN-γ signaling pathways involving key molecules such as NF-κB and phosphatidylinositol 3-kinase (PI3K), lead to changes in transcription control as part of the inflammation response [21, 22].

1.2.2.2 Cell growth and apoptosis

The effect of IFN-γ on apoptosis in macrophages is still subject to controversy. Several studies show that apoptosis is induced by IFN-γ, whereas others report that it serves as an anti-apoptotic signal [9, 23]. IFNs can activate the PI3K-Akt signaling pathway, and generate either pro-survival or apoptotic signals depending on the cellular context [3, 24]. In most cases, survival of the cell is crucial for the generation of IFN-γ induced proteins necessary for the destruction of the invading organism [3]. On the other hand, apoptosis might also be the right choice for the destruction of tumor cells. For instance, IFN-γ induces up-regulation of Fas protein which is responsible for the activation of cell death [25].

The anti-apoptotic transcription factor, NF-κB, is stimulated by proinflammatory cytokines and plays a crucial role in macrophages [26]. NF-kB regulates genes responsible for both the innate and the adaptive immune response [21]. In resting cells, NF-κB is bound to IκB protein and remains inactive in the cytoplasmic compartment. Extracellular stimulation induces signaling pathways that converge to free NF-κB from IκB [10]. NF-κB, then translocates to the nucleus to regulate the expression of multiple target genes to respond to the inflammation, the immune response, inflammatory response, cell adhesion, cell growth, and apoptosis (Fig. 1.2) [21].

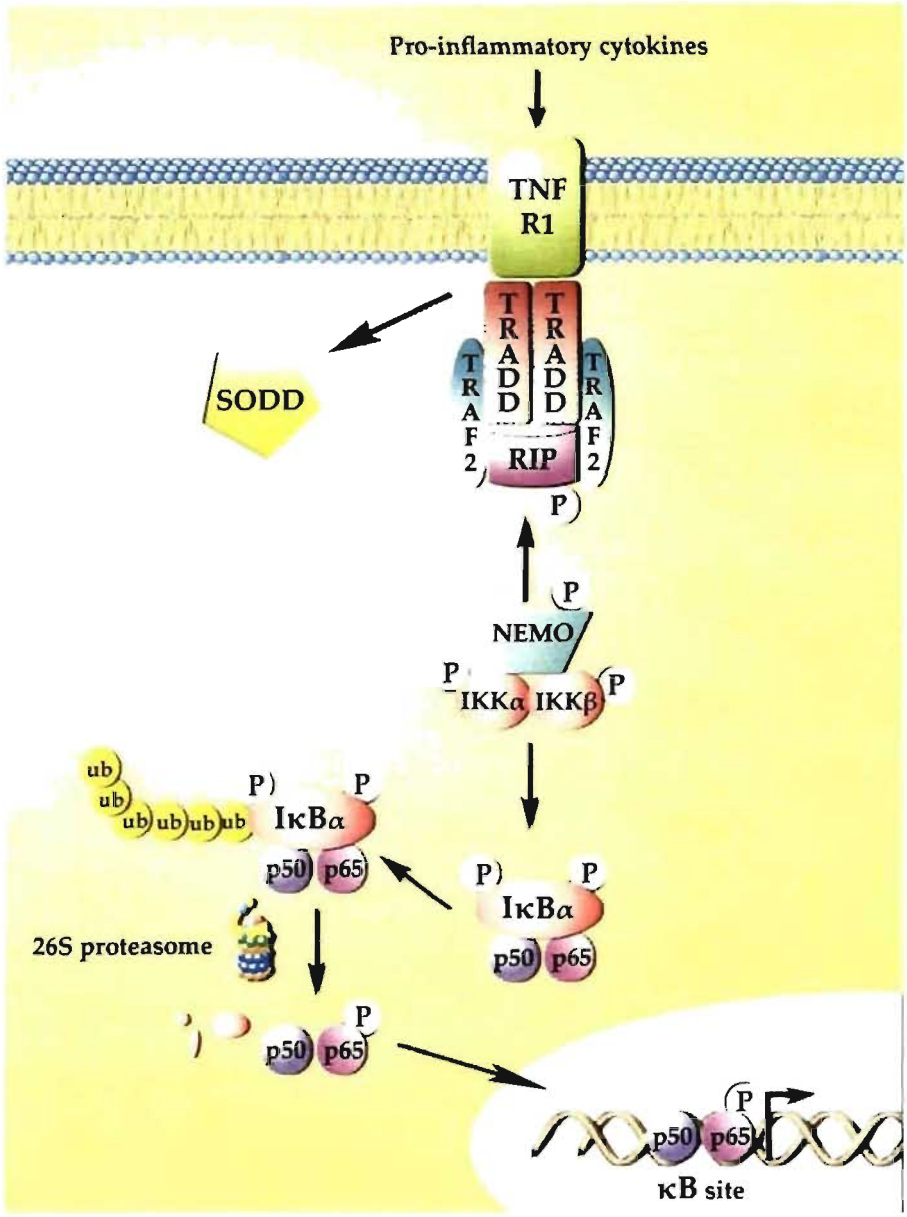

Figure 1.2: **The classical NF-κB signaling pathway during inflammatory response.** Pro-inflammatory cytokines such as IFN-γ and TNF-α activate tumour necrosis factor receptor 1 (TNFR1) which triggers silencer of death domain (SODD) release and recruitment of TNF-receptor-associated death domain protein (TRADD), receptor-interacting protein (RIP) and TNF-receptor-associated factor 2 (TRAF2) to the membrane. Subsequently, IκB kinase (IKK)-complex is recruited to the TNFR1 receptor by TRAF2 [21]. Activated IKK phosphorylates IκB, which induces conformational change of IκB and exposes lysine residues for ubiquination. Thus, IκB becomes target for degradation by 26S proteasome and releases NF-κB dimers (p50 & p65) from the cytoplasmic NF-κB-IκB complex [10]. Free NF-κB translocates to the nucleus and binds to DNA for the regulation of gene transcription.

1.2.2.3 mRNA translation

IFN-γ can also block cell growth and inhibit viral replication by deactivating the mRNA translation protein machinery. Most invading organisms such as bacteria and parasites have their own metabolism and only rely on the host for nutrients. On the other hand, viruses take over the host's protein synthesis machinery for their own replication [27]. For example, poliovirus and influenza virus specifically shut down the transcription and protein synthesis machinery respectively of the host cell so that the host cell replication, transcription and translation machinery will be dedicated for the synthesis of viral proteins [7].

IFN-γ activation will mainly inhibit the translation of viral mRNAs during virus replication. The dsRNA will activate IFN-inducible RNA-dependent protein kinase (PKR), which will in turn phosphorylate eIF-2α subunit to inactivate viral protein synthesis [28].

On the other hand, IFN is also known to induce protein expression of IFN-sensitive genes that act as direct or indirect mediators of their biological effect. Since protein synthesis requires considerable amounts of metabolic energy (ATP & GTP) and amino acids, this event is highly controlled [3]. The initiation step corresponds to the decisive point during mRNA translation to determine the fate of protein synthesis. Hence, extracellular stimuli mediate signal transduction of two different pathways (Ras-MAPK and PI3K/Akt/mTOR), which converge and rigorously regulate the specific activity of key initiation translation factors (Fig. 1.3) [22, 29, and 30].

In summary, IFN-γ stimulation was demonstrated to be directly involved in blocking virus replication and in the synthesis of critical proteins for the inflammation response. Yet, similarly to apoptosis, the precise role of IFN-γ effect on mRNA translation is still not clearly defined [3].

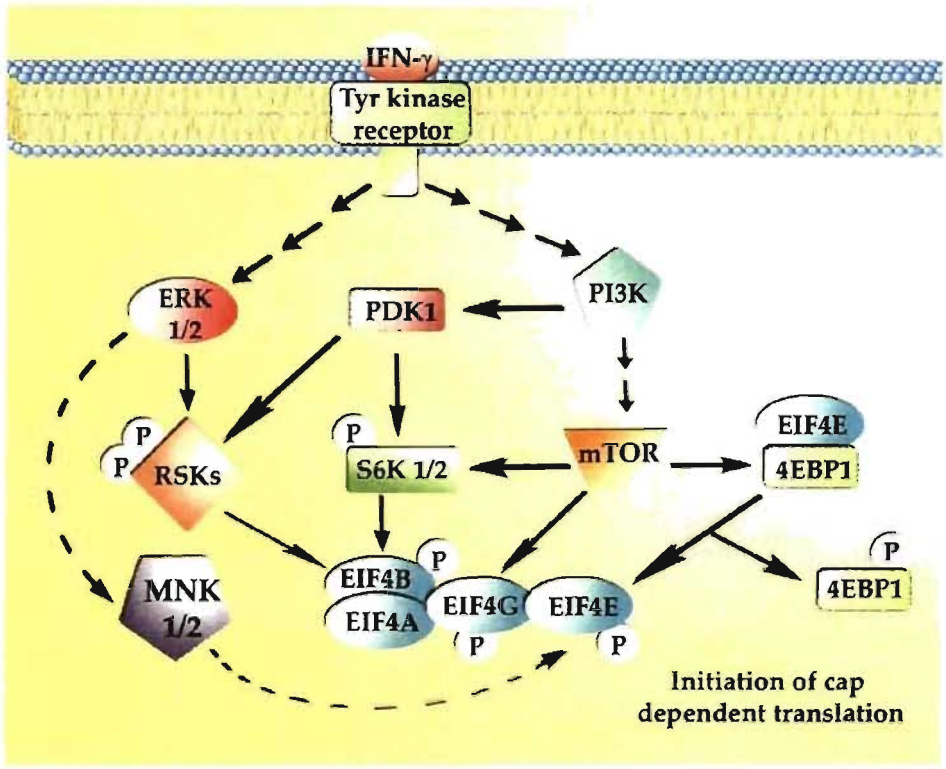

Figure 1.3: **IFN-γ activation of Ras-MAPK and PI3K/Akt/mTOR signaling pathways to initiate mRNA translation.** IFN-γ induction leads to the activation of the PI3K and Ras pathways [29]. Consequently, PDK1 and ERK1/2 phosphorylate and stimulate ribosomal protein S6 kinases (RSKs) [22]. Also, activated mammalian target of rapamycin (mTOR) phosphorylates 4EBP1, eIF4G and p70 S6K. Induced p70 S6K kinase and RSKs phosphorylate eIF4B resulting in initiation of mRNA translation [31]. In contrast, phosphorylation of 4EBP1 disrupts its interaction with eIF4E. In the free state, eIF4E gets phosphorylated by MAP kinase signal-interacting kinase 1/2 (MNK 1/2), which activates its binding to the cap for translation initiation [29].

1.2.2.4 Phospholipid signaling

Another major pathway activated in response to extracellular stimuli consists of PLCs, phosphoinositide kinases and phosphatases, which are responsible for the change in phosphoinositide concentration. As discussed in the mRNA translation signaling pathways, PI3K was shown to play a major role upon IFN-γ activation. Nonetheless, PI3K also produces a potent messenger phospholipid $PI(3,4,5)P_3$ from $PI(4,5)P_2$. Phosphatase and tensin homologue deleted on chromosome ten (PTEN) protein and inositol polyphosphate

phosphatase-like 1 (SHIP-2) can terminate this pathway by transforming $PI(3,4,5)P_3$ into $PI(4,5)P_2$ and $PI(3,4)P_2$, respectively [32].

The phosphoinositide, $PI(4,5)P_2$, is involved in large number of cellular processes such as cell survival, membrane transport and bacterial uptake and transport. For example, $PI(4,5)P_2$ participates in the cytoskeleton remodelling by promoting actin filaments polymerization to form pseudopods. Activated macrophages develop membrane protusions for locomotion and final capture of the prey [33]. Figure 1.4 clearly illustrates the cell morphology change upon 24 h IFN-γ stimulation.

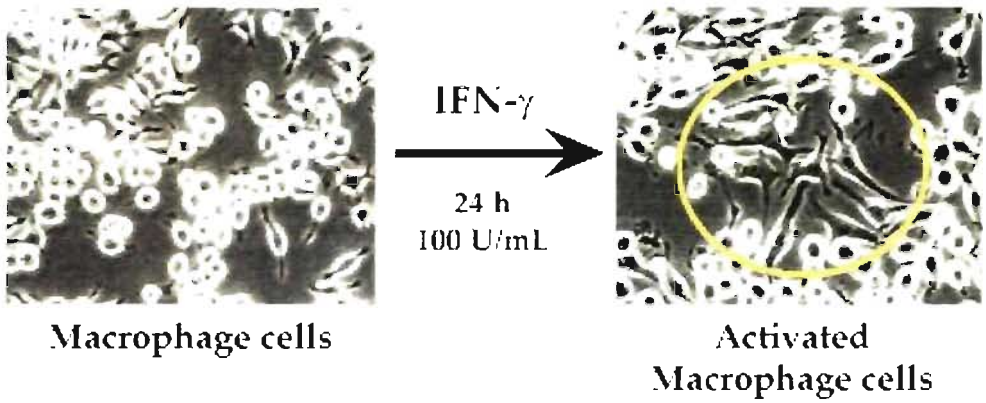

Figure 1.4: **Microscopic examination of J774 macrophage cells highlighting morphological changes taking place upon IFN-γ stimulation.**

Furthermore, hydrolysis of $PI(4,5)P_2$ leads to the production of arachidonic acid (AA), which also plays an important role in inflammatory response. Once AA is released, it interacts with the cytosolic factor, $p47^{phox}$, further involved in the activation of the NAPDH oxidase complex [34]. Interestingly, the change in phospholipid composition within macrophages in response to IFN-γ leads not only to cytoskeleton rearrangements but also the induction of cytotoxic molecules.

1.2.2.5 Production of cytotoxic molecules

To completely eliminate the invading organism, macrophages need to produce specific harmful metabolites. To do so, IFN-γ-activated macrophages produce two types of strong cytotoxic molecules, reactive oxidative species (ROS) and reactive nitrogen species

(RNS) by induction of the NADPH-dependent phagocyte oxidase [9]. The NADPH complex is localized in the plasma membrane of the phagocytic cup and is composed of cytochrome b_{558} ($gp91^{phox}$ and $gp22^{phox}$), $p47^{phox}$, $p40^{phox}$ and $p67^{phox}$, Rac and Rap1. Superoxide ($O_2^{\cdot}$) is produced in the phagosome by accepting electrons from the NADPH oxidase complex from the cytosolic side of the membrane [35].

The NADPH oxidase complex is only complete and active during macrophage stimulation. In resting cells, the components of the complex are located in the cytosolic compartment of the cell [35]. Upon IFN-γ activation, many different signaling pathways lead to its formation. For instance, neutrophil cytosolic factors, $p47^{phox}$, $p40^{phox}$ & $p67^{phox}$, are recruited to the membrane by phosphorylation [35]. $p47^{phox}$ can also be translocated to the plasma membrane through the interaction with activated arachidonic acid (Fig. 1.5) [36]. Two different signaling pathways originating from the phospholipids and the phox proteins converge to synergistically stimulate NADPH oxidase complex.

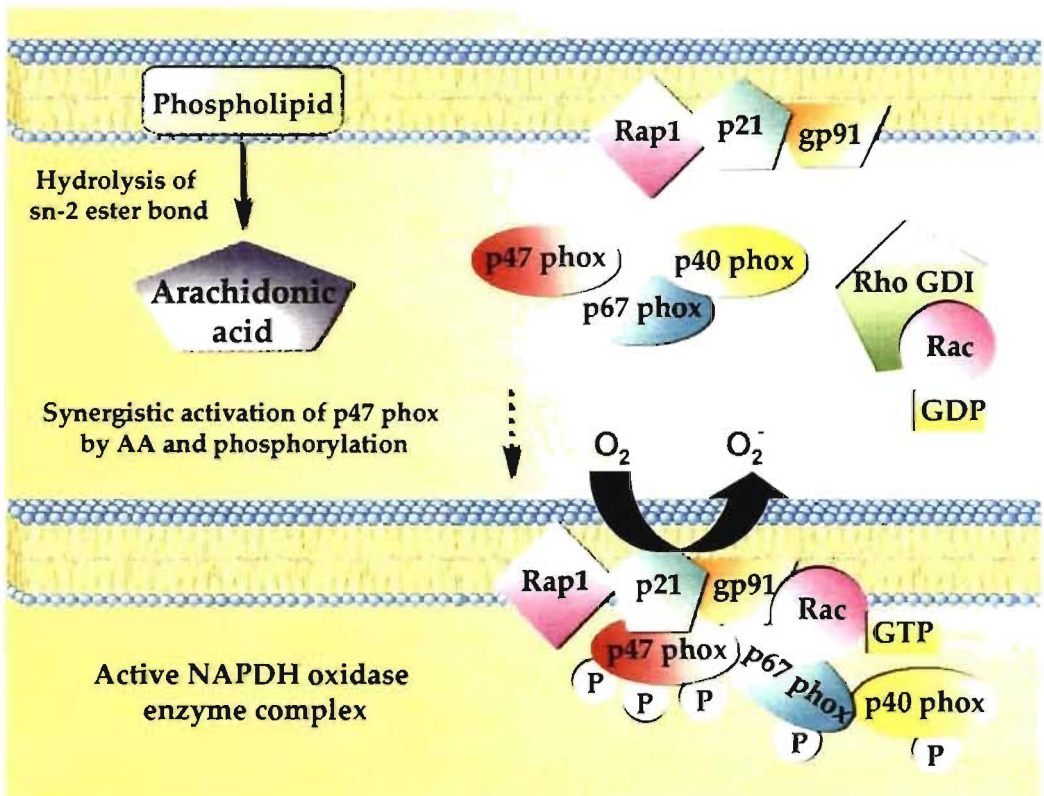

Figure 1.5: **Upon IFN-γ administration, induction of cytosolic factors ($p47^{phox}$, $p40^{phox}$ and $p67^{phox}$) recruitment to the membrane to form the NADPH oxidase complex through phosphorylation and interaction with arachidonic acid.**

In summary, important pathways such as JAK-STAT, PI3K-Akt-mTOR, NF-κB, and NAPDH oxidase, were shown to be affected by IFN-γ activation. These changes in the gene and protein regulation, cell survival and phospholipid composition are important to prepare the macrophage against viral infection and finally lead to phagocytosis and pathogen destruction.

1.3 Phosphoproteomics

Upon extracellular stimuli activation, a cascade of signaling events is triggered to transmit the message from the membrane to the nucleus and induce changes in different cell function such as cytoskeletal structure, protein expression and gene transcription [37]. The proteins engaged in these stimulated pathways may undergo post-translational modifications (PTMs) such as ubiquitination, phosphorylation, acetylation and methylation to regulate their function, localization, binding specificity and stability [38]. Protein phosphorylation is the most abundant PTM and it is involved in various essential cell functions such as cell division, proliferation, apoptosis and protein translocation [39]. In eukaryotic cells, the most common phosphorylation occurs on hydroxyamino acids such as serine, threonine and tyrosine residues with a ratio of about 1000:100:1, respectively (Fig. 1.6) [40].

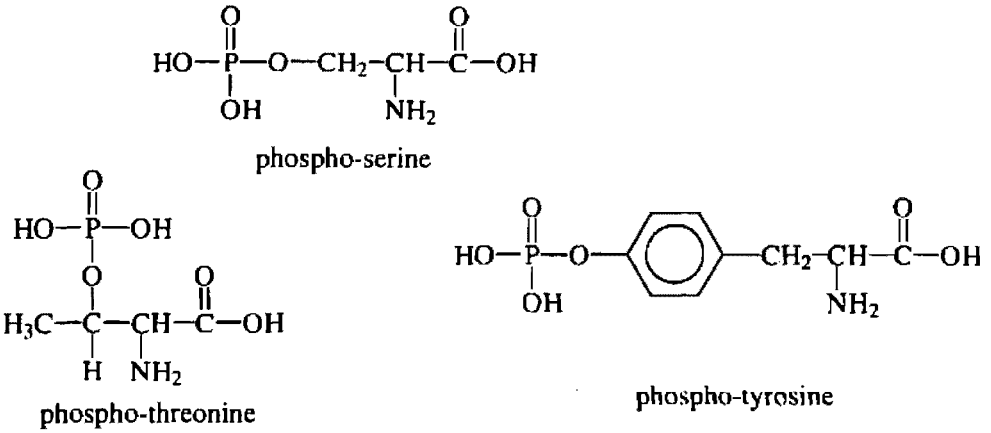

Figure 1.6: **Chemical structure of phosphorylated serine, threonine and tyrosine residues [41].**

Detection of phosphoproteins is rather difficult since only 1-2% of proteins are found in the phosphorylated form at any given time during signaling pathways [42]. The phosphorylation status of a particular protein depends upon the equilibrium between the activities of the corresponding kinases and phosphatases. Since the phosphatase reaction dominates and the phosphate group is very labile, the chance to observe a phosphoprotein is

very low [5]. Also experimental analysis of phosphoproteins is not an easy task because the phosphoamino acid only corresponds to a small fraction of the whole protein sequence [40].

To counteract these problems, cell biologists use three main techniques for phosphoprotein detection: ^{32}P radioactive labeling, Western blotting and 2D-gels. The most popular method is ^{32}P radioactive labeling since enrichment of the sample is not required and the detection signal is very sensitive (fmol) and quantifiable [42]. Yet, working with radioactive substances is not very desirable due to their toxic nature. Also, ^{32}P labeling can be tedious and sometimes even impossible since phosphate turnover rate is slow and only small amounts of radioactive phosphate are incorporated and may thereby escape detection [37].

As an alternative, Western blotting is another very sensitive (fmol) technique, which uses mono/poly-clonal antibodies directed against phosphorylated amino acids in order to detect phosphoproteins transferred from a 1D or 2D gel to a membrane [40]. However, serine and threonine residues possess a very small and structurally similar group, which makes it harder to obtain selective affinity interaction of the antibody to phosphoserines and phosphothreonines and the applicability of this method is reduced [37].

The last classical technique, 2D-gels, allows high-resolution separation of proteins from a complex sample according to their size and isoelectric point. However, 2D-gels analysis contains many drawbacks such as low-abundance protein (ng) detection and solubility problems of membrane proteins [43]. These molecular biology tools can provide quick information on the presence of one relatively abundant phosphoprotein but cannot identify the specific phosphorylation site. As an alternative, mass spectrometry has shown to be an excellent approach that surpasses most of the limitations encountered by the classical biological methods [42].

1.3.1 Mass spectrometry approaches for phosphopeptide detection

In recent years, mass spectrometry techniques and approaches have been developing rapidly and with success for the analysis of the phosphoproteome [5]. Initially, Edman degradation in combination with ^{32}P labeling allowed the peptide identification of many proteins including the phosphoprotein, β-casein [44]. Yet, this technique was not very

efficient since the amino acid cleavage did not consistently occur [41]. Nowadays, tandem mass spectrometers such as the hybrid quadrupole/time of flight hybrid (Q-TOF), Linear Trap Quadrupole (LTQ)-Orbitrap and Fourier transform ion cyclotron resonance (FTIRC) can provide identification of phosphopeptides with high resolution and sensitivity levels (fmol). Still, phosphoproteomic analysis by MS encounters major limitations due to the phosphopeptide ion suppression [5]. To enhance their detection, phosphopeptides are selectively isolated or modified using immunoprecipitation, enrichment methods, chemical modification and alkaline phosphatase treatment prior to MS analysis [45].

1.3.1.1 Immunoprecipitation assay

Phosphopeptides are present in very small amounts compared to the non-phosphorylated peptides in a cell extract [42]. For this reason, immunoprecipitation methods using phosphospecific antibodies are required for an enhanced detection. General pTyr antibodies have been used for the enrichment of complex cell extracts. Antibodies directed against the specific amino acids sequence containing the phosphorylated residue (Tyr/Ser/Thr) is also used for immunoprecipitation assay. Cell lysates are initially incubated with phosphospecific antibodies and then the immunocomplex is collected with protein A-Sepharose beads. The isolated phosphoproteins are resolved by SDS-PAGE analysis to be further analyzed by MS [46, 47].

Overall, immunoprecipitation assay has shown to achieve successful outcomes with anti-phosphotyrosine antibody [48]. Yet, it is still quite expensive and inconvenient to use antibodies for such large-scale experiments. Also, the serine and threonine antibodies independent of sequence context have not been used extensively due to their low specifity [5]. However, when antibodies are directed against a specific peptide containing Ser/Thr residues, the enrichment level is more significant [4].

Many novel phosphorylated proteins have been identified using immunoprecipitation assay, especially with tyrosine antibody [48]. However the use of this method is somewhat more limited than the other enrichment procedure since it is highly dependent upon the efficiency of the phosphospecific antibodies.

1.3.1.2 Phosphopeptide enrichment methods

Two other similar approaches routinely used for phosphoprotein enrichment are TiO_2 and IMAC micro-columns [45, 49]. The principle of IMAC enrichment mainly exploits the high affinity of negatively charged phosphopeptides towards metal-chelated (usually Ga^{3+} and Fe^{3+}) stationary phase [50]. In order to reduce non-specific binding by acidic side chains of glutamic acid and aspartic acid, a pH lower than the carboxyl group pKa (pKa of Asp is 3.65 and pKa of Glu is 4.25) and higher than the phosphoric acid pKa (2.15) is used [51]. Yet, unspecific binding to acidic residues (glutamic acid & aspartic acid), electron donors (histidine) and hydrophobic peptides is still a major pitfall [5]. To overcome this problem, Ficarro *et al.* [52] esterified all carboxylic acid groups prior to enrichment, which enabled the reduction of unspecific binding by at least two orders of magnitude. However, reaction conditions have to be chosen correctly in order to avoid incomplete methylation of the carboxylic groups and side reactions.

Recently, Larsen *et al.* [49] introduced a highly selective and efficient stationary phase, titanium dioxide (TiO_2), for phosphopeptide enrichment. A much higher enrichment level and recovery level was obtained by dissolving the sample in trifluoroacetic acid (TFA), acetonitrile (ACN) and 2,5-dihydroxybenzoic acid (DHB). The exact binding mechanism of TiO_2 to the phosphate group is still unclear but TiO_2 was found to have higher selectivity towards singly phosphorylated peptides. On the other hand, it was also reported that IMAC ligands have higher affinity for multi-phosphorylated peptides [53]. Hence, Thingholm *et al.* [54] created the SIMAC technique by combining both strategies to improve phosphorylation sites coverage.

Generally, IMAC and TiO_2 application is performed off-line using Zip Tip or micro-columns [50, 55]. To simplify the extraction procedure and minimize sample handling and loss, the chromatographic medium can be integrated into micro-capillary, which is combined to nano-LC/ESI-MS. On-line IMAC or TiO_2 enrichment can be controlled by an interface, which is compatible to any LC and MS [56, 57]. TiO_2 and IMAC enrichment is commonly used since it allows pre-concentrating the sample, retaining phosphopeptides, and removing reagents not compatible to MS [58]. Another major advantage is that less

suppression effect occurs due to enhancement of phosphopeptides and removal of non-phosphorylated peptides.

Even thought, immunoprecipitation, TiO_2 and IMAC micro-tips significantly improve phosphopeptide detection by decreasing sample complexity, detection by MS still remains challenging due to the chemical properties of the phosphate group. In positive ion mode, the negatively charged phosphate group decreases the ionization efficiency of the peptide. Also, since phosphate groups are very labile on phosphoserine and threonine, MS/MS spectrum is very poor which makes it harder for peptide sequencing [5]. In brief, enrichment procedures significantly improve phosphopeptide recovery but are still limited for complete phosphopeptide detection.

1.3.1.3 Chemical modification methods

Many studies have attempted to enrich phosphopeptides by replacing the phosphate group by an affinity tag. The most popular reaction, β-elimination, exposes phosphoserines and phosphothreonines to strongly alkaline conditions (LiOH or $Ba(OH)_2$ at pH 12) and yields a more reactive dehydroalanine and dehydroaminobutyrine species, respectively. The modified residue can act as a Michael acceptor and reacts with thiol based nucleophiles such as dithiothreitol (DTT) and 1,2-ethanedithiol (EDT) (Fig. 1.7) [59]. The phosphorylated amino acid can be identified by a mass shift resulting from the derivatization (-21 Da for β-elimination and Michael addition with 2-aminoethanethiol) [60].

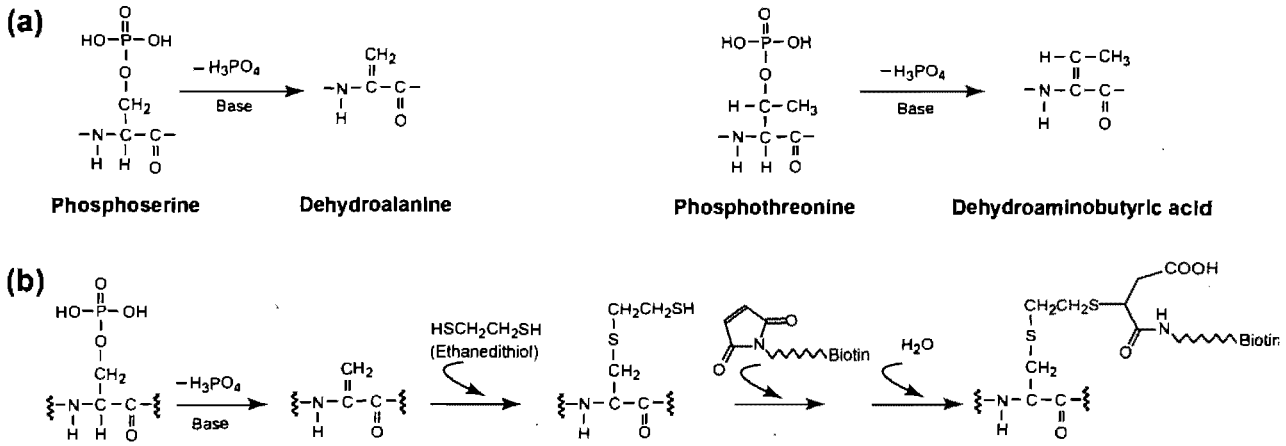

Figure 1.7: **(a) β-elimination reaction of phosphoserine and phosphothreonine. (b) Addition of a thiol group and biotin tag on phosphoserine for further enrichment on avidin columns [5].**

Phosphopeptide derivatization method has greatly improved and now allows detection down to femtomolar range [42]. A distinct advantage of this technique over enrichment procedures is that removal of the phosphate group prior to mass spectrometry facilitates positive ion detection. Nevertheless, this strategy still suffers from many drawbacks. First, contrary to immunoprecipitation approach, chemical derivatization is not applicable to tyrosine phosphorylation since it would require breakage of the very stable aromatic ring [5]. In addition, O-linked sugar moieties may also undergo β-elimination and obtain same intermediates as the phosphorylation residues [42]. Finally, incomplete derivatization of the phosphate moiety will result in decrease of phosphopeptide signal intensity after β-elimination.

Overall, chemical derivatization of phosphopeptide has demonstrated to be very efficient for the detection of phosphopeptides. Yet, this method is dependent upon the extent of completion of the reaction and unwanted reactions, which might be responsible for the increase of complexity of the sample and phosphopeptide losses [42].

1.3.1.4 *Alkaline phosphatase treatment*

Removal of the phosphate group by a phosphatase enzyme is another popular strategy used to avoid the ion suppression limitation of phosphopeptides in MS. The enriched protein digest is split in two where one half is incubated with alkaline phosphatase in basic conditions [61]. Following MS analysis of the treated and control sample, all the peptides correlated by a mass shift of 80 Da are designated as potential phosphopeptides [62]. If there are more than one phosphorylation site in a peptide, then mass shifts of multiples of -80 Da will be observed.

One major drawback of alkaline phosphatase treatment is that the phosphorylation sites remain indistinguishable from other hydroxyl amino acids. To overcome this problem, Liao *et al.* used several specific proteases such as endoproteinase Glu-C, Asp-N and trypsin to degrade the phosphopeptide into smaller fragments and locate exactly the phosphorylation site [61]. Also, Torres *et al.* addressed this issue by combining the advantages of IMAC, on-target dephosphorylation and hypothesis driven MALDI MS/MS [63]. This approach enabled the identification of four phosphate group on the C-terminus of the metazoan histone mRNA regulator (dSLBP), showing that alkaline phosphatase treatment is the method of choice to overcome the ion suppression of phosphopeptide in complex mixtures during MS detection.

In short, enrichment of the phosphopeptide samples and modification of the phosphate group are key strategies for an enhanced phosphopeptide analysis. In addition, further method optimization can also be performed on the analytical separation prior to MS detection to obtain higher phosphopeptide coverage.

1.3.1.5 *Separation methods*

Highly complex samples can be separated and analyzed using high performance liquid chromatography (HPLC) coupled to a ESI-MS [64]. Peptides are first loaded onto a nano-column containing C_{18} material and then eluted at a slow flow rate (200-600 nL/min) using a gradient of water and ACN. Coupling the nano-LC system to the mass spectrometer has been very successful for the separation of phosphopeptides and a decrease in ion

suppression [5]. However, since multi-phosphorylated peptides are very hydrophilic, they may not stick onto the hydrophobic column and will elute in the column flow-through [62].

Alternatively, to enhance detection of phosphorylated peptides, the sample mixture can initially be separated on a strong cation exchange (SCX) column followed by chromatographic separation into the C_{18} column. Hydrophilic phosphopeptides are enriched in early fractions, resulting in better detection [5].

In summary, mass spectrometry provides a viable alternative to more traditional methods for phosphorylation analysis. Yet, the dual constraints of low yield of phosphopeptide and the mixture complexity required methods of separation and enrichment prior to MS analysis. Affinity enrichment procedures such as IMAC and TiO_2 micro-columns, chemical derivatization and anti-phosphospecific antibodies, increased the proportion of phosphopeptides in a complex mixture. However, the choice of which method is most appropriate is dependent upon the quantity of protein available, which residue are expected to be phosphorylated and the degree of sample purification. Nevertheless, recent high-sensitive mass spectrometers have proven to significantly enhance phosphoprotein identification in simple and complex samples [65, 66].

1.4 Mass spectrometry

The mass spectrometer (MS) is an instrument used for determining the molecular mass and structure of biomolecules, drugs, proteins and oligonucleotides. This analytical tool is composed of three different sections: the ionization source, the mass analyzer and the detector [67]. In proteomics-based experiments, the sample is initially digested by trypsin and then the peptide mixture can undergo chromatographic separation or is directly introduced into the MS [68]. Upon ionization in the source, the ions travel into the analyzer where they will be separated according to their mass (m) –to-charge (z) ratio (*m/z*). The signal collected from all these ions is transformed to generate *m/z* spectrum [67]. Lastly, the raw chromatograms are processed through specialized softwares that further enable the profiling and identification of the proteins in the sample (Fig. 1.8) [69].

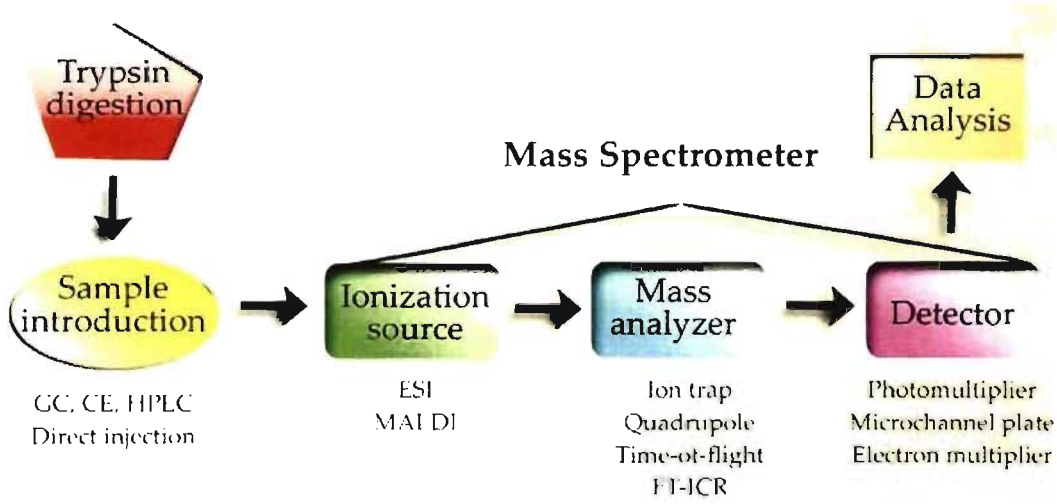

Figure 1.8: **General mass spectrometry-based proteomics.**

Some instruments contain two or more analyzers, which can be used for structural and sequencing studies [67]. Several different types of MS are available commercially such as the triple quadrupole, hybrid triple quadrupole/linear ion trap (Q-TRAP), matrix assisted laser desorption ionization-time of flight (MALDI-TOF), hybrid quadrupole/time of flight hybrid (Q-TOF), Fourier transform ion cyclotron resonance (FTICR) and the linear trap quadrupole (LTQ)-Orbitrap. All of these instruments offer different applications in the field of MS.

1.4.1 Electrospray ionization

The most common ionization method used for biological applications is the electrospray ionization (ESI). This technique was first introduced by Fenn in 1984 [64]. The analysis can be performed in positive or negative ion mode depending on the proton affinity of the sample. ESI can be coupled to a HPLC or a CE since the analyte is converted from a liquid to a gaseous phase [70].

The atmospheric pressure interface of an ESI source is composed of a capillary where the sample solution is exposed to very high voltage (3-5 kV) applied to the tip. A stream of nebulising gas (nitrogen) can also be present around the capillary to facilitate the nebulisation of the analytes [71]. As the charged liquid first exits the emitter's tip, a cone shape, known as a Taylor cone, briefly forms (Fig. 1.9). With the assistance of the drying gas (nitrogen), droplets decrease in size by solvent evaporation which forces the charges in the molecules closer together [71]. A Coulombic explosion occurs when there are too many charges being confined within a too small area and start repelling each other (Rayleigh limit), causing the droplets to divide into two smaller droplets. This process repeats itself until the solvent is completely evaporated and the droplets have split up to become one single charged molecule (Fig. 1.9) [67]. This ionization process is very fast and occurs within milliseconds.

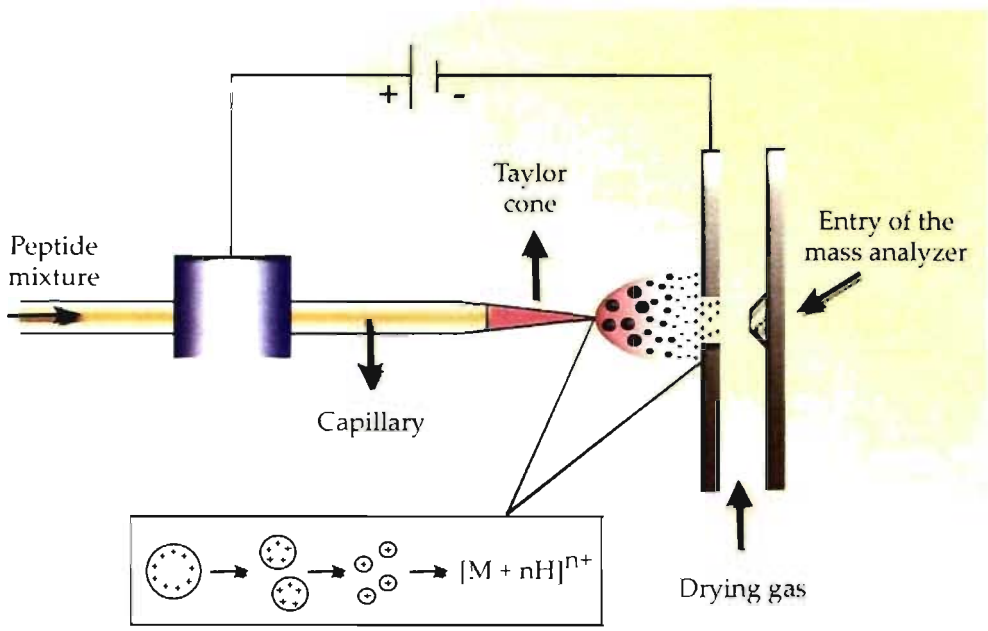

Figure 1.9: **Electrospray ionization chamber.**

A new method named nano-electrospray ionization uses flow rate of sample injection of 20-40 nL/min and minimizes loss of analyte [71]. The decrease in droplet size and inner diameter of the emitter enabled an ionization efficiency of two orders of magnitude greater than the conventional ESI [64]. Hence important parameters that influence the electrospray stability are the voltage applied, the flow rate and the emitter size. Overall, ESI provides a continuous stream of multiply charged ions that can be introduced in a multitude of mass analyzers.

1.4.2 LTQ-Orbitrap mass spectrometer

As technology progresses, more important advancements take place in the mass spectrometry field. For instance, several years ago, detection of about few hundreds phosphopeptides in a complex cell extract was considered very high for mass spectrometry analysis [52]. Recently, a new and very powerful mass spectrometer, the LTQ-Orbitrap, enabled the identification of almost 1000 phosphopeptides for large-scale phosphoproteomic analysis [66]. This observation shows that the extent to which biological information can be gained is completely dependent upon the analytical performance of the MS. The Linear Trap Quadrupole (LTQ)-Orbitrap recently invented by Makarov is one of the most efficient hybrid mass analyzer.

The orbitrap mass analyzer is an electrostatic trap containing an inner and outer electrode. Ions are injected tangentially in the trap and move in complex spiral patterns all around the inner electrode [72]. A Fourier transform performs the mass analysis based on image current detection of oscillation frequencies [73]. For this reason, the FTICR and orbitrap have similar level of mass accuracy and resolution [5]. The orbitrap has a mass accuracy below 2 ppm, a high dynamic range (~5000) and a maximum resolving power of 100,000 that can be reached in 1.6 sec of analysis and 400 *m/z* [73, 74]. Even though the orbitrap is able to perform MS/MS analysis, a lower sensitivity is observed due to the loss of ions in the C-trap. Hence, it is more practical to link the orbitrap to another mass analyzer, the linear ion trap, which will perform MS/MS analysis with much higher sensitivity. This hybrid of mass analyzers is referred to as Linear Trap Quadrupole (LTQ)-Orbitrap (Fig 1.10).

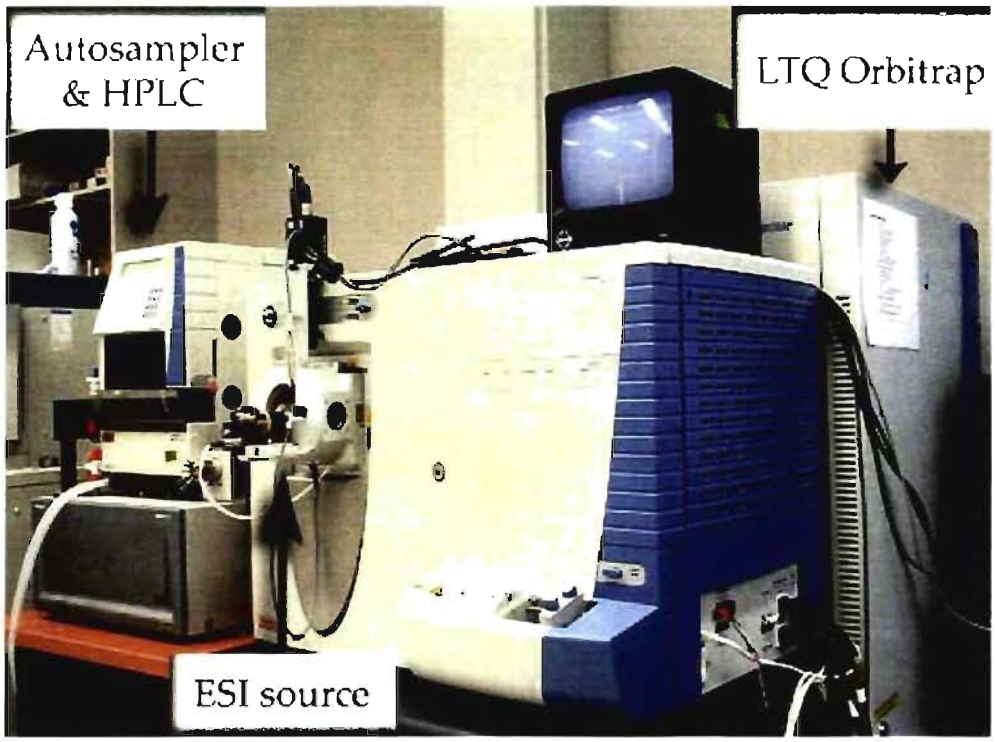

Figure 1.10: **LTQ-Orbitrap hybrid mass spectrometer (Thermo Electron) coupled to a nano-flow LC (Eksigent) with a Spark-Holland autosampler (Thermo Electron).**

The LTQ-Orbitrap is composed of three main elements; the linear quadrupole ion trap, the C-trap and the orbitrap (Fig. 1.11). Initially, the ions are accumulated into the linear quadrupole ion trap and then transferred into the C-shaped storage trap (C-trap). The C-trap is used to store and collisionally cool ions, which are subsequently pulsed into the orbitrap [74].

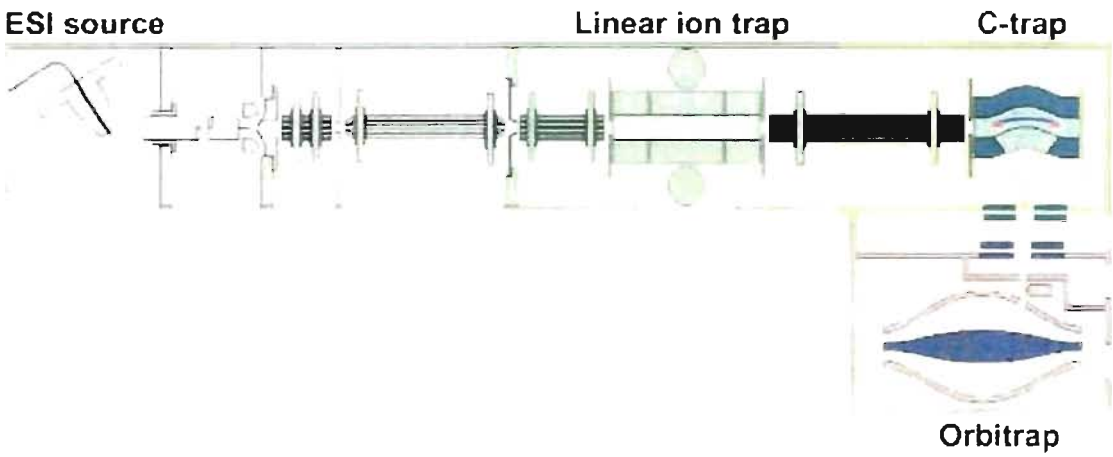

Figure 1.11: **A schematic representation of the LTQ-Orbitrap mass spectrometer [73].**

The MS and MS/MS analysis can be recorded independently or in tandem with both mass analyzers (linear quadrupole ion trap and orbitrap) according to the experimental requirements. The most popular approach used for peptide identification is to combine the fast MS^n capabilities of the linear ion trap with the high resolution and mass accuracy of the orbitrap [73]. For the tandem MS analysis, the ion trap stores and stabilizes ions by applying a RF voltage. Maximum resolution and sensitivity is achieved by cooling down the ions with a damping gas. By increasing the RF voltage, ions are destabilized and ejected from the trap. As a result, only one peptide is kept where bond cleavage occurs upon vibrational excitation [67]. In a total time of 1 sec, the duty cycle of the LTQ-Orbitrap consists of 3-5 MS/MS analysis for one survey scan [73].

In summary, this higher number of acquired MS/MS spectrum considerably enhances the overall number of peptide identification. Also the false positive rate of high-throughput peptide analysis is significantly smaller due to the instrument's high mass accuracy.

1.4.3 Tandem MS

Tandem MS is mainly applicable for small drug molecules and peptides. MS/MS spectrum offers structural information which can be pieced together to generate the complete peptide sequence. The process consists of isolating a particular ion, which subsequently collides with neutral gas atoms (nitrogen, argon or helium) in the collision cell. Ions will absorb the kinetic energy which induces breakage of peptide bonds to form product ions [67]. All these fragmented ions are separated according to their *m/z* by the mass analyzer and finally provide a fingerprint pattern of the precursor ion under investigation [75]. Throughout one survey scan of a chromatographic run, the most abundant ion at a given time is kept in the trap and is further fragmented to obtain the MS/MS scan [69]. The success of d*e novo* sequence interpretation largely depends upon the mass accuracy and resolution of the instrument.

Three different peptide bonds (NH-CH, CH-CO and CO-NH bond) can be fragmented depending on the MS conditions. Upon bond breakage, two fragments are created where one is charged and the other neutral depending on the chemistry and proton affinity of the two species [67]. In all, there are six different possible fragment ions; a, b and c ions when the charge is retained on the N-terminus and x, y and z ions for C-terminal charged molecules. Since it requires less energy, the most common fragmentation pattern is the b and y type ions (Fig. 1.12) [75].

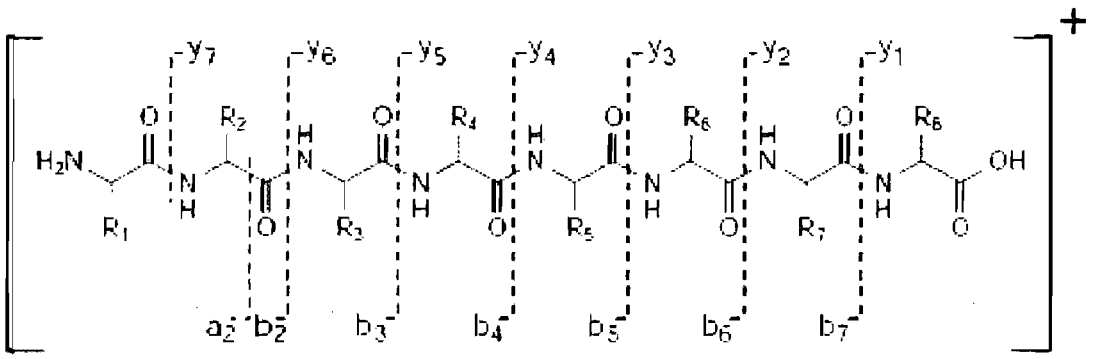

Figure 1.12: **Peptide fragmentation in low collisional energy illustrating b and y ions [69].**

During tandem mass spectrometry, the phosphate moiety of phosphopeptides is predominantly lost and usually serves as a signature for phosphopeptides. Since the P—O bond is much weaker than a peptide bond for Ser/Thr phosphorylated precursor, a satellite ion, $[M+H-98]^+$, is generated during fragmentation [76]. The unsaturated form of the serine (69.03 Da) and threonine (83.05 Da) will indicate the presence of a phosphate moiety in a MS/MS spectrum [71]. On the other hand, the phosphate group on tyrosine phosphorylated peptides usually remains attached to the side chain during MS/MS analysis due to tyrosine's stable ring structure [77]. Hence, the phosphorylated tyrosine can be identified with a mass of 243.18 Da (163.18 + 80 Da) on the MS/MS spectrum.

The MS/MS spectrum can be interpreted manually or through different specialized algorithms (Mascot, Sequest and ProteinProspector) that try to match the fragments ions to theoretical values expected from a large protein database [69].

1.4.4 Data processing

1.4.4.1 MS/MS ion search using Mascot

In proteomics studies, Mascot from Matrix Science (http://www.matrixscience.com/) is a very popular database engine used to identify proteins from MS/MS spectrum and protein databases. Mascot is a useful tool for the interpretation of less informative MS/MS spectrum or complex protein mixtures [69]. Prior to the Mascot search, necessary information about the MS experiment needs to be added in the Mascot search engine page in order to minimize the false positive rate especially for the large scale proteomic analysis (Fig. 1.13).

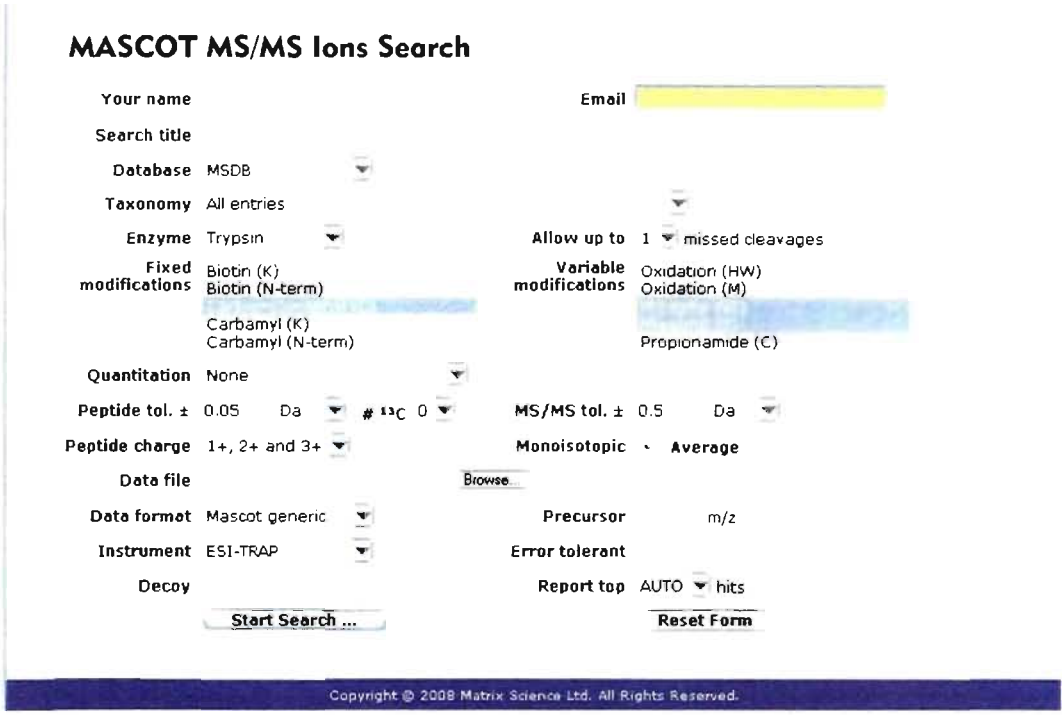

Figure 1.13: **Mascot search engine page showing all parameters for a MS/MS ion search.**

The general approach consists of first downloading the file containing all MS/MS spectra (fragment ions with their intensity, *m/z* and RT) to Mascot. Then, the most suitable database (MSDB, IPI, SwissProt and NCBInr) and species are determined according to the proteins characteristics. The sample preparation is taken into consideration by choosing the enzyme responsible for the digestion, the number of allowed missed cleavage sites and the

fixed and variable modifications. Finally, the mass accuracy of the mass analyzer for the MS and MS/MS analysis is indicated to set a mass tolerance range for confident peptide detection. As a result, a list containing the peptide's sequence, matching protein, *m/z*, RT, *z* and Mascot score is generated.

Overall, Mascot is a great tool for quick and high-throughput protein identification. To obtain a complete analysis of the proteomic study, Mascot identification must be combined with a quantification method.

1.4.4.2 Mass Sense & peptide clustering

For the quantification analysis of complex protein mixtures, different types of methods are available using relative or absolute measurements and label-free or derivatized protein mixtures. Mass Sense and peptide clustering are in-house label-free bioinformatics softwares developed by Jaitly *et al.* [78].

From raw MS files, Mass Sense software computes with high confidence a contour map with four different coordinates; *m/z* value, retention time (RT), charge (*z*) and abundance (Fig. 1.14). From the manual validation of this software, the false positive and false negative rate corresponded to 4.6 % and 7.4 %, respectively [78]. A score value is attributed to each identified peptide ion reflecting the correlation between observed and expected abundance ratio of isotopic ions. In addition, an excel list is generated displaying the *m/z* value, z, RT, intensity and Mass Sense score for each peptide. Hence, Mass Sense is capable to display statistically significant fold-change in abundance across cellular replicates and conditions.

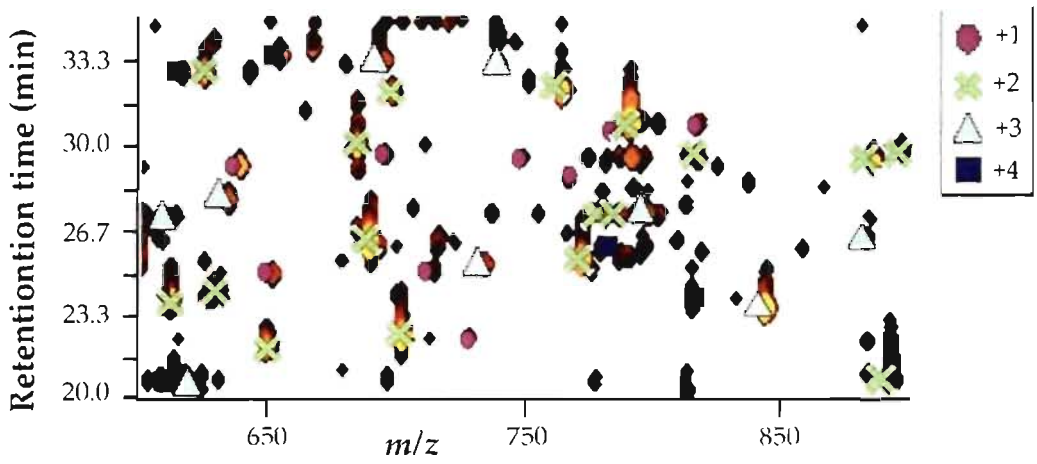

Figure 1.14: **Contour plot generated by Mass Sense.** Peptide abundance is represented by a colour gradient from yellow (most abundant) to black (least abundant). Peptide's charge is illustrated by a symbol described in the legend.

The Peptide Cluster Miner software enables the comparison of peptide intensities of several replicates or samples in different conditions. Peptides with similar *m/z*, RT and charge within the tolerance range, are clustered together. As a result, a list displaying all the peptides with their corresponding abundance in each different condition is generated. In a similar fashion, the clustered peptides can be aligned to the peptide identification list from the Mascot search. Hence, this tool allows the generation of expression profiles for the better understanding of identified peptide abundance change across different conditions.

2. Combined enzymatic and data mining approaches for comprehensive phosphoproteome analyses; application to cell signaling events of interferon-γ stimulated macrophages

Marcantonio, M., Trost, M., Courcelles, M., Desjardins, M., and Thibault, P. (2008)
Molecular & Cellular Proteomics, 7: 645-660.

2.1 Abstract

Protein phosphorylation is a central cell signaling event that underlies a broad spectrum of key physiological processes. Advances in affinity chromatography and mass spectrometry are now providing the ability to identify and quantitate thousands of phosphorylation sites simultaneously. Comprehensive phosphoproteome analyses still present sizable analytical challenges in view of suppression effects and the variable quality of MS/MS spectra. This work presents an integrated enzymatic and data mining approach enabling the comprehensive detection of native and putative phosphopeptides following alkaline phosphatase digestion of titanium dioxide (TiO_2)-enriched cell extracts. The correlation of retention times of more than 750 phospho- and dephosphopeptide pairs from J774 macrophage cell extracts indicated that removal of the phosphate groups can impart a gain or a loss in hydrophobicity that is partly explained by the formation of salt bridge with proximal amino groups. Dephosphorylation also led to an average 2-fold increase in MS sensitivity which facilitated peptide sequencing. More importantly, alkaline phosphatase digestion enhanced the overall population of putative phosphopeptides from TiO_2-enriched cell extracts providing a unique approach to profile multi-phosphorylated cognates that would have remained otherwise undetected. The application of this approach is demonstrated for differential phosphoproteome analyses of mouse macrophages exposed to IFN-γ for 5 min. TiO_2 enrichment enabled the identification of 1143 phosphopeptides from 432 different proteins of which 125 phosphopeptides showed a 2-fold change upon IFN-γ exposure. The use of alkaline phosphatase nearly doubled the number of putative phosphopeptides assignments leading to the observation of key IFN-γ signaling events involved in vesicle trafficking, production of reactive oxygen species and mRNA translation.

2.2 Introduction

In biological systems, signal transduction pathways are primarily guided through post-translational modifications (PTMs) of proteins to transmit information from extracellular stimuli into the cytoplasm and nuclei of cells for changes in cytoskeletal structure, vesicle transport and gene transcription [37]. Protein phosphorylation is the most abundant reversible PTM and a major regulator of protein activity or stability. About one third of proteins encoded by the human genome are assumed to be phosphorylated during their life cycle [79]. Phosphorylation can occur on several residues, but it is mostly found on hydroxyamino acids such as serine, threonine and tyrosine residues with a ratio of about 89:10:1 [80]. Because protein phosphorylation holds a central role in signaling networks, considerable effort is attributed to the development of methods for phosphoprotein characterization. Highly sensitive detection techniques are required because phosphoproteins represent only a small proportion of any given cell extracts (typically ~1-2%) [42]. Most conventional methods such as two-dimensional-gels, ^{32}P radioactive labeling and Western blotting have limited features, which do not enable them to comprehensively profile phosphoproteome change or identify the exact phosphorylation site.

To overcome this challenging task, mass spectrometry has emerged as a sensitive, rapid and effective tool for accurate and specific localization of post-translational modifications such as protein phosphorylation. Nevertheless the negatively charged phosphate group on phosphopeptides renders their MS analysis more difficult than their non-phosphorylated counterpart. For instance, MS/MS spectra of phosphopeptides are less interpretable than their non-phosphorylated counterpart due to the abundant fragment ion corresponding to the loss of the labile phosphate group (80 or 98 Da). Also database search engines are better adapted to the correlation of linear sequences compared to peptides with labile functionalities. In positive ion mode, this difficulty is compounded with the under-represented population of phosphopeptide abundance due to suppression effects in an overwhelming large population of non-phosphorylated peptides [79]. The coupling of the nano-LC system to the mass spectrometer has been very successful for the separation of

phosphopeptides and led to a decrease in ion suppression [5]. However, because multi-phosphorylated peptides are very hydrophilic, they may not be retained on the hydrophobic column and will elute in the column flow-through [62]. On the other hand, Steen *et al.* [81] used a small set of synthetic phosphopeptides and their dephosphorylated cognate to indicate that the challenge in phosphopeptide identification is primarily due to the low abundance of this PTM rather than their lower ionization efficiency.

Phosphopeptide enrichment is an indispensable step for the analysis of large-scale phosphoproteomics to reduce sample complexity and to enhance their detection. Immobilized Metal Ion Chromatography (IMAC) using Fe(III) or Ga(III) and titanium dioxide (TiO_2) micro-columns are most commonly used as selective isolation method of phosphopeptides [42]. These techniques allow pre-concentrating the sample, retaining phosphopeptides, and removing salts and detergents not compatible to MS [58]. Yet one major pitfall is the unspecific binding of acidic residues (glutamic acid and aspartic acid), electron donors (histidine) and hydrophobic peptides [5]. To overcome this problem, Ficarro *et al.* [52] converted all carboxylic groups to the corresponding methyl esters using HCl-saturated, dried methanol before IMAC enrichment. In addition, Larsen *et al.* [53] demonstrated that 2,5-dihydroxybenzoic acid (DHB) significantly improved phosphopeptide recovery by selectively displacing acidic peptides from the TiO_2 stationary phase. However, depending on the column material, the phosphopeptide populations enriched seem to differ and the suppression effect of phosphopeptides is still evident in enriched complex samples [82]. This raises the question if many more phosphopeptides are still not detected due to their weak ionization efficiency in positive ion mode. Several teams have tried to approach this issue by chemically modifying the phosphate group by β-elimination/Michael addition reactions, which will enhance the level of detected phosphopeptides [59, 83]. Yet, this method is dependent upon the reaction yield and unwanted side-reactions and is only applicable to Ser and Thr residues. The study of tyrosine phosphorylation is mainly achieved by immunoprecipitation with anti-pTyr monoclonal antibodies [84]. However, large-scale analysis of phosphotyrosine using specific antibodies commercially available can be relatively expensive and would not provide any information on serine and threonine phosphorylation. Another strategy adapted recently identified phosphopeptides in a sample using alkaline phosphatase (AP) treatment

applicable to all hydroxyamino acids, even tyrosine residues [63, 85, 86]. The major drawback from AP approach is the information of the phosphorylation site on the peptide is lost.

In the present study, we describe a combined enzymatic and data mining approach to comprehensively identify trace-level phosphopeptides from cytosolic protein extracts of macrophage cells. This strategy is further demonstrated for differential phosphoproteome analyses of macrophages from control and IFN-γ challenge experiments. Several phosphoproteins involved in vesicle trafficking, reactive oxygen species (ROS) production and mRNA translation were identified as significantly over or under-expressed upon early macrophage activation. The collection of a large number of phosphopeptides containing even multi-phosphorylated species treated with AP enabled a more extensive study on the comparison between phosphopeptides and their dephosphorylated cognate using in-house bioinformatic tools. The higher intensity and the appearance of new putative phosphorylated peptides confirmed the reduced ionization efficiency of phosphopeptides in positive ion mode. The correlation of retention time between phosphopeptides and their dephosphorylated counterparts also provided a meaningful approach to determine changes in hydrophobicity upon dephosphorylation.

2.3 Experimental Procedures

2.3.1 Materials

Acetonitrile (ACN) was purchased from Fisher Scientific (Whitby, ON, Canada). Formic acid (FA), ammonium acetate and ammonium bicarbonate were obtained from EM Science (Mississauga, ON, Canada). Ammonium hydroxide, trifluoroacetic acid (TFA), acetic anhydride, α-casein, DTT, iodoacetamide, imidazole, sucrose, urea and acetic acid were purchased from Sigma-Aldrich. Tyr$(PO_3H_2)^4$-Angiotensin II Human was obtained from Calbiochem. BCA protein assay, immobilized TPCK trypsin, bond breaker tris(2-carboxyethyl)phosphine (TCEP) solution and phosphopeptide isolation kit One SwellGel® gallium disc/column were purchased from Pierce. Fetal bovine serum (FBS), penicillin-streptomycin, L-glutamine and DME/High glucose Dulbecco's modified eagle's medium were purchased from HyClone (Perbio, Nalgene).

2.3.2 Preparation of standard proteins

A solution of eight reduced and iodoacetamide-alkylated protein standards (40 fmol/μL each) was prepared from individual digests of bovine serum albumin, rabbit phosphorylase *b*, yeast alcohol dehydrogenase, bovine deoxy-ribonuclease, horseradish peroxidase C1A, bovine glyceraldehyde 3P dehydrogenase, *Escherichia coli* β-galactosidase, and bovine carboxypeptidase A (Michrom Bioresources, Auburn, CA). α-Casein was digested with immobilized trypsin in 50 mM ammonium bicarbonate overnight at 37°C and then evaporated to dryness.

2.3.3 Cell cultures

J774 (murine macrophage cells) were cultured in Dulbecco's modified Eagle's medium (DMEM), pH 7.4, supplemented with 10% heat inactivated fetal bovine serum (FBS), 2 mM L-glutamine and antibiotics (100 mg/mL penicillin & 100 mg/mL streptomycin), at 37°C in 5% CO_2 atmosphere. Cells were plated in 100 mm Petri dishes at

a density of 20 million cells per dish corresponding to approximately 330 μg of cytosolic protein extracts. For IFN-γ challenge experiments, J774 cell cultures were incubated for 5 min with mouse interferon-γ (PBL Biomedical Laboratories) (100 U/mL).

2.3.4 Protein extraction and immobilized trypsin digestion

Cells were washed with 1X PBS to remove culture media. Cells were resuspended in 8.5% sucrose (w/w)/3 mM imidazole and broken with a metal douncer homogenizer. Nuclei were removed by centrifugation at 860 g for 15 min. Cell lysates were ultracentrifuged at 150,000 g for 30 min to discard membrane proteins. Cytosolic proteins in the supernatant were precipitated by acetone. Proteins were resuspended in 1% SDS/50 mM ammonium bicarbonate for phosphopeptide TiO_2 enrichment or in 8 M urea/50 mM ammonium bicarbonate for IMAC Ga^{+3} micro-columns phosphopeptide enrichment. Proteins were reduced in 0.5 mM TCEP for 20 min at 37°C and then alkylated in 50 mM iodoacetamide for 20 min at 37°C. 50 mM DTT was added to the protein solution to react with excess iodoacetamide. Total protein amount was quantitated by BCA protein assay. Proteins were digested in 1 M urea or 0.1% SDS, 50 mM ammonium bicarbonate with immobilized TPCK trypsin overnight at 37 °C and high agitation speed (250 μL of trypsin per mg of sample). The digest mixture was acidified with trifluoroacetic acid (TFA) and then evaporated to dryness.

2.3.5 Phosphopeptide isolation

Two different affinity-based methods (IMAC Ga^{3+} and TiO_2 micro-columns) for phosphopeptide enrichment were used in this study. For the IMAC isolation protocol, J774 cell digests were resuspended in 5% FA and incubated for 20 min at room temperature in SwellGel Ga(III) disc/column. IMAC beads were washed with 0.1% FA (two times), 30% ACN/0.07% FA (two times), and finally water. Lastly, phosphorylated peptides were eluted with 2 x 25 μL of 0.1% ammonium acetate pH 9.6. For the TiO_2 procedure, sample loading, washing and elution were performed by applying gas pressure from a nitrogen tank to the TiO_2 micro-tips. Each micro-column was used once to avoid contamination. In-house TiO_2 (5 μm, GL Sciences, Japan) micro-columns were equilibrated with 10 μL 3% TFA, 70%

ACN. The digest mixture was redissolved in 350 mg/mL 2,5-dihydroxybenzoic acid (DHB) (Aldrich), 3% TFA, 70% ACN. Unless otherwise indicated, 250 µg (50 µL) of protein digests (equivalent to 15 x 10^6 cells) were loaded onto a 1.25 mg TiO_2 micro-column. The column was washed first with 10 µL of 350 mg/mL DHB, 3% TFA, 70% ACN and then 2 times with 30 µL of 3% TFA, 70% ACN. The bound phosphopeptides were eluted with 30 µL (or 50 µL for the IMAC comparison experiment) of 1% ammonium hydroxide pH 10. The eluate was acidified with 1 µL of TFA and 20 µL of the enriched sample was injected on the LTQ-Orbitrap mass spectrometer. Unless otherwise indicated, samples were prepared in triplicate for each condition under study.

2.3.6 Alkaline phosphatase treatment

The reaction consisted of incubating half of the sample for 2 h at 37°C at high agitation speed with 20 Units of calf intestine AP (New England BioLabs) per 175 µg of protein in basic conditions. For the analysis of standard proteins, 175 µg of digested α-casein and 10 pmol of eight known non-phosphorylated proteins with 0.1 mM phenylmethyl sulphonyl fluoride (PMSF) were resuspended in 50 mM ammonium bicarbonate and then treated with 20 Units of AP. For the TiO_2-enriched J774 phosphopeptides, half of the eluate (15 µL) was treated with 20 Units (2 µL) of AP and 2 µL of 1% ammonium hydroxide pH 10 was added to the other half of TiO_2-eluate. After dephosphorylation, treated and non-treated samples were acidified with 1 µL of TFA and injected on the LTQ-Orbitrap mass spectrometer. For *N*-acetylation of TiO_2 enriched α-casein phosphopeptides, dried samples were initially resuspended in 40 µL of 50mM ammonium bicarbonate and then derivatized with 100 µL of acetylation reagent (anhydrous MeOH: acetic anhydride 3:1). After a 30 min derivatization period at room temperature, samples were evaporated on a SpeedVac concentrator prior to AP digestion.

2.3.7 LC-MS/MS analysis

LC-MS/MS analyses were performed on a LTQ-Orbitrap hybrid mass spectrometer (Thermo Electron, San Jose, CA) coupled to a nano-flow LC (Eksigent, Dublin) with a Spark-Holland autosampler (Thermo Electron, San Jose, CA). The analytical column (10

cm length, i.d. 150 μm) and trap column (4 mm length, i.d. 360 μm) were packed in-house with C_{18} Jupiter (3 μm & 300 Å) material (Nalgene, Phenomenex, Torrance, CA). Peptides were eluted from the reverse phase column into the mass spectrometer using a gradient from 2% to 25% B over 63 min followed by a gradient from 25% to 40% over 15 min with a flow rate of 600 nL/min (A: 0.2% FA in water, B: 0.2% FA in ACN). MS spectra were acquired in FTMS positive ion mode for 1 sec from *m/z* 400 to *m/z* 1600 with a resolution of 60,000. Mass calibration used Calmix (caffeine, MRFA, and ultramark) and typically provided mass accuracy within 15 ppm on average for all nanoLC-MS/MS experiments without using a lock mass. The nanoelectrospray voltage and MS/MS fragmentation amplifier voltage were set to 1.6 V and 1.3 V, respectively. The mass spectrometer operated in data-dependent mode where a survey scan is initiated in full scan at high mass accuracy in the Orbitrap followed by tandem MS in the linear ion trap of the 3 most abundant precursor ions. A dynamic exclusion window was applied to prevent MS/MS analysis of previous selected ions 80 sec after its acquisition. Only multiply charged ions with intensity above 10,000 counts were selected for MS/MS sequencing. Tandem MS analysis operated in a total time of 1 sec from one third of precursor ion *m/z* to *m/z* 2000.

2.3.8 Database searching with mass spectrometry data

Data were analysed with Xcalibur (version 2.0 SR1) software and peak lists were generated using Mascot distiller (version 2.1.1, Matrix Science, London, UK) software and LCQ_plus_zoom script. Database searches were performed against an IPI mouse database containing 52,326 entries [87] (version 3.24, released November 2006) using Mascot (version 2.1, Matrix Science) selecting mouse species for J774 cell extract analysis. Data of α-casein and eight non-phosphorylated proteins were searched against in-house compiled database where the sequences were taken from UniProtKB/Swiss-Prot database (release 9.0, October 31 2006). Parent ion and fragment ion mass tolerances were both set at +/- 0.05 and 0.5 Da, respectively. One missed cleavage was allowed for trypsin digestion and phosphorylation (STY), oxidation (M), deamidation (NQ) and carbamidomethylation (Cys) were selected as variable modifications. All protein identifications and IPI entry numbers were reported for peptide sequences matching more than one protein entry. A Mascot search against a concatenated target/decoy database consisting of a combined forward and

reverse version of the IPI mouse database was performed to establish a cutoff score threshold for a false-positive rate of less than 2% ($p < 0.02$) [88]. The location of the phosphorylation site was based on the highest ranking assignment with a Mascot score ≥5 to the next leading candidate. All possible phosphorylation sites were reported if the Mascot scores could not provide sufficient discrimination amongst the leading candidates.

2.3.9 Peptide detection and clustering

Raw data files (.raw) generated from the LTQ-Orbitrap acquisition software were converted into text files representing all ions according to their corresponding *m/z* values, retention time, peak widths, intensity and charge state using in-house peptide detection software [78]. Intensity values above a user-defined intensity threshold (10,000 counts) were considered. Segmentation analyses were performed across different sample sets using hierarchical clustering with criteria based on their respective *m/z*, charge and time within user-defined tolerance (±0.05 *m/z* and ±1 min). Normalization of retention time is then performed on the initial peptide cluster list using a dynamic and nonlinear correction. A moving-average time-window interpolation scheme is used to compute the time shifts for each peptide across the different data sets. For replicate LC-MS injections, this alignment confines the retention time distribution to less than ± 0.1 min (< 0.3% relative S.D.) on average. The generated unique list of peptide clusters allowed the direct comparison of peptide abundance between samples in different conditions to identify those showing reproducible and statistically meaningful changes in abundance. Also peptide clusters were aligned with phosphopeptide identification file from Mascot according to set *m/z* and retention time tolerance (±0.05 *m/z* and ±1 min). In addition, to compare the retention time and abundance of phosphopeptides and their dephosphorylated counterpart, specific algorithms were developed to cluster peptide ions from control and phosphatase-treated samples that displayed changes in retention time up to 5 min and precise mass shifts for one or multiple phosphate groups (HPO_3: 79.9663 Da).

2.4 Results

2.4.1 Evaluation of phosphopeptide enrichment methods

Large-scale proteomics analyses of phosphopeptides have been very difficult due to the strong signal suppression taking place in the presence of a high number of non-phosphorylated peptides [79]. Phosphate group affinity media such as titanium dioxide (TiO_2) and metal ions (Ga^{3+} and Fe^{3+}) are the most analyzed and optimized enrichment methods for the isolation of phosphopeptides [45, 82]. In this study, the phosphopeptide enrichment performance of TiO_2 micro-tips introduced by Larsen *et al.* [53] was compared with the phosphopeptide isolation kit One SwellGel Ga(III) disc/column from Pierce. In total, 679 peptides were identified with a Mascot score above 25 from the TiO_2-enriched sample where 76.9% corresponded to phosphopeptides. On the other hand, Ga^{3+} metal ions extraction method obtained a much lower phosphopeptide enrichment level (37.0%) from the 451 identified peptides (Fig. 2.1, and Table 2.1).

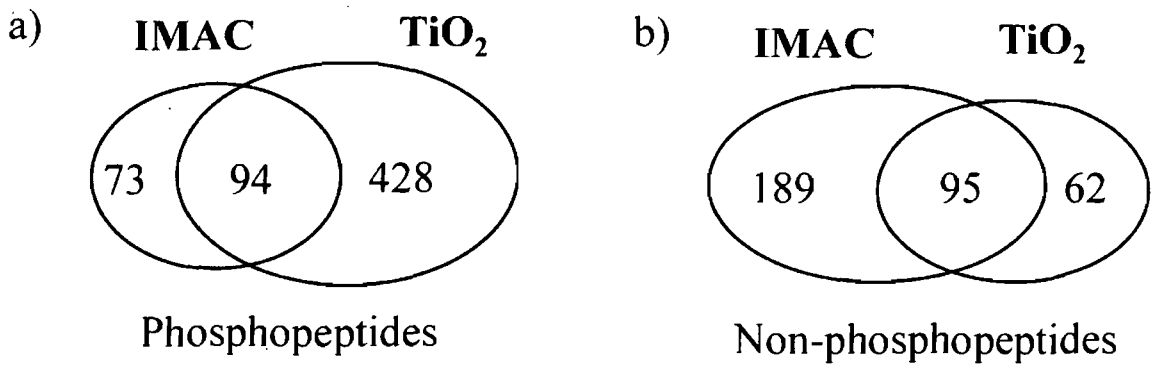

Figure 2.1: **Comparison of IMAC (Ga^{3+}) and TiO_2 enrichment procedures.** Venn diagrams showing the number of unique and common J774 (a) phosphopeptides and (b) non-phosphorylated peptides using both isolation methods.

Table 2.1: **Comparison of TiO_2 and IMAC (Ga^{3+}) phosphopeptide enrichment methods using 250 µg J774 cell extract**

	Phosphopeptides	Non-phosphopeptides	Total	Enrichment level
Total (IMAC)	167	284	451	37.0%
Total (TiO_2)	522	157	679	76.9%
Common	94	95		
Unique (IMAC)	73	189		
Unique (TiO_2)	428	62		

A large divergence in selectivity towards phosphopeptides and non-phosphorylated peptides was noted using different affinity media and enrichment protocols. Interestingly, 70% and 18% of phosphopeptides isolated by the IMAC and TiO_2 technique corresponded to multi-phosphorylated peptides, respectively. This comparison suggested that TiO_2 micro-columns are less likely to retain peptides with multiple phosphate groups but offer a stronger affinity towards singly phosphopeptides. Since TiO_2 micro-tips offered a much higher number and proportion of phosphopeptides than the SwellGel Ga(III) discs from Pierce, further experiments requiring enrichment of phosphopeptides were performed using TiO_2 micro-tips.

Subsequently, the overall characteristics of TiO_2 beads were evaluated to ensure most optimal phosphopeptide enrichment of J774 macrophage cell extract. First, a column capacity assay was performed in triplicate using five different loading amounts of J774 tryptic digest (63, 125, 250, 500, 1000 µg). The same level of α-casein (0.4 ng/µg cell extract) and 1 pmol of $Tyr(PO_3H_2)^4$-Angiotensin II were spiked for different sample loading of cell extracts. Upon LC-MS/MS analysis, more than 80% of assigned peptides corresponded to phosphopeptides except for the 63 µg injection of cell extract. Also, the highest number of identified phosphopeptides (Mascot score >25) was obtained when loading 250 µg cell extract onto TiO_2 micro-tips. Similarly, expression profiling analysis indicated that 250 µg of cell extract provided the most abundant level of phosphopeptides. Figure 2.3a shows that the recovery level of α-casein phosphopeptides such as VPQLEIVPN**pS**AEER and TVDME**pS**TEVFTK, reached a maximum at 250 µg and then decreased for larger amount of cell extracts. The same trend was also observed for phosphopeptides from J774 digest (Fig. 2.2a). In contrast, non-phosphorylated peptides showed a different behavior on TiO_2 beads whereby the number of unspecific binding significantly increased above 250 µg of cell extract (Fig. 2.2b). The second standard,

Tyr$(PO_3H_2)^4$-Angiotensin II (DRV**pY**IHPF), which was equally loaded on each micro-column, was less retained by TiO_2 beads as more protein digest was loaded onto the micro-tip (Fig. 2.3a). At 250 μg of J774 cell extract, only ~35% of Tyr$(PO_3H_2)^4$-Angiotensin II was lost whereas ~65% was not retained by the TiO_2 beads when twice the amounts of cell extract was loaded. Hence, all experiments performed in this study used 250 μg of cell extract for 1.25 mg TiO_2 micro-tips since most phosphopeptides are retained on the column and higher enrichment level is obtained.

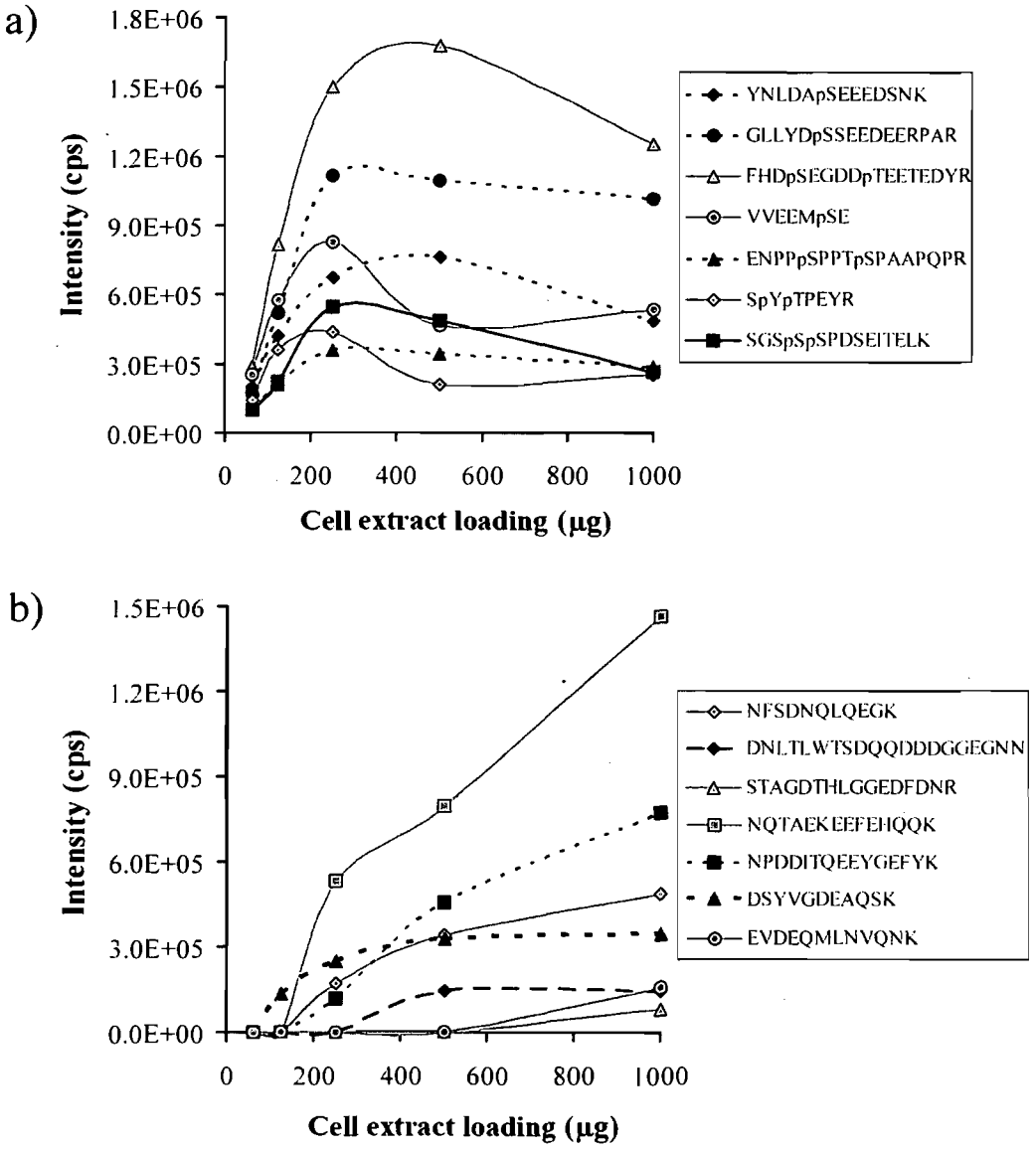

Figure 2.2: **Capacity test of 1.25 mg TiO_2 micro-tips using spiked phosphopeptides from J774 cytosolic cell extract (n=3).** Intensity of various J774 (a) phosphopeptides and (b) non-phosphorylated peptides identified at different loading amounts of J774 cell extract onto the micro-column.

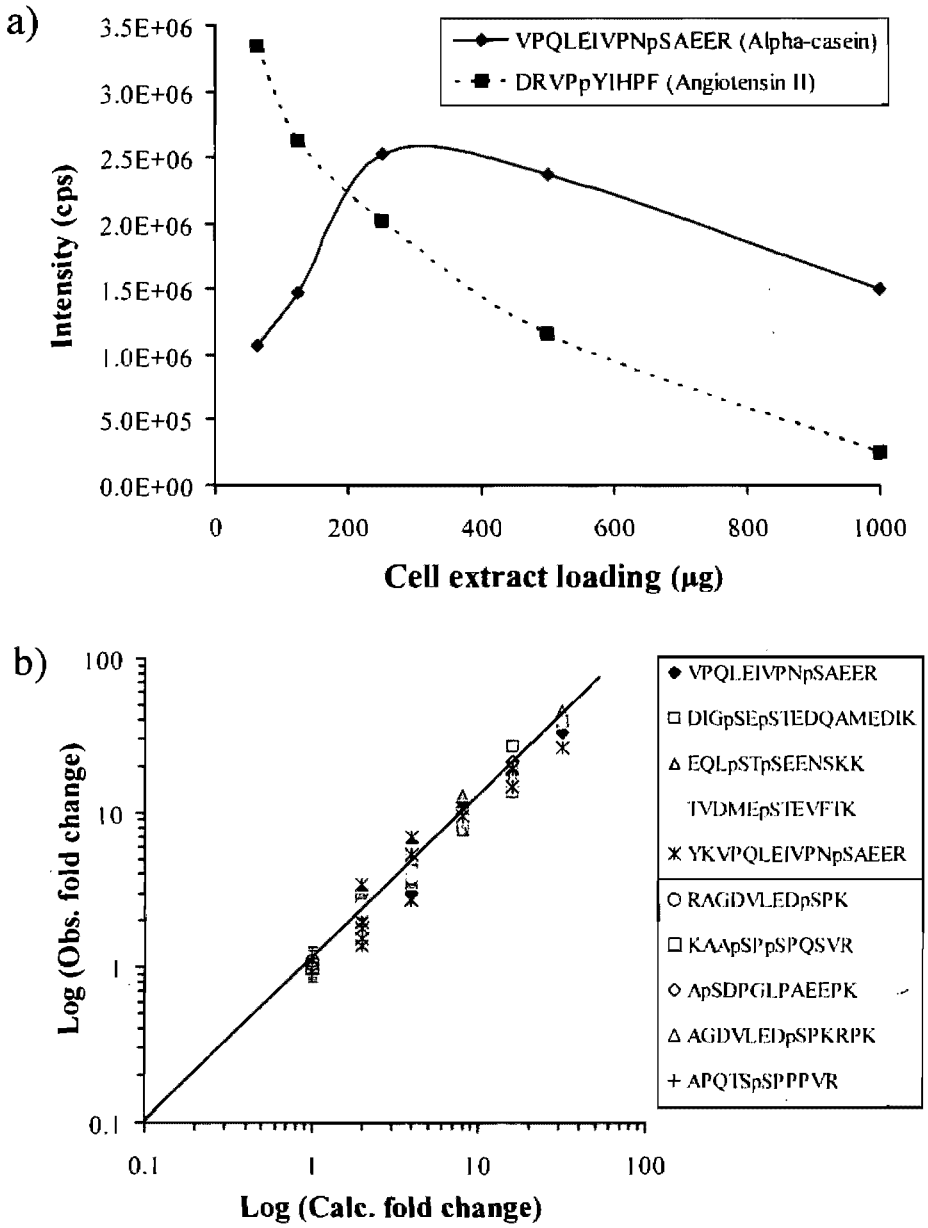

Figure 2.3: **Loading capacity and linear dynamic range of TiO_2 enrichment procedure.** (a) Capacity test of 1.25 mg TiO_2 micro-tips using spiked phosphopeptides from J774 cytosolic cell extract (n=3). Intensity of α-casein (m/z 830.9^{2+} VPQLEIVPN**pS**AEER) and [Tyr$(PO_3H_2)^4$]-Angiotensin II (m/z 563.7^{2+} DRV**pY**IHPF) phosphopeptide spiked into J774 protein digest versus various amounts of J774 cell extract loaded on the micro-tips. Optimal loading amount of J774 protein digest was 250 µg. (b) Plot of (log-log) observed versus calculated fold change of TiO_2-enriched α-casein amounts spiked into a 250 µg J774 protein digest (n=3). A linear relation was observed for spiked α-casein phosphopeptides (m/z 830.9^{2+} VPQLEIVPN**pS**AEER, m/z 972.4^{2+} DIG**pS**E**pS**TEDQAMEDIK+oxidation, m/z 770.3^{2+} EQL**pST**p**S**EENSKK, m/z 741.8^{2+} TVDME**pS**TEVFTK+oxidation, m/z 976.5^{2+} YKVPQLEIVPN**pS**AEER) with an average RSD of 34.2%. Average observed fold change for each J774 enriched phosphopeptides (m/z 633.8^{2+} RAGDVLED**pS**PK, m/z 644.3^{2+} KAA**pS**P**pS**PQSVR, m/z 645.8^{2+} A**pS**DPGLPAEEPK, m/z 746.4^{2+} AGDVLED**pS**PKRPK, m/z 608.8^{2+} APQTS**pS**PPPVR) showed no change in intensity with an average RSD of 17.9%.

In a separate study, the sensitivity and linearity response of TiO_2 enrichment procedure was examined by loading α-casein (0, 25, 50, 100, 200, 400 & 800 fmol) spiked into 250 μg of J774 cell extract onto 1.25 mg TiO_2 micro-tips (n=3). The α-casein quantity ratio between different spike levels was determined to obtain the calculated fold change, which was then compared with the observed fold change obtained from intensity ratios of α-casein phosphopeptides of the LC-MS experiments. A graph of the observed and calculated fold change was plotted to determine the correlation between the estimated and experimental ratio. The changes in intensity measurements were also compared with five identified phosphopeptides (Mascot scores >25) of different intensities (RAGDVLED**pS**PK, KAA**pSPpS**PQSVR, A**pS**DPGLPAEEPK, AGDVLED**pS**PKRPK and APQTS**pS**PPPVR) and originating from J774 cell extract. As expected, no significant change in intensity (average fold change ≤ 1.05) was noted for phosphopeptides present in the original J774 macrophage cell extracts (Fig. 2.3b). In contrast, a linear recovery for the five most abundant α-casein phosphopeptides (VPQLEIVPN**pS**AEER, DIG**pS**E**pS**TEDQAMEDIK, TVDME**pS**TEVFTK, EQL**pST**p**S**EENSKK, and YKVPQLEIVPN**pS**AEER) was observed with an average correlation coefficient of r^2 of 0.988 over two orders of magnitude in spike levels. A log-log plot of calculated and observed ratio is shown in Figure 2.3b for all pair-wise combination of spike levels. As indicated, a linear correlation between observed and calculated ratio was obtained over the spike range examined. Also, the TiO_2 isolation technique provides sensitive enrichment of phosphopeptides because α-casein digests spiked in 250 μg of cell extract were still detected at levels as low as 25 fmol (0.6 ng). Overall, the linear recovery of spiked α-casein digest provided evidence that even specific phosphopeptides present in complex cell extracts yield a linear response across different abundance levels. Differential phosphoproteome profiling can be performed to monitor abundance changes of enriched phosphopeptides across different cellular conditions.

2.4.2 Evaluation of alkaline phosphatase treatment

Many methods have been used in the past to confirm the presence of phosphorylation on a protein of interest [59, 63, 83, 85, 86]. Dephosphorylation of the phosphopeptide is the most straightforward and specific approach to confirm phosphorylation of the cognate peptide. For instance, comparison of two-dimensional gels

with the native protein and the AP-treated sample can specifically determine if the protein is phosphorylated [89]. In this study, we report the application and analytical potentials of this method for large-scale proteomics analyses. The availability of enrichment methods providing high proportion of phosphopeptides (>80%) such as TiO_2 micro-tips facilitates such differential display analyses by maximizing the number of putative assignments. This strategy consisted of treating half of the TiO_2-enriched J774 phosphopeptides with AP for 2 h at 37°C in basic conditions and identifying all putative phosphorylated peptides using mass spectrometry and in-house bioinformatic tools (Fig. 2.4).

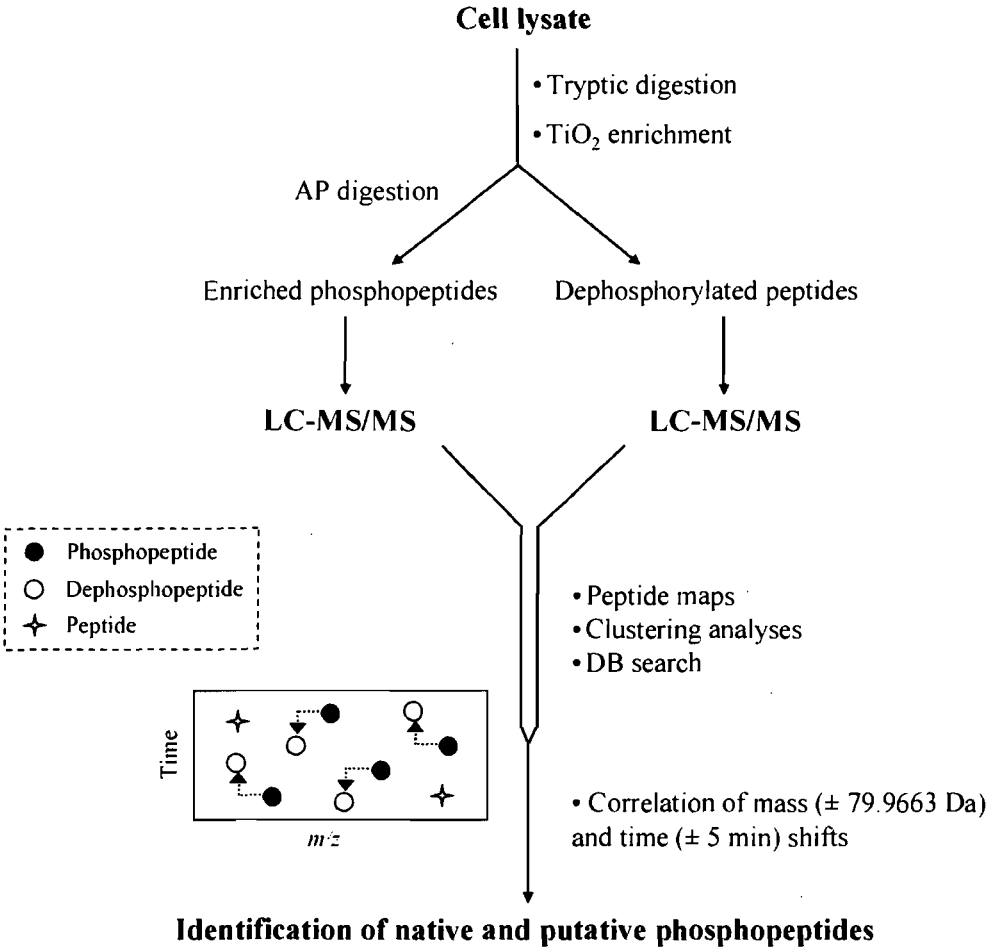

Figure 2.4: **Overview of the analytical strategy combining enzymatic and data mining approaches.** J774 protein digest was initially enriched with TiO_2 micro-tips and subsequently half of the eluate is treated with AP. Phosphopeptides treated and non-treated with AP were analyzed on a LTQ-Orbitrap mass spectrometer. In-house bioinformatic software processed the data for subsequent matching of phosphopeptides and their dephosphorylated cognate by a set retention time and a mass difference (+ 5 min and 79.9663 Da) corresponding to phosphorylation.

The purity of the AP was first established from a silver stain gel of the enzyme preparation which showed a prominent band at 69 kDa for the expected enzyme with low abundance (<1%) of protein contaminants (data not shown). The approach was then validated using a mixture of eight known non-phosphorylated proteins (glutamate dehydrogenase, aldolase, lactotransferrin, bovine serum albumin, alcohol dehydrogenase, catalase, glycerokinase & lactoperoxidase) as a negative control. The non-phosphorylated protein mixture revealed no significant change in abundance when subjected to AP treatment where 97.5% of ion clusters showed less than 1.5-fold change (Fig. 2.5a and b). The negative control confirmed that no proteolytic activity is present in the AP mixture other than dephosphorylation. Hence all changes observed following enzyme incubation are primarily attributed to the loss of the phosphate group.

The specificity of this enzyme was also established using α-casein, which served as positive control. Preliminary experiments performed on native α-casein tryptic digest enabled the identification of six singly- and doubly-phosphorylated peptides. Consistent with previous investigations, peptides comprising a higher number of phosphorylated amino acids including QMEAE**pS**I**pSpSp**SEEIVPN**pS**VEQK and NTMEHV**pSpSpS**EESII**pS**QETYK, were notably absent or of very low abundances [59, 90]. In contrast, the analysis of the same non-enriched α-casein tryptic digest following AP treatment revealed all 10 dephosphorylated tryptic peptides including the penta-phosphorylated peptide QMEAE**pSIpSpSpS**EEIVPN**pS**VEQK. From the comparison of peptide abundance across non-treated and AP-treated α-casein, 51.7 % peptide clusters corresponded to non-phosphorylated peptides with changes in intensities lower than 1.5-fold change (Fig. 2.5d). Also, the expression profile shows that 11.6 % of peptide cluster representing the phosphopeptide population are only present in the control sample. On the other hand, 36.7 % of potential dephosphorylated peptides are either observed with greater than 1.5-fold increase in intensity or uniquely detected in the AP-treated samples. The scatter plot of the corresponding analysis is shown in Figure 2.5c and illustrates all peptide clusters with similar intensities along the *45° line*, whereas the peptides on the *vertical* and *horizontal lines* correspond to all ions only found in the phosphorylated and dephosphorylated forms.

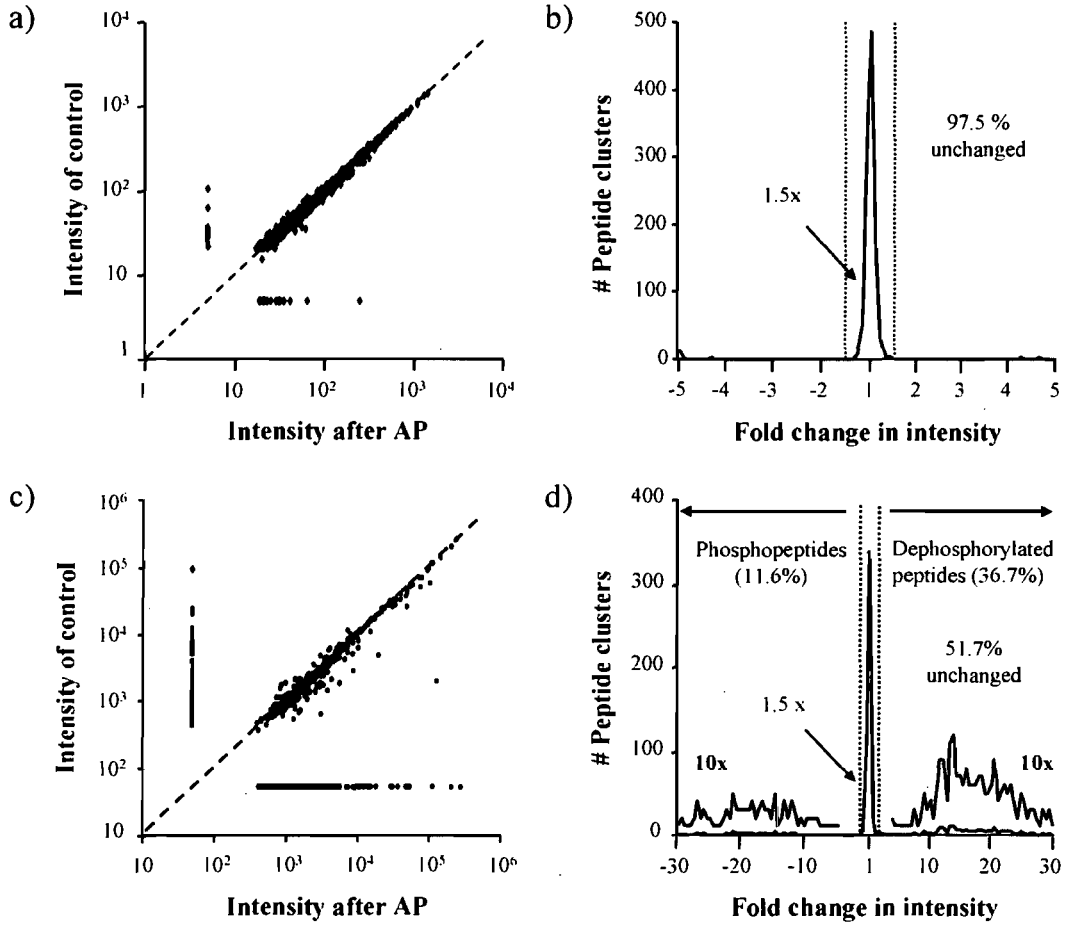

Figure 2.5: **Changes in peptide abundance of positive and negative control following AP treatment.** Scatter plot of ion intensity for (a) eight protein digests non-phosphorylated (200 fmol, 1073 peptide clusters) and (c) α-casein digest (200 fmol, 767 peptide clusters) with and without AP treatment. *Vertical* and *horizontal* lines indicate peptide ions observed only in control (phosphopeptides) and after AP treatment (dephosphorylated peptides), respectively. Expression plot showing the change in intensity of peptide ions for (b) eight protein digests (200 fmol) and (d) α-casein digest (200 fmol) following AP treatment.

In total, 31 α-casein phosphopeptides with different charges and a tryptic peptide with a missed cleavage site were matched to their dephosphorylated counterpart by correlating changes in retention time (±5 min) and mass shifts (79.9663 Da). Examples of two α-casein phosphopeptides (YKVPQLEIVPN**pS**AEER and TVDME**pS**TEVFTK) correlated to their dephosphorylated counterparts through the lost of one phosphate group are shown in Figure 2.6. However, another phosphopeptide (NTMEHV**pSpSpS**EESII**pS**QETYK) was only detected upon AP treatment probably because it contained four phosphorylation sites (Fig. 2.6).

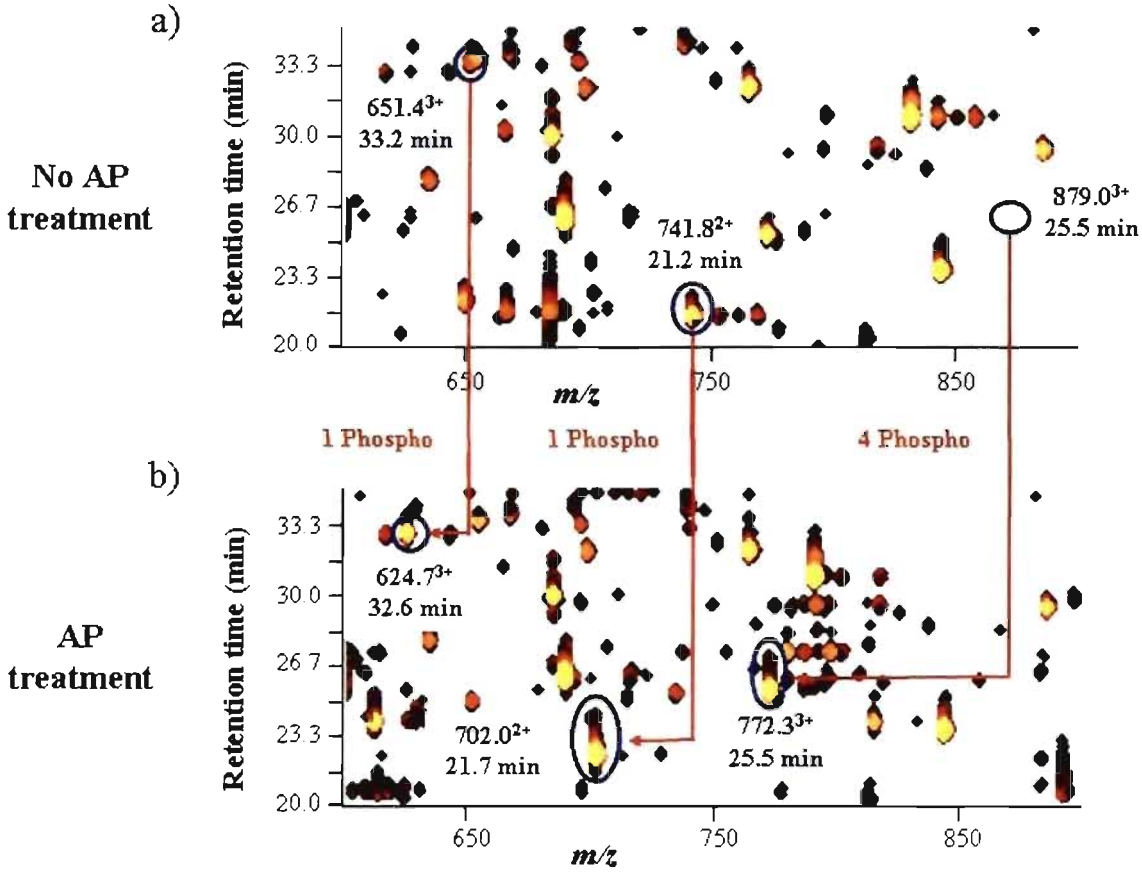

Figure 2.6: **Comparison of non-treated and AP-treated α-casein contour plots.** (a) Singly phosphorylated peptides from α-casein present on the peptide map of the non-treated α-casein (*m/z* 651.4^{3+} YKVPQLEIVPN**pS**AEER & *m/z* 741.8^{2+} TVDME**pS**TEVFTK + oxidation). (b) AP-treated α-casein peptide map showing the presence of the corresponding dephosphorylated counterpart (*m/z* 624.7^{3+} & *m/z* 702.0^{2+}) and the appearance of a new peptide (*m/z* 772.3^{3+} NTMEHV**pSpSpS**EESII**pS**QETYK + oxidation) never detected previously in the phosphorylation form.

Correlation of phosphopeptides with their dephosphorylated cognates allowed a direct comparison of their intensity and their elution time in LC-MS. Significant variations of retention time and abundance were noted for different pairs of phosphorylated peptides and their non-phosphorylated counterparts. For instance, peptide pair VPQLEIVPN**pS**AEER/ VPQLEIVPNSAEER had a retention time difference of less than 0.5 min and an intensity variation close to 1-fold. In contrast, the elution time for the doubly phosphorylated peptide, DIG**pS**E**pS**TEDQAMEDIK, increased by ~1.5 min upon dephosphorylation, a change that was also accompanied by a 2-fold increase in intensity for

the corresponding peptide. Comparison of α-casein phosphopeptides to the AP-treated peptides revealed that dephosphorylation enhances ionization efficiency and confers unexpected changes in retention time that cannot be rationalized with simple structural rules. Rationalization of phosphopeptides behavior in LC-MS thus required a pool of phospho- and dephospho peptides for more meaningful statistical analyses.

2.4.3 Phosphopeptide behavior in LC-MS

Two major limitations attributed to the presence of the negatively charged phosphate group on the peptide are the suppression in ionization efficiency and the decrease in retention time on reverse-phase chromatography [62, 79]. To address this problem, Steen *et al.* [81] have investigated phosphopeptide behavior in LC-MS by selecting a small set of phosphopeptides. In this study, we present a more comprehensive analysis of the retention time and intensity change performed on the large pool of tryptic TiO_2- enriched J774 phosphopeptides, including several multi-phosphorylated peptides, treated with AP.

Initially, peptide lists obtained for the control and AP-treated samples were clustered together using in-house bioinformatic tools. A total of 14,147 peptide clusters were obtained where 759 (5%) corresponding to unspecific binding of non-phosphorylated peptides on TiO_2 micro-tips were found in both conditions. To minimize the rate of false positive identification, common peptides were removed from the list for subsequent correlation of mass (79.9663 Da) and retention time (±5 min) shifts between phosphopeptides and their dephosphorylated counterparts. The list of detected phosphopeptides matched with their dephosphorylated counterpart was aligned with the Mascot identification file (Mascot score >20) of phosphopeptides using in-house bioinformatic software. Similarly, in cases where only the dephosphorylated peptide was identified, putative phosphopeptides were determined by matching the detected phosphopeptide-dephosphorylated peptide pairs to the Mascot list (Mascot score >30) of assigned dephosphorylated peptides containing at least one Ser, Thr or Tyr residues. In total, 686 unique peptides (764 peptides when considering sequences with multiple phosphorylation sites) were matched to their dephosphorylated counterpart where 234 were

putative phosphopeptides with a higher distribution of singly phosphorylation on serine residues (Table 2.2). It is noteworthy that we observed 531, 40, 3 phosphopeptides corresponding to Ser, Thr and Tyr phosphorylation sites, a relative distribution that is consistent with that observed by other groups [80].

Table 2.2: **Statistics on overall distribution of correlated phosphopeptides and their dephosphorylated counterparts from J774 AP study**

Category	No. of examples
# Assignment	686
# Phosphopeptides	452
# Putative phosphopeptides	234
Phosphopeptides with 1, 2, 3 or 4 phospho sites	348, 87, 16, 1
Putative phosphopeptides with 1, 2, 3 or 4 phospho sites	121, 73, 33, 7
Phosphorylated residues (Ser:Thr:Tyr)	531, 40, 3 (92.5%, 7.0%, 0.5%)

Figure 2.7a shows that non-phosphorylated peptides have very similar intensities before and after AP treatment, whereas the phosphopeptides and putative phosphopeptides showed an average fold-change of 1.5 and 2.0, respectively. It is noteworthy that dephosphorylated peptides uniquely found after AP treatment but not observed as phosphopeptides (624 identified peptides of which 210 were already known in the literature) were not considered in this comparison. Higher proportion (> 60 %) of multi-phosphorylated (two, three and four HPO_3 groups) peptides have an intensity increase greater than 2-fold upon dephosphorylation compared to the singly phosphorylated peptides (~33%). These results support the proposal that phosphorylation can suppress MS signal in positive ion mode [79].

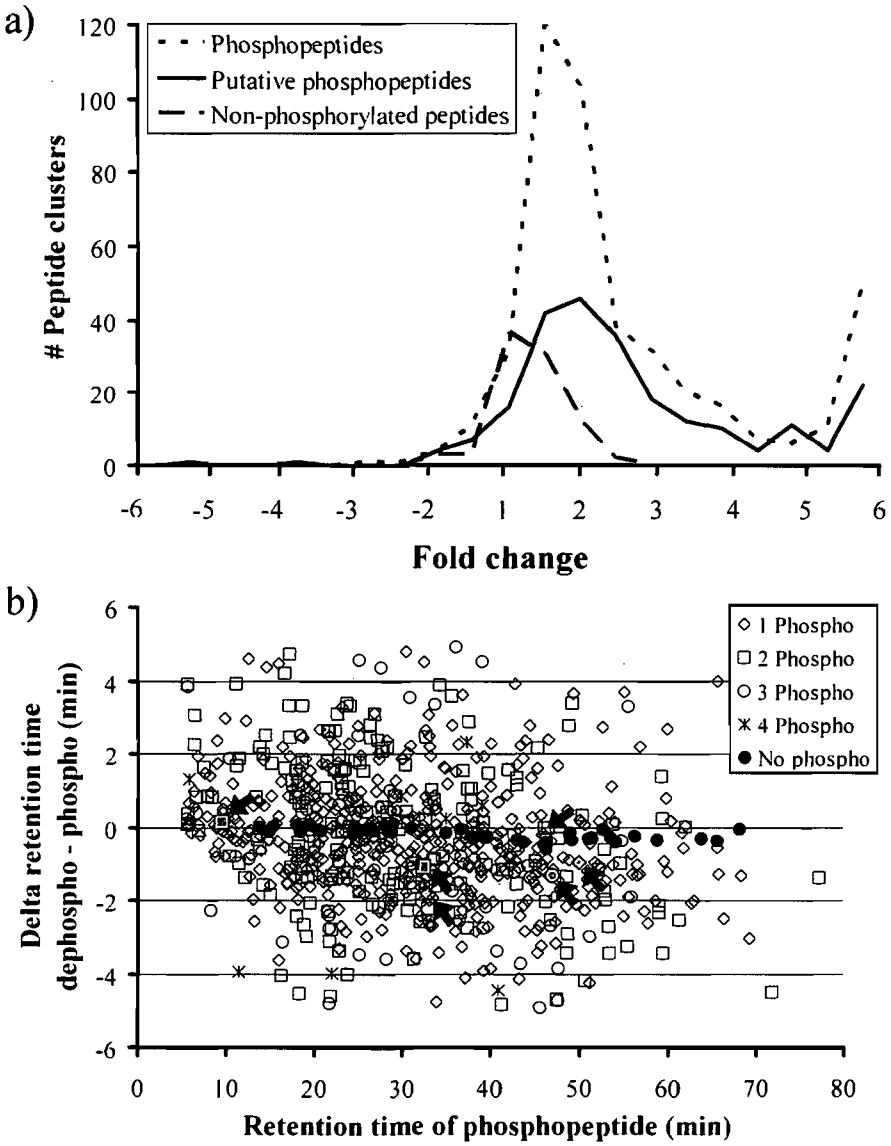

Figure 2.7: **Phosphopeptide behavior in LC-MS following alkaline phosphatase treatment (*n*=3).** (a) The intensity fold change (ratio of dephosphorylated peptide over phosphopeptide) distribution for phosphopeptides (351), putative phosphopeptides (224) and non-phosphorylated peptides (41) identified with a Mascot score >20. The average fold change for the latter were 1.5, 2.0 and 1.0, respectively. Putative phosphopeptides were determined by matching the detected phosphopeptide-dephosphorylated peptide pairs to the Mascot list of assigned dephosphorylated peptides containing at least one Ser, Thr or Tyr residues. Following AP treatment, more than 40% of dephosphorylated peptides had an abundance increase higher than 2-fold, whereas this was the case for only 2% of the non-phosphorylated peptides. (b) Variation of retention time for correlated phospho- and dephosphorylated peptides in a two-step linear gradient from 2% to 25% B over 63 min followed by a gradient from 25% to 40% over 15 min. Phosphopeptides (369) and putative phosphopeptides (271) were distributed across ± 5 min retention time upon AP treatment whereas non-phosphorylated peptides (41) only had an elution time difference less than 0.6 min compared to the AP-treated peptides (Mascot score >20). Arrows indicate phosphopeptides from α-casein.

Our studies have also revealed that a large number of phosphopeptides displayed a more hydrophobic character than their dephosphorylated counterpart. No significant change in retention time was observed for the 41 non-phosphorylated peptides (Mascot score >30 & <0.6 min variation) upon AP treatment (Fig. 2.7b). On the other hand, only 55% of matched phosphopeptides had a retention time difference (RT dephospho – RT phospho) less than 1 min whereas 24 and 21% had a decrease or increase in retention time of more than 1 min respectively. For convenience, phosphopeptides corresponding to spiked α-casein are indicated by an *arrow* on Figure 2.7b. Interestingly, several multi-phosphorylated peptides (28%) eluted much later (>1 min) than their dephosphorylated counterpart, and ~30% had a smaller retention time (Fig. 2.7b). The unexpectedly large population of phosphopeptides of greater hydrophobicity than their dephosphorylated counterparts was intriguing and warranted further investigations.

Several peptide characteristics were evaluated to understand the phosphopeptide behavior in LC-MS analysis. We systematically examined physicochemical properties of phosphopeptides such as peptide length, pI, hydrophobicity, charge, polarity and amino acid composition to correlate structural changes with corresponding shift in retention times. Regrettably, none of these properties could be correlated with the observed retention time shift. We next looked at the location of basic and acidic residues and N-terminus from the phosphate group within the singly phosphorylated peptide. Only one distinct distribution examined showed that phosphorylated residues proximal to the N-terminus typically eluted later than their dephosphorylated counterpart (Fig. 2.8). Also, phosphate groups closer to the C-terminus had elution time difference >1 min upon dephosphorylation. On the other hand, the location of phosphorylation site for peptides with unchanged retention time upon dephosphorylation showed no particular trend (Fig. 2.8). One possible explanation for this effect can be attributed to the salt bridge formation between phosphate groups and the basic residue. In this case, the electrostatic interactions can diminish the overall polarity of the phosphopeptide thus conferring a more hydrophobic character compared with its dephosphorylated counterpart where no salt bridge can be formed.

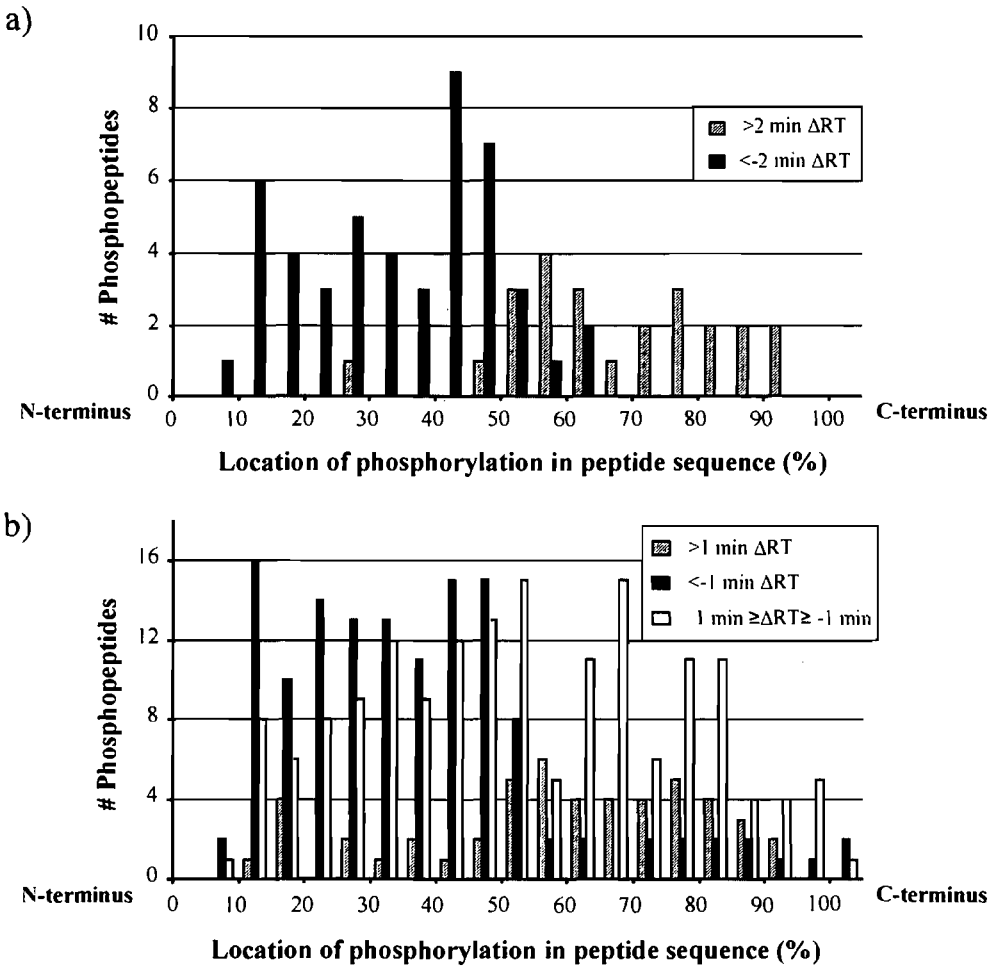

Figure 2.8: **Distribution of matched phospho- and dephosphorylated peptides with different Δ retention time according to the phosphate group position from both C and N-terminus.** (a) Representation of singly phosphorylated peptides with a Δ retention time (AP-treated RT - non AP-treated RT) >2 min and <-2 min. (b) Distribution of singly-phosphorylated peptides with an unchanged (between 1 and -1 min), positive (>1 min) and negative (<-1 min) Δ retention time. Phosphopeptides containing phosphate groups closer and further to the N-terminus have negative and positive retention time shifts, respectively. On the other hand, phosphopeptides with unchanged retention shift have modification sites distributed across all the peptide sequence.

To test this proposal, we enriched α-casein tryptic digest with TiO_2 micro-columns, derivatized free amino groups with acetic anhydride and compared the shift in retention time of the corresponding peptides following AP treatment. The differences in retention times were also compared to those of non-acetylated peptides (Fig. 2.9). Without *N*-acetylation, α-casein phosphopeptides showed positive and negative retention time shifts when compared to the elution of their dephosphorylated counterparts. It is noteworthy that

the non-phosphorylated peptide NANEEEYSIGSSSEESAEVATEEVK and its *N*-acetylated derivative showed no significant change in retention time following AP treatment irrespective of the number of N-acetylated groups. However, upon AP treatment a positive shift in retention time was observed for the *N*-acetylated phosphopeptides indicating an increase of the hydrophobicity of the corresponding dephosphorylated peptides. Two exceptions to this were noted for the phosphopeptides DIGSES**pT**EDQAMEDIK and FQ**pS**EEQQQTEDELQDK where the acetylated derivative could not be detected in positive ion mode presumably due to their overall negative charge. Interestingly, these phosphopeptides were also more hydrophobic than their dephosphorylated counterpart.

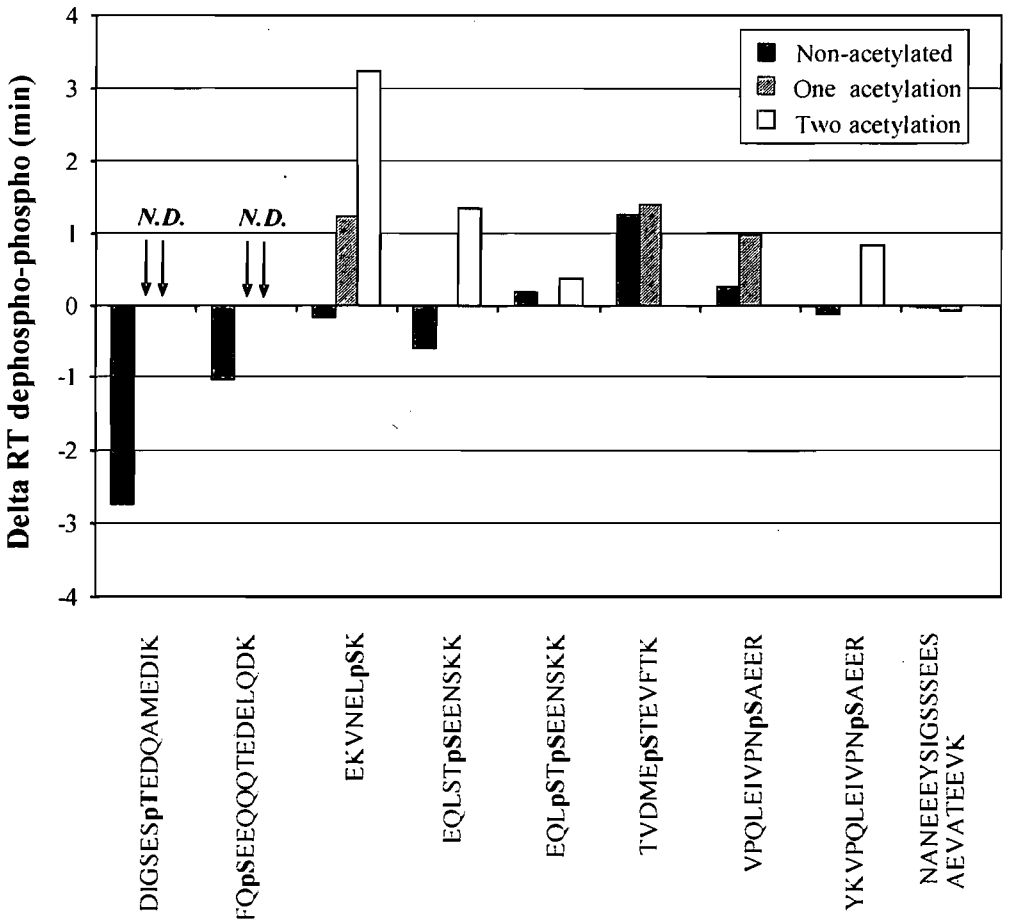

Figure 2.9: **Comparison of retention time shifts of α-casein phosphopeptides and their N-acetylated counterpart following AP treatment.**

Although these results are consistent with a salt bridge model, secondary structural changes on the peptide conformation following AP could also influence the extent of retention time shift. Further structural studies on these aspects are currently underway and will be reported separately.

2.4.4 Application of alkaline phosphatase treatment for large-scale phosphoproteomic analyses

The AP approach was further evaluated for a more comprehensive characterization of the differentially expressed phosphoproteome following stimulation of J774 mouse macrophage cells by IFN-γ. Initially, control and macrophage cells incubated with IFN-γ for 5 min were digested with trypsin and phosphopeptides were isolated using TiO_2 affinity media prior to their LC-MS/MS analyses on a LTQ-Orbitrap mass spectrometer. The reproducibility of three replicates of control and IFN-γ treated samples was initially assessed to validate meaningful expression changes of identified phosphopeptides. More than 95% of peptide clusters showed less than 80% intensity variation indicating that peptides with ≥2-fold change in abundance provided statistically meaningful variation. Following peptide clustering analysis, expression profiling was performed to compare the phosphopeptide abundance in two different conditions. All reproducible changes taking place between control and IFN-γ treated samples were represented on a volcano plot (Fig. 2.10a). The comparison of the macrophage phosphoproteome with and without IFN-γ indicated that 68% of all 6170 ion clusters showed less than 2-fold change in abundance across biological replicates and conditions (n=3) whereas 12% (763) and 20% (1218) ion clusters showed more than 2-fold over- and under-expression, respectively.

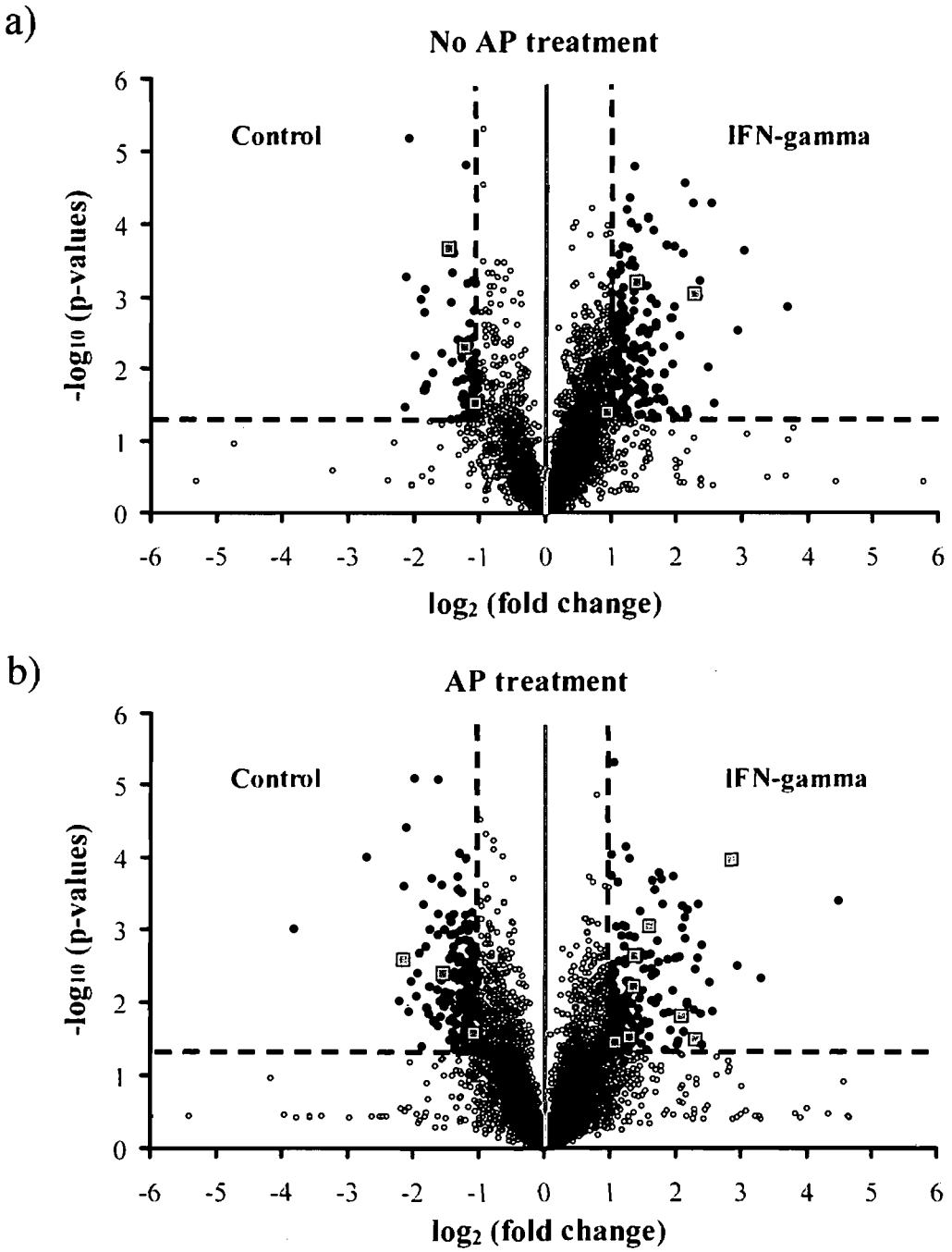

Figure 2.10: **Volcano plot distribution of (a) non-treated and (b) AP-treated cytosolic extracts of J774 control and IFN-γ treated (5 min).** Only peptide clusters containing intensity values in all three replicates of the control and IFN-γ treated samples were considered. *Solid* line divides peptide clusters more abundant in control and IFN-γ samples. *Dashed* lines delimit peptide populations showing 2-fold change in abundance with p-values <0.05. Squares identify all phospho and dephospho-peptides listed in Table 2.4.

Also, LC-MS/MS analysis with the LTQ-Orbitrap mass spectrometer resulted in 716 and 917 phosphopeptides (Mascot score >20, n=3) in the control and IFN-γ stimulated samples, respectively (Table 2.3). In total, 1143 unique phosphopeptides from 432 different proteins were detected where 125 phosphopeptides showed a 2-fold change upon IFN-γ administration.

Table 2.3: **Summary of identification obtained from different approaches**

	Non-treated		AP-treated	
	Control	IFN-γ	Control	IFN-γ
# Phosphopeptides	716	917	1306*	1569*
# Non-phosphorylated peptides	171	225	—	—
# Phosphoproteins identified	291	340	577*	638*
# Putative phosphopeptides	—	—	716	872

**New assignments (i.e. without non-phosphopeptides found in control)*

To obtain a higher number of phosphopeptides, half of the TiO_2-enriched control and IFN-γ treated (5 min) J774 cell extract were incubated with AP and analyzed on the LTQ-Orbitrap mass spectrometer. Comparison of both volcano plots in Figures 2.10, a and b, showed a ~2-fold increase in putative phosphopeptides after AP treatment. In fact, 61.4% (8493) and 32.9% (4558) of peptide clusters showed 2-fold increase in the AP-treated and non-treated control J774 cell extract, respectively. Similar results were obtained for the AP-treated IFN-γ sample (63.4%, 8439 peptide clusters and 30.9%, 4111 peptide clusters), further supporting the notion that phosphopeptide ions are under-represented in positive ion peptide maps due to suppression effects [79]. Upon enzyme treatment, better MS/MS spectral quality was obtained for the dephosphorylated peptides, and a higher score was assigned by Mascot (Fig. 2.11, c and d, and 2.12, b and d). In fact, more than 90% of identified phosphopeptides had a significant higher score following AP treatment. For instance, 65% of dephosphorylated peptides showed an increase of 20 in their corresponding Mascot score compared to the phosphorylated counterpart. Not only the confidence level of identification increased but the number of putative phosphopeptides identified doubled to 1306 and 1569 for control and IFN-γ sample, respectively (Table 2.3). Also, less than 7.6 % of the entire pool of AP-treated samples corresponded to incompletely dephosphorylated peptides probably originating from very abundant phosphopeptides or peptides structurally incompatible to AP dephosphorylation.

Putative phosphopeptides can be identified from peptide ions showing an increase in abundance higher than 2-fold upon phosphatase treatment. For instance, the peptide EVEEDSEDEEMSEDEDDSSGEEEVVIPQKK (*m/z* 1147.8^{3+}) from nucleolin protein showed a 13-fold increase in abundance upon AP treatment. Yet the corresponding phosphopeptide was never detected in the non-treated sample proving that phosphopeptides do not ionize as efficiently as their dephosphorylated counterpart. This lower ionization efficiency can be probably explained by the high number of phosphorylation sites (four) already known in the literature for this peptide (EVEED**pS**EDEEM**pS**EDEDD**pSpS**GEEEVVIPQKK). In short, the AP strategy provides a meaningful tool to uncover the presence of putative phosphopeptides where only the dephosphorylated counterpart is present in the AP-treated sample. This analysis also provides a mean to determine stoichiometry of phosphorylated and non-phosphorylated peptides by comparing changes in intensity ratio of the dephosphorylated peptides in the control and AP-treated samples.

Moreover, the mass shift (HPO_3: 79.9663 Da) associated with phosphorylation together with the variation in intensities and retention times were integrated in data mining softwares to identify potential phosphopeptide candidates following AP treatment. Peptide maps of control and phosphatase-treated macrophage cell extracts were compared and results obtained indicated that 2723, 1457, 495, 194 and 85 (3920, 1918, 582, 259 & 105 for IFN-γ) peptide ion pairs were correlated with the addition of one, two, three, four and five phosphate groups, respectively. For instance, the phosphopeptide (EELA**pS**DLEEMATSSAK) originating from nucleolar protein Nop56 [91] was identified in the AP-treated (*m/z* 855.9^{2+}, 57.5 min) and non-treated control (*m/z* 895.9^{2+}, 57.6 min) sample (Fig. 2.11a-d). Interestingly, more than 7325 and 7384 potential phosphopeptides in the control and IFN-γ mixtures were only detected in the AP-treated sample and were absent in the corresponding non-treated sample. For instance, Figures 2.11a-b showed the presence of the putative phosphopeptide, TQSLQDFPVAD<u>S</u>EEEAEEEFQK, from Tuftelin-interacting protein 11 [92] only after AP treatment, and the phosphorylation site is already known in the literature (pS211).

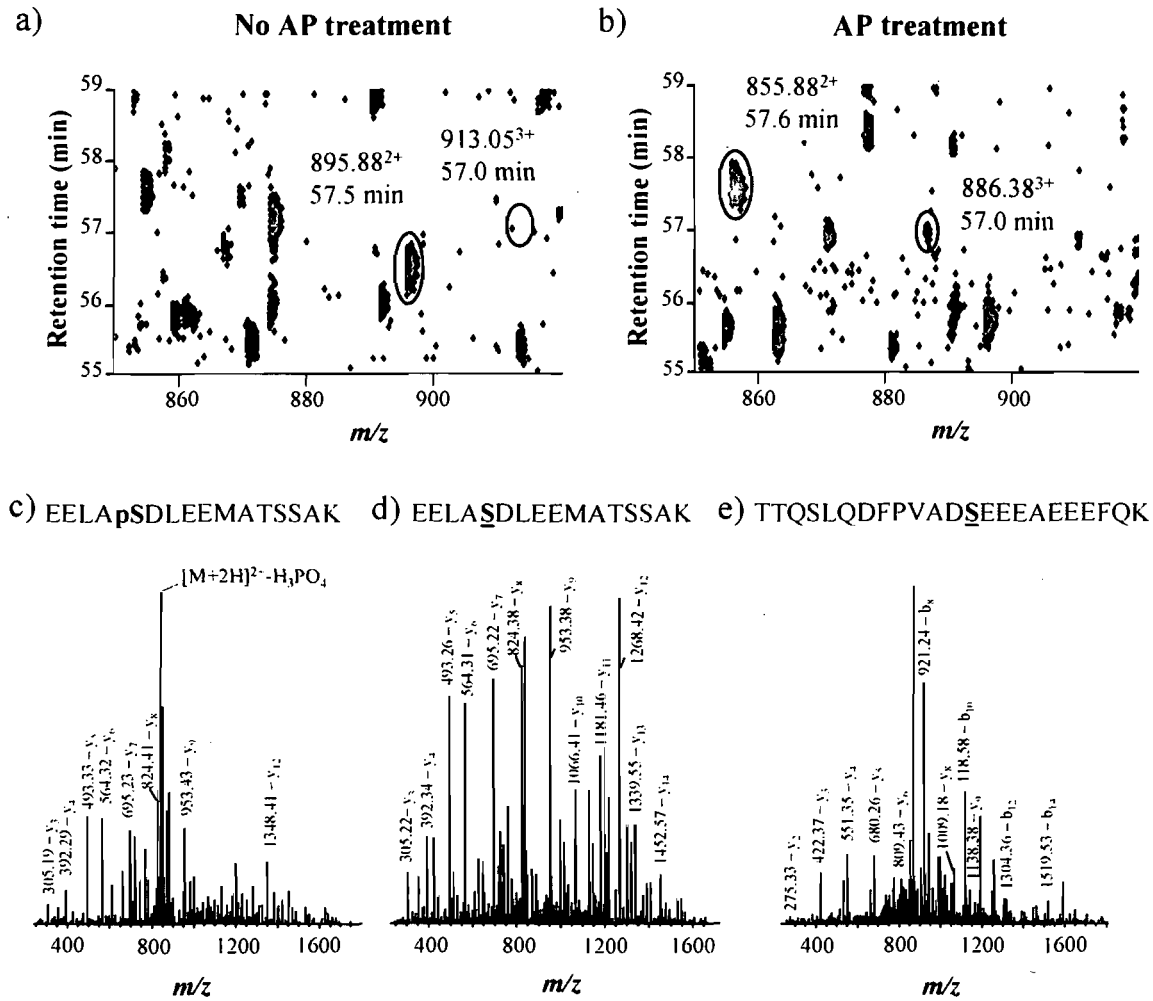

Figure 2.11: **Identification of phosphopeptide candidates using alkaline phosphatase.** Contour profile of *m/z* versus time for phosphopeptide-enriched extract from J774 (a) without and (b) with AP. MS/MS spectra for (c) *m/z* 895.88^{2+} (Mascot score 71) and (d) *m/z* 855.88^{2+} (Mascot score 121) corresponding to Nucleolar protein Nop56 and (e) *m/z* 886.38^{3+} (Mascot Score 35) corresponding to Tuftelin-interacting protein 11.

All identified phosphopeptides listed in Table 2.4 are highlighted as *squares* in the volcano plot in Figures 2.10a-b. Among phosphoproteins showing statistically meaningful change in abundance was cytosolic phospholipase A2 ($cPLA_2$) [93] (CSV**pS**LSNVEAR, pS727) where a 2.6-fold increase in abundance was observed upon IFN-γ treatment in the phosphorylated and dephosphorylated form (Fig. 2.12, a and c). Also, IFN-γ treatment induced dephosphorylation of eukaryotic translation initiation factor 4B (eIF4B) [3] (**pS**LENETLNK, pS445) which is involved in mRNA translation.

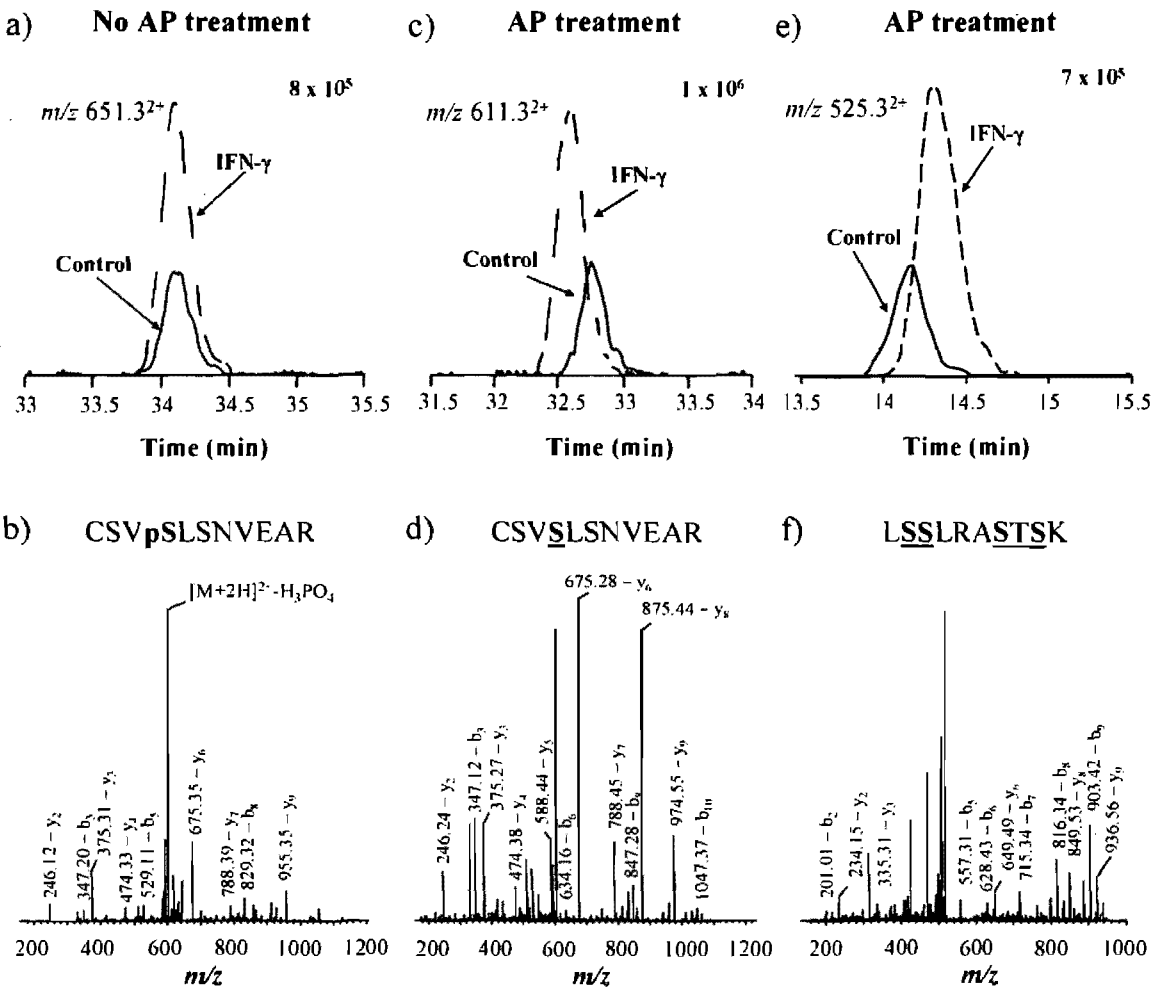

Figure 2.12: **Identification of differentially expressed phosphoproteins from J774 following 5 min IFN-γ stimulation.** Reconstructed ion chromatograms of $cPLA_2$ (a) phosphopeptide *m/z* 651.3^{2+} with (b) its corresponding dephosphorylated counterpart *m/z* 611.3^{2+} and 40S ribosomal protein S6 (c) dephosphopeptide *m/z* 525.3^{2+} showing differential abundance in control and IFN-γ exposed cells. *Solid* lines correspond to control digests and *dotted* lines to IFN-γ treated samples. MS/MS spectra of precursor ions (b) *m/z* 651.3^{2+} (Mascot score 56) (d) *m/z* 611.3^{2+} (Mascot score 87) and (f) *m/z* 525.3^{2+} (Mascot score 57) confirming identification of $cPLA_2$ in control and AP treatment, and the 40S ribosomal protein S6 after AP treatment only.

Table 2.4 indicates that only a small number of phosphoproteins such as $cPLA_2$ and eIF4B showed stoichiometric change in phosphorylation upon IFN-γ treatment, suggesting an under representation of the phosphopeptides population leading to an incomplete characterization of the corresponding signaling pathways. Hence, AP treatment was applied to further characterize differentially regulated phosphoproteins in response to IFN-γ

stimulation. A volcano plot representing AP-treated control and IFN-γ stimulated J774 cells showed that 69.7% of all 10,763 peptide clusters were within 2-fold intensity change whereas 15.5% (1664) and 14.8% (1594) had a decrease and increase in peptide abundance, respectively (Fig. 2.10b). The high number of newly detected putative phosphopeptides led to the identification of more early signaling and regulatory events including the enhanced phosphorylation of ROS complex members such as $p40^{phox}$ (GV**S**PQGAIMDR, S161), which was not identified in the previous analysis, and the phosphosite was never before reported in the literature (Table 2.4). Another interesting finding was AP-3 complex protein (RHSSLPTE**S**DEDIAPAQR) involved in vesicle formation and was only detected upon AP treatment with a known phosphosite at Ser760 [94]. In addition, the phosphatase approach enabled a more complete characterization of the initiation of mRNA translation mediated by IFN-γ. Changes in phosphorylation of important phosphoproteins such as putative RNA-binding protein Luc7-like 1 (**S**EEKEAGEI) and 40S ribosomal protein S6 (L**SS**LRA**STS**K) were also identified further confirming the importance of mRNA translation upon macrophage activation [3]. Figure 2.12e shows the change in abundance upon IFN-γ treatment of 40S ribosomal protein S6 following AP treatment. It is noteworthy that no phosphopeptide containing one, two or three phosphate groups was detected in any of the control samples examined. In brief, the AP approach enabled a more comprehensive representation of all phosphoproteins involved in the signal transduction pathways of IFN-γ stimulated macrophages.

Table 2.4: **Putative phosphopeptides showing differential abundance in 5 min IFN-γ stimulated J774 cytosol extracts upon AP treatment**

Putative phosphopeptides	Proteins	Function	Fold change	
			Non-treated (p-values)	AP-treated (p-values)
CSV**pS**LSNVEAR	Cytosolic phospholipase A2 ($cPLA_2$)	ROS production	2.6 (0.001)	2.6 (0.002)
GV**S**PQGAIMDR	Neutrophil cytosol factor 4 ($p40^{phox}$)	ROS production		4.9 (0.032)
FSEMMDHMGGDEDVDLPEVDGAD DDSQDSDDEK	Prostaglandin E synthase 3	Production of PGE2		-2.1 (0.027)
H**pS**GQDVHVVLK	NSFL1 cofactor p47	Vesicle trafficking	-2.1 (0.030)	-2.9 (0.004)
RHSSLPTESDEDIAPAQR	AP-3 complex subunit delta-1	Vesicle trafficking		2.1 (0.038)
QP**S**IELP**S**MAVA**S**TK	Lymphocyte-specific protein 1 isoform 2	Vesicle trafficking	4.8 (0.001)	3.0 (0.001)
LSSLRA**S**TSK	40S ribosomal protein S6	mRNA translation		2.5 (0.029)
SEEKEAGEI	Putative RNA-binding protein Luc7-like 1	mRNA translation		7.2 (0.0001)
IDASKNEEDEGHSNSSPR	Heterogeneous nuclear ribonucleoprotein D0 (AUF1)	mRNA translation		4.3 (0.016)
KAA**pS**LTEDR	Eukaryotic translation initiation factor 4-γ 1 isoform b (eIF4G1)	mRNA translation	1.8 (0.044)	2.6 (0.006)
pSLENETLNK	Eukaryotic translation initiation factor 4B (eIF4B)	mRNA translation	-2.7 (0.0002)	-4.5 (0.003)
pTPEFLR	Elongation factor 1-γ (eEF-1B gamma) isoform 1	mRNA translation	-2.3 (0.005)	ND

2.5 Discussion

In summary, we report the analytical potentials of a strategy using AP to detect a higher number of phosphopeptides in complex mixtures. The AP approach was validated with a negative and positive control, which confirmed that the enzyme had high selectivity and enabled specific dephosphorylation of a wide range of substrates. In fact, the mixture of non-phosphorylated peptides showed no change in abundance upon enzyme incubation further supporting the notion that AP has no proteolytic activity other than dephosphorylation. Also, the high performance of the AP approach, even for multi-phosphorylated peptides, was greatly demonstrated through the analysis of the standard phosphoprotein, α-casein.

For a successful application of the AP treatment on large-scale experiments, enrichment of phosphopeptides is absolutely required to simplify the mixture and obtain enhanced MS detection. The evaluation of two different phosphopeptide isolation procedures using TiO_2 and IMAC (Ga^{3+}) micro-columns revealed that TiO_2 extraction offered a higher number of phosphopeptides and enrichment level than the IMAC procedure. Also as stated by Bodenmiller *et al.* [82], we confirmed that complementary phosphopeptide populations are obtained with TiO_2 and IMAC (Ga^{3+}) isolation methods. TiO_2 seemed to have higher affinity towards singly phosphorylated peptides and DHB loading solution definitely helped to displace most non-phosphorylated acidic residues. On the other hand, IMAC retained mostly multi-phosphorylated peptides but provided a much lower enrichment level (~37%) than TiO_2 micro-tips (~77%). Thingholm *et al.* [95] also reported this difference in selectivity of both stationary phases (IMAC and TiO_2) towards phosphopeptide and further suggested to combine both enrichment methods for optimal recovery. For our analysis, phosphopeptides were isolated using only TiO_2 micro-tips since it provided the best overall performance. The optimal loading capacity of TiO_2 enrichment procedure was 250 μg of cell extract loaded onto a 1.25 mg TiO_2 offering a linear recovery of spiked α-casein ranging from 25 to 800 fmol.

Enrichment of phosphopeptides has been the most straightforward approach to identify phosphopeptides and their corresponding phosphorylation site. Yet it has been demonstrated that some peptides remain undetected in positive ion mode MS possibly

due to their multiple phosphorylation. Hence to obtain the most complete coverage of all phosphopeptides in the sample, several groups have recently shown that treating the enriched mixture with AP reveals the presence of a high number of phosphopeptides [63, 85], [86], [96]. One major drawback of AP approach is that no information on the location of the phosphorylated site is revealed, a limitation that is even more evident when more than one potential residue is present. However, this approach will still provide insight on potential phosphopeptides which can be further identified by targeted MS/MS analysis. In-source activation can be used to promote the formation of phosphopeptides fragments baring the dehydroalanine or dehydrobutyrine moieties for confirmation by MS/MS. For large scale experiments, AP treatment is still the preferred strategy over β-elimination to directly confirm the presence of the phosphate group on the protein. In fact, phosphatase treatment on TiO_2-enriched J774 mouse macrophage protein digest showed that a large fraction of phosphopeptides were only detected upon dephosphorylation. These results further strengthen the notion that the mass spectrometry analysis of phosphorylated peptides is limited. The identification level almost doubled upon AP treatment confirming that positive ion detection coupled to reverse-phase LC method is not fully optimized to detect all phosphopeptides. Further understanding of phosphopeptide behavior in LC-MS is required to better predict phosphopeptide detection in positive ion mode. Our study showed that dephosphorylated peptides can vary significantly in abundance following AP treatment with a large proportion (~40 %) showing a 2-fold increase in intensity upon dephosphorylation. The occurrence of new peptides upon AP treatment demonstrates that some phosphopeptides cannot be detected by MS in positive ion mode. Likewise, Nielsen *et al.* [97] provided evidence that posttranslational modifications such as phosphorylation on hydrophobic peptides yielded a lower ESI signal response. Steen *et al.* [81] suggested otherwise by showing that most tested phosphopeptides still had similar ionization efficiency compared to their unphosphorylated cognates. Yet their work reflected the behavior of only few selected synthetic peptides where a small number comprised doubly phosphorylated peptides.

Another interesting observation mentioned by Steen *et al.* [81] and Ishihama *et al.* [85] was that some phosphopeptides actually eluted much later than their dephosphorylated cognate. Similarly our study revealed that a high proportion of dephosphorylated peptides were more hydrophilic than their phosphopeptide

counterparts. So far, this study is the first one presenting a large list of detected phosphopeptides to rationalize phosphopeptide behaviour in LC-MS. Theoretically, removal of a phosphate group should lead to an increase in hydrophobicity of the peptide, yet these results show otherwise. Many different parameters (peptide length, pI, hydrophobicity, charge, polarity, and amino acid composition) were studied to probe the reason behind this surprising change in RT upon dephosphorylation. However, from those characteristics, no coherent reasoning was found to completely explain changes in retention times occurring upon dephosphorylation. Hence we looked more closely at the influence of salt bridges on a phosphopeptide conformation. Our data suggested that possible intramolecular electrostatic interactions take place between the N-terminus and phosphate group rendering the peptide more hydrophilic upon dephosphorylation. Since phosphopeptides are dissolved in acidic conditions of pH 3.0 for LC-MS analysis, the phosphate group is negatively charged because of its lower p*Ka* of 1-2. Hence salt bridges can occur between phosphate groups and the positively charged N-terminus reducing overall charge and rendering the phosphopeptides more hydrophobic. This proposal was also supported from the retention time behavior of α-casein *N*-acetylated phosphopeptides where an increase in retention time was consistently observed upon AP treatment in contrast to the non-derivatized phosphopeptides. In a similar fashion, few studies have shown that introduction or removal of a phosphate group completely destroys the stability and conformation of the peptide since salt bridges are disrupted from basic or N-terminal residues [98, 99]. Conformational studies of phosphopeptides secondary interactions are presently in progress to further characterize possible effects that will reveal a more complete reasoning of the model.

Subsequently, the analytical potentials of AP strategy were conveyed through the further understanding of a biological model. Over the past decades, the identification of phosphorylation sites has become a primordial need for the full understanding of cell division, cancer therapy and even signal transduction in inflammatory response. To survive from viral infections, several mechanisms have evolved to recognize and eliminate invading organisms [100]. Inflammatory response is commonly initiated by the secretion of IFN-γ by T-cells that activates important antiviral mechanisms such as the JAK-STAT pathway in macrophages. In the present experiment, we did not observe any phosphopeptide associated with the JAK-STAT pathways possibly due to their relatively low abundance in cytosol extracts and the incompatibility of their

physicochemical characteristics with the present LC-MS systems (i.e. high hydrophilicity and *m/z* values outside of scanning range). However, we identified several phosphoproteins associated with bactericidal activities of macrophages. Indeed, many additional downstream substrates are stimulated through phosphorylation and direct the elimination of the microbe by phagocytosis or the release of reactive oxygen species (ROS) and hydrolytic enzymes [3]. Hence, phosphoproteome analysis in stimulated macrophages is essential for a better understanding of the innate immunity to potential pathogens. Pathogen destruction by phagocytosis is an important step for the inflammatory response [101]. Upon IFN-γ stimulation, Hefner *et al.* [102], demonstrated that $cPLA_2$ is activated through Ser727 phosphorylation by mitogen- and stress-activated protein kinase 1 (MSK1) involved in the JAK/STAT pathway. Stimulated $cPLA_2$ hydrolyzes membrane phospholipids from the *sn*-2 position to release arachidonic acid (AA) which in turn translocates $p47^{phox}$ to the cell membrane. [103]. Concomitantly, IFN-γ priming of macrophages triggers phosphorylation of $p40^{phox}$, $p47^{phox}$ and $p67^{phox}$ which are translocated from the cytoplasm to the membrane to associate with cytochrome b_{558} and form the NADPH oxidase enzyme complex [101]. Hence the phosphorylation change taking place in both pathways is necessary for the translocation of neutrophil cytosolic factors to the cell membrane. The resulting activated complex catalyzes the electron transfer from NADPH to O_2 to generate a burst of toxic superoxide (O_2^-) which helps in the killing of phagocytosed microorganisms. In our preliminary phosphoproteome analysis using TiO_2 enrichment only, we observed a limited number of kinase substrates such as $cPLA_2$ (Ser727) which showed stoichiometric changes in phosphorylation following IFN-γ stimulation. However, a greater number of differentially phosphorylated proteins involved in the production of ROS including $p40^{phox}$ were detected upon AP treatment.

The advantages of dephosphorylating phosphopeptides also allowed the characterization of another IFN-γ stimulated pathway covering the formation of vesicles. Vesiculation is generated by 5 different adaptor proteins, AP1, AP2, AP3, coat protein I (COPI) and coat protein II (COPII). AP-3 complex originates from the Golgi and endosomal membranes [104]. Studies have shown that upon phosphorylation, the AP-3 complex is recruited by VAMP-2 to form the coat assembly for pseudopod extension and vesicle formation involved in the pathway to lysosomes [105, 106]. In our study, the putative phosphopeptide RHSSLPTE**S**DEDIAPAQR from AP-3 complex

protein had an ~2-fold increase in abundance upon macrophage activation. To our knowledge, no paper has yet reported the possible direct linkage of IFN-γ priming to the enhanced phosphorylation of AP-3 complex and subsequent vesiculation.

In addition, our study allowed further characterization of the mRNA translation signaling pathway mediated by the action of IFN-γ. Cytokine stimulation has the ability to block cell growth and inhibit viral replication. Yet, it will also induce mRNA translation and protein synthesis of selective IFN-sensitive genes [31]. The regulatory mechanisms of protein synthesis is known to be mediated very quickly (minutes) through changes of phosphorylation state of translational machinery components reflecting the variations observed upon 5 min incubation of IFN-γ with J774 cells [107]. So far, an incomplete description of protein synthesis signaling pathway has been obtained for cells stimulated by IFN-γ [3]. Scheper *et al.* [108] demonstrated that eukaryotic translation initiation factor 4B (eIF4B) binds the 5'-cap structure of the mRNA more tightly in its dephosphorylation form. Likewise, our analysis revealed a 4.5 fold decrease in phosphorylation of the eIF4B phosphopeptide (**pS**LENETLNK) upon IFN-γ treatment. In addition, our study detected an increase in phosphorylation for eIF4G (KAA**pS**LTEDR, Ser1211) upon IFN-γ induction. Earlier reports proposed the implication of eIF4G1 phosphorylation in the mTOR pathway but no clear functional effect has yet been recognized [107]. Also, it has been previously shown that the mTOR pathway required phosphatidylinositol 3-kinase (PI3K) activation induced by type II IFN signaling with p70 S6K/rpS6 and 4E-BP1 as putative downstream effectors [3]. Upon cytokine induction, the p70 S6 kinase is rapidly activated by phosphorylation, which will in turn phosphorylate 40S ribosomal protein S6 on Ser235-236. During the initiation step, 40S ribosomal protein S6 is recruited to the mRNA for the identification of the start codon [107]. Until now, only the phosphorylation of 40S ribosomal protein S6 upon IFN-γ was shown to regulate mRNA translation but the exact function remained unclear [107]. After AP treatment, we were able to identify the 40S ribosomal protein S6 phosphopeptide, L**SS**LRA**STS**K, with three possible phosphorylation sites already known in the literature (Ser235-236, 240) including those responsible for the regulation of mRNA translation. Upon IFN-γ stimulation we identified significant changes in the phosphorylation state of other proteins involved in the protein synthesis machinery such as elongation factor 1-γ (eEF-1B-γ) isoform 1 and heterogeneous

nuclear ribonucleoprotein D0. The direct implication of these phosphoproteins with inflammatory response has not been reported in the literature.

The AP strategy enabled a more comprehensive study of the change in phosphorylation following IFN-γ signaling highlighting known and novel activation pathways in macrophages. Validation of potential phosphorylation sites can be subsequently obtained using independent techniques such as Western blotting and site mutagenesis. We anticipate that the broader application of AP in quantitative phosphoproteome studies of TiO_2-enriched protein extracts will provide a complementary and meaningful analytical strategy to uncover signaling pathways that remain elusive with current methodology.

2.6 References

3. Platanias, L.C., *Mechanisms of type-I- and type-II-interferon-mediated signalling.* Nat Rev Immunol, 2005. **5**(5): p. 375-86.

5. Mann, M., et al., *Analysis of protein phosphorylation using mass spectrometry: deciphering the phosphoproteome.* Trends Biotechnol, 2002. **20**(6): p. 261-8.

29. Lekmine, F., et al., *Interferon-gamma engages the p70 S6 kinase to regulate phosphorylation of the 40S S6 ribosomal protein.* Exp Cell Res, 2004. **295**(1): p. 173-82.

35. Kaufmann, H., J.E. Bailey, and M. Fussenegger, *Use of antibodies for detection of phosphorylated proteins separated by two-dimensional gel electrophoresis.* Proteomics, 2001. **1**(2): p. 194-9.

40. Reinders, J. and A. Sickmann, *State-of-the-art in phosphoproteomics.* Proteomics, 2005. **5**(16): p. 4052-61.

42. Loyet, K.M., J.T. Stults, and D. Arnott, *Mass spectrometric contributions to the practice of phosphorylation site mapping through 2003: a literature review.* Mol Cell Proteomics, 2005. **4**(3): p. 235-45.

49. Ficarro, S.B., et al., *Phosphoproteome analysis by mass spectrometry and its application to Saccharomyces cerevisiae.* Nat Biotechnol, 2002. **20**(3): p. 301-5.

50. Larsen, M.R., et al., *Highly selective enrichment of phosphorylated peptides from peptide mixtures using titanium dioxide microcolumns.* Mol Cell Proteomics, 2005. **4**(7): p. 873-86.

55. Corthals, G.L., R. Aebersold, and D.R. Goodlett, *Identification of phosphorylation sites using microimmobilized metal affinity chromatography.* Methods Enzymol, 2005. **405**: p. 66-81.

56. Thompson, A.J., et al., *Characterization of protein phosphorylation by mass spectrometry using immobilized metal ion affinity chromatography with on-resin beta-elimination and Michael addition.* Anal Chem, 2003. **75**(13): p. 3232-43.

59. Aebersold, R. and D.R. Goodlett, *Mass spectrometry in proteomics.* Chem Rev, 2001. **101**(2): p. 269-95.

60. Torres, M.P., et al., *Phosphatase-directed phosphorylation-site determination: a synthesis of methods for the detection and identification of phosphopeptides.* J Proteome Res, 2005. **4**(5): p. 1628-35.

75. G. Jaitly, E.B., N. Jaitly, K. Eng, C. Pomiès and P. Thibault, *Comprehensive profiling of unlabeled peptide ions from large-scale proteomics experiments using one and two dimensional nanoLC-MS/MS.* 2007(Submitted).

76. McLachlin, D.T. and B.T. Chait, *Analysis of phosphorylated proteins and peptides by mass spectrometry.* Curr Opin Chem Biol, 2001. **5**(5): p. 591-602.

77. Olsen, J.V., et al., *Global, in vivo, and site-specific phosphorylation dynamics in signaling networks.* Cell, 2006. **127**(3): p. 635-48.

78. Steen, H., et al., *Phosphorylation analysis by mass spectrometry: myths, facts, and the consequences for qualitative and quantitative measurements.* Mol Cell Proteomics, 2006. **5**(1): p. 172-81.

79. Bodenmiller, B., et al., *Reproducible isolation of distinct, overlapping segments of the phosphoproteome.* Nat Methods, 2007. **4**(3): p. 231-7.

80. Zhou, H., J.D. Watts, and R. Aebersold, *A systematic approach to the analysis of protein phosphorylation.* Nat Biotechnol, 2001. **19**(4): p. 375-8.

81. Zheng, H., et al., *Phosphotyrosine proteomic study of interferon alpha signaling pathway using a combination of immunoprecipitation and immobilized metal affinity chromatography.* Mol Cell Proteomics, 2005. **4**(6): p. 721-30.

82. Ishihama, Y., et al., *Enhancement of the efficiency of phosphoproteomic identification by removing phosphates after phosphopeptide enrichment.* J Proteome Res, 2007. **6**(3): p. 1139-44.

83. Wu, H.Y., V.S. Tseng, and P.C. Liao, *Mining Phosphopeptide Signals in Liquid Chromatography-Mass Spectrometry Data for Protein Phosphorylation Analysis.* J Proteome Res, 2007.

84. Kersey, P.J., et al., *The International Protein Index: an integrated database for proteomics experiments.* Proteomics, 2004. **4**(7): p. 1985-8.

85. Elias, J.E. and S.P. Gygi, *Target-decoy search strategy for increased confidence in large-scale protein identifications by mass spectrometry.* Nat Methods, 2007. **4**(3): p. 207-14.

86. Makrantoni, V., et al., *Rapid enrichment and analysis of yeast phosphoproteins using affinity chromatography, 2D-PAGE and peptide mass fingerprinting.* Yeast, 2005. **22**(5): p. 401-14.

87. Feng, S., et al., *Fe3+ immobilized metal affinity chromatography with silica monolithic capillary column for phosphoproteome analysis.* Proteomics, 2007. **7**(3): p. 351-60.

88. Gautier, T., et al., *Nucleolar KKE/D repeat proteins Nop56p and Nop58p interact with Nop1p and are required for ribosome biogenesis.* Mol Cell Biol, 1997. **17**(12): p. 7088-98.

89. Wen, X., et al., *Structural organization and cellular localization of tuftelin-interacting protein 11 (TFIP11).* Cell Mol Life Sci, 2005. **62**(9): p. 1038-46.

90. Flati, V., S.J. Haque, and B.R. Williams, *Interferon-alpha-induced phosphorylation and activation of cytosolic phospholipase A2 is required for the formation of interferon-stimulated gene factor three.* Embo J, 1996. **15**(7): p. 1566-71.

91. Trinidad, J.C., et al., *Comprehensive identification of phosphorylation sites in postsynaptic density preparations.* Mol Cell Proteomics, 2006. **5**(5): p. 914-22.

92. Thingholm, T.E., et al., *SIMAC - A phosphoproteomic strategy for the rapid separation of mono-phosphorylated from multiply phosphorylated peptides.* Mol. Cell. Proteomics, in press.

93. Marcantonio M., M.T., M. Desjardins, and P. Thibault. *Combined enzymatic and data mining approaches for comprehensive phosphoproteome analyses in sub-cellular protein extracts of macrophages.* in *Proc. of 54th ASMS conference on Mass Spectrometry and allied topics.* 2006. Seatlle, WA.

94. Nielsen, M.L., et al., *Physicochemical properties determining the detection probability of tryptic peptides in Fourier transform mass spectrometry. A correlation study.* Anal Chem, 2004. **76**(19): p. 5872-7.

95. Errington, N. and A.J. Doig, *A phosphoserine-lysine salt bridge within an alpha-helical peptide, the strongest alpha-helix side-chain interaction measured to date.* Biochemistry, 2005. **44**(20): p. 7553-8.

96. Mayne, L., et al., *Stabilizing Effect of a Multiple Salt Bridge in a Prenucleated Peptide.* J. Am. Chem. Soc., 1998. **120**(41): p. 10643-10645.

97. Ferret, P.J., et al., *Auto-protective redox buffering systems in stimulated macrophages.* BMC Immunol, 2002. **3**: p. 3.

98. Park, J.B., *Phagocytosis induces superoxide formation and apoptosis in macrophages.* Exp Mol Med, 2003. **35**(5): p. 325-35.

99. Hefner, Y., et al., *Serine 727 phosphorylation and activation of cytosolic phospholipase A2 by MNK1-related protein kinases.* J Biol Chem, 2000. **275**(48): p. 37542-51.

100. Sellmayer, A., et al., *Arachidonic acid increases activation of NADPH oxidase in monocytic U937 cells by accelerated translocation of p47-phox and co-stimulation of protein kinase C.* Cell Signal, 1996. **8**(5): p. 397-402.

101. Faundez, V., J.T. Horng, and R.B. Kelly, *A function for the AP3 coat complex in synaptic vesicle formation from endosomes.* Cell, 1998. **93**(3): p. 423-32.

102. Salem, N., et al., *A v-SNARE participates in synaptic vesicle formation mediated by the AP3 adaptor complex.* Nat Neurosci, 1998. **1**(7): p. 551-6.

103. Faundez, V.V. and R.B. Kelly, *The AP-3 complex required for endosomal synaptic vesicle biogenesis is associated with a casein kinase Ialpha-like isoform.* Mol Biol Cell, 2000. **11**(8): p. 2591-604.

104. Proud, C.G., *Signalling to translation: how signal transduction pathways control the protein synthetic machinery.* Biochem J, 2007. **403**(2): p. 217-34.

105. Scheper, G.C., et al., *Phosphorylation of eukaryotic initiation factor 4E markedly reduces its affinity for capped mRNA.* J Biol Chem, 2002. **277**(5): p. 3303-9.

3. Molecular dissection of early interferon-γ cell signaling events in macrophages via quantitative phosphoproteomics

Marcantonio, M., Trost, M., Bridon G., Courcelles, M., Desjardins, M., and Thibault, P. (2008) *Molecular & Cellular Proteomics,* in revision.

3.1 Abstract

IFN-γ induction of macrophages activates several signaling networks primarily modulated by reversible phosphorylation to overcome inflammatory diseases. The impact of IFN-γ stimulation is well-defined for the JAK/STAT pathway but is still poorly understood in other cell signaling events. In the present study, phosphoproteome analysis in macrophages using the sensitive mass spectrometry-based strategy provided a better understanding of the immune response. We conducted kinetic profiles up to 180 min of IFN-γ administration to mouse J774 macrophages in order to follow phosphoproteome dynamics. Phosphopeptides from tryptic digests of cytosolic proteins were isolated using TiO_2 affinity media and analyzed by LTQ-Orbitrap mass spectrometry. Amongst the different trends observed, a higher proportion of phosphopeptides showed a change in phosphorylation after 5 and 30 min of IFN-γ administration. In a more extensive study, a total of 2,831 non-redundant phosphopeptides were identified for J774 cell extracts treated for 0, 5 and 30 min with IFN-γ using 2D-LC-MS/MS analysis. This number included 1,673 new phosphorylation sites providing novel insights on IFN-γ stimulated pathways. According to kinase prediction and motif analyses, phosphopeptides containing consensus sequences recognized by CK2, CDK2 and MAPK14 kinases were up-regulated upon IFN-γ treatment. Phosphoprotein networking analysis indicated that mRNA translation and apoptotic pathways are regulated by early and late signaling events, respectively. Protein networks showed statistically meaningful changes in abundance for key phosphoproteins involved in protein synthesis, apoptosis, cytotoxic molecules formation as well as phospholipid signaling. The identification of known and novel phosphoproteins (PEA-15, RSK-2 and NF-κB) involved in the apoptotic pathway suggested a potential activation of cell death upon cytokine priming. Overall, the identification of important phosphorylation events upon IFN-γ induction led to a more comprehensive characterization of cytokine signaling pathways in macrophages.

3.2 Introduction

Cell signaling of the immune system consists of an interconnected network of pathways associated with various regulatory processes to induce acute inflammatory response. Specialized cells such as macrophages are responsible for ingesting and degrading dead cells and various pathogens through phagocytosis. Then, peptides from the degraded particles are presented to T cells for subsequent activation of the adaptive immune response [109].

Inflammatory response is commonly initiated by the secretion of interferon-γ (IFN-γ) from T-cells, which subsequently activates macrophages [12]. For several years, IFN-γ was used as a therapeutic agent to treat infectious diseases such as chronic myelogenous leukemia and hepatitis B and C [84, 110]. This cytokine binds to the membrane receptor IFNAR1, which in turn activates several signaling pathways in macrophages [1]. The first well studied signaling network involved the nuclear translocation and initiation of gene transcription by STATs following JAK phosphorylation [111]. Many important proteins implicated in cytoskeleton rearrangement, cell cycle progression, gene transcription, mRNA translation and production of reactive oxidative species (ROS) and nitric oxide (NO) intermediates were already shown to partake during IFN-γ macrophage activation [9, 109].

IFN-γ regulated pathways are primarily guided through post-translational modifications (PTMs) of proteins. Several studies have shown the important implication of protein phosphorylation-dephosphorylation throughout IFN-γ mediated cascades [111, 112]. Protein phosphorylation is the most abundant reversible PTM and a major regulator of protein activity or stability. Addition of negative charge from the phosphate group can cause major conformational changes affecting the protein's interacting partners, localization and activity [39]. This regulation is so extensive that more than one third of all proteins are thought to be phosphorylated at any given time during their life cycle [84]. Since phosphorylation holds a central role in signaling networks, comprehensive phosphoproteome analysis is required to fully understand the signaling mechanisms through which IFN-γ stimulates macrophage cells. Although, several antiviral effects of IFN-γ are well known, no extensive study on the phosphoproteomic kinetics of early time-points has yet been generated on macrophage cells.

Large-scale phosphorylation analysis on other organisms such as yeast, Jurkat and Hela cells has been already documented in the literature using proteome chip technology and mass spectrometry [80, 113, and 114]. For instance, Zheng *et al.* analyzed by MS the phosphorylation effect of IFN-α on Jurkat cells using esterification/IMAC combined with phosphotyrosine immunoprecipitation [84]. In the past few years, mass spectrometry combined with enrichment strategies became a method of choice for the detection of thousands of phosphopeptides due to its high sensitivity and speed of analysis [80, 115]. Yet, mapping of phosphorylation sites in positive ion mode is difficult because of low stoichiometry of phosphorylation and the phosphopeptide population is under-represented due to ionization suppression effects [79, 116]. Hence the combination of enrichment (TiO_2 and IMAC) and separation (Strong Cation Exchange & SDS-PAGE) procedures with the liquid chromatographic mass spectrometry (LC-MS) analysis is essential to enhance phosphopeptides detection [5, 114].

Large-scale mass spectrometry analyses generate sizable lists of phosphoproteins which require bioinformatic and data mining tools for comprehensive identification. Few tools are available to correlate proteins together and assemble networks. For instance, STRING generates protein-protein interaction maps using published two-hybrid studies or identification of interacting partners by affinity purifications and mass spectrometry [117]. Furthermore, additional information can be revealed on activated signaling pathways by determining the kinase motifs on detected phosphopeptides using kinase prediction tools and motif-x [118].

Here, we present a sensitive MS-based phosphoproteomic approach combined with TiO_2 enrichment to profile changes in cytosolic phosphoprotein abundances in response to IFN-γ activation of mouse macrophage cell line J774. We used a label-free detection method along with a peptide and a Fuzzy c-means clustering (FMC) method to profile phosphopeptide dynamics up to 180 min following IFN-γ administration. The most significant changes occurred 5 and 30 min after macrophage activation. Subsequently, 2D-LC/MS analysis on TiO_2-enriched phosphopeptides activated for 0, 5 & 30 min with IFN-γ generated 2831 unique phosphopeptides. Functional (phosphoproteins network) combined with non-labeled expression-based proteomics enabled the identification of activated signaling pathways in macrophages. Transduction pathways linked to apoptosis, mRNA translation, ROS production and phospholipid signaling were found to be modulated by phosphorylation changes upon IFN-γ treatment.

3.3 Experimental Procedures

3.3.1 Materials

Sequencing Grade Modified Trypsin was obtained from Promega (Madison, WI US). Acetonitrile (ACN) and formic acid (FA) were purchased from Fisher Scientific (Whitby, ON, Canada). Ammonium bicarbonate was obtained from EM Science (Mississauga, ON, Canada). Ammonium hydroxide, trifluoroacetic acid (TFA), DTT, iodoacetamide, imidazole and sucrose were purchased from Sigma-Aldrich (Oakville, ON, Canada). BCA protein assay and bond breaker TCEP solution were purchased from Pierce (Rockford, IL). Fetal bovine serum (FBS), penicillin-streptomycin, L-glutamine and DME/High glucose Dulbecco's modified eagle's medium were obtained from HyClone (Perbio, Nalgene).

3.3.2 Cell cultures, protein extraction and trypsin digestion

The preparation of J774 murine macrophage cells and cytosolic protein extraction is described in detail in Marcantonio *et al.* [116]. For IFN-γ challenge experiments, J774 cell cultures were incubated for 0, 5, 10, 30, 60 and 180 min with 100 U/mL mouse IFN-γ (PBL Biomedical Lab).

Since phosphopeptides were isolated with TiO_2 micro-tips, precipitated cytosolic proteins were resuspended in 1% SDS/50 mM ammonium bicarbonate. Proteins were reduced in 0.5 mM TCEP for 20 min at 37°C and then alkylated in 50 mM iodoacetamide for 20 min at 37°C. 50 mM DTT was added to the protein solution to react with excess iodoacetamide. Total protein amount was quantitated by BCA protein assay. Protein digestion was performed in 0.1% SDS, 50 mM ammonium bicarbonate with Sequencing Grade Modified Trypsin overnight at 37 °C and high agitation speed (1 μg trypsin: 100 μg protein). The digest mixture was acidified with TFA and then evaporated to dryness.

3.3.3 Phosphopeptide isolation

The TiO_2 enrichment procedure was performed as described before [53, 116]. The 2,5-dihydroxybenzoic acid (DHB) was replaced by lactic acid to avoid interference in 2D-LC analysis. For the 1D-LC-MS analysis, 20 μL of acidified eluate was injected

on the LTQ-Orbitrap mass spectrometer. For the SCX-LC-MS analysis, eluates from five TiO_2 micro-columns were pooled together, acidified with TFA and then evaporated to dryness. Samples were resuspended in 10 µL of 0.2% formic acid/ 2% ACN and completely injected on the LTQ-Orbitrap mass spectrometer. Unless otherwise indicated, samples were prepared in triplicate for each condition.

3.3.4 LC-MS/MS analyses and Mascot database searching

In this study, 1D- and 2D-LC-MS analyses were performed on the LTQ-Orbitrap hybrid mass spectrometer (Thermo Electron, San Jose, CA) coupled to a nano-flow LC (Eksigent, Dublin) with a Spark-Holland autosampler (Thermo Electron, San Jose, CA) as described previously [116]. The 2D-LC-MS experiment comprised also a SCX column (300 Å and 5 µm, Nanoease Waters) on line with the pre-column and analytical column. Peptides were eluted from the SCX column using five different ammonium acetate salt pH 3.0 fractions (0, 50, 100, 500 & 2000 mM) in 0.2% FA/2% ACN. In this case, the C_{18} analytical gradient started from 2% to 33% B over 54 min followed by a gradient from 33% to 60% over 10 min with a flow rate of 600 nL/min (A: 0.2% FA in water, B: 0.2% FA in ACN).

Subsequently, all MS/MS spectra were processed through Mascot Distiller (version 2.1.1, Matrix Science) and Mascot (version 2.1, Matrix Science, London, UK) software. A Mascot search against a concatenated target/decoy database consisting of a combined forward and reverse version of the IPI mouse database (v3.24) was performed to establish a cutoff score threshold for a false-positive rate of less than 1% ($p < 0.01$) [88].

3.3.5 Peptide detection and clustering

Raw data files (.raw) generated from the LTQ-Orbitrap acquisition software were converted into *csv* files representing all ions according to their corresponding *m/z* values, retention time, intensity and charge state using in-house peptide detection software [78]. Intensity values above a user-defined intensity threshold (10,000 counts) were considered. Clustering of peptides across different samples was performed using in-house software. Upon obtaining Mascot search results, the clustering program matched each Mascot entry to a peak top from the MS data. The matching between MS

and MS/MS is based on the correlation of similarity in *m/z* and retention time (±0.035 *m/z* and ±1 min) following time normalization. Peptides from different samples with similar *m/z*, retention time (±0.035 *m/z* and ±1 min) and identical assigned sequences by Mascot are grouped together to form clusters. Using the cluster average *m/z* and corrected retention time, peptides from samples where no MS/MS or no Mascot search results were obtained, are then added. In order to confidently add peptides, a list of neighbors in the surrounding area (±5 *m/z* and ±4 min) is compared against a reference list of neighbors for each cluster. A minimum of three common neighbors must exist before a peptide is added to a cluster. The generated unique list of peptide clusters allowed the direct comparison of peptide abundance between samples in different conditions to identify those showing reproducible and statistically meaningful changes in abundance.

3.3.6 Fuzzy c-means clustering

Temporal profiles of phosphopeptides' clusters for each IFN-γ incubation time were created using a fuzzy c-means (FMC) clustering software titled "Soft clustering of time series gene expression data" (Mfuzz, 2007, v1.6.0) available at http://itb.biologie.hu-berlin.de/~futschik/software/R/Mfuzz/index.html. A detailed description of the FMC clustering device is found in Olsen *et al.* [80]. Only phosphopeptides with intensity values found in at least two of the three replicates of each condition were used for the plotting. Raw intensities instead of ratios were taken for the generation of time profiles. The cluster number (c) and the fuzzification parameter (m) were 6 and 1.5, respectively, since most defined and significant kinetic trends were obtained.

3.3.7 Kinase and motif prediction tools

The Prediction of PK-specific Phosphorylation site (PPSP), NetworKIN and Motif-x analyses were performed on all identified phosphopeptides with a Mascot score >25 and also on up- & down regulated phosphopeptides with at least 2-fold change and a p-value <0.1.

For kinase motif prediction, a Perl script automated with the PPSP software (2006, LCD & USTC) was used to determine the kinase consensus site with a high specificity

(http://bioinformatics.lcd-ustc.org/PPSP/). PPSP was proven to be a very powerful and accurate tool holding a large number of protein kinase groups [119]. The search was performed against mouse IPI database.

Concomitantly, protein kinases targeting phosphorylation sites were also established using NetworKIN software (v2.0, 2008) (http://networkin.info/search.php). This tool not only considers consensus sequence motifs like PPSP but also the direct or indirect protein association networks from STRING database [120]. In doing so, the linked experimental prediction of the kinases responsible for the identified phosphopeptides improves the accuracy and confidence level. In this case, the human database was used for the kinase prediction since NetworKIN considers human and mouse species to have very similar protein coverage and characteristics.

Over-represented patterns from phosphopeptides sequence were extracted using motif-x software (http://motif-x.med.harvard.edu/motif-x.html, v1.2 10.05.06, 2005) [118]. Motif-x's strategy consists of building successive motifs and comparing it to a dynamic statistical background. Identified phosphosites were centered with six amino acids flanking on each side of the hydroxyamino acid. Parameters set for the width, occurrences, significance and background were 13, 20, 0.000001 and IPI Mouse Proteome, respectively.

3.3.8 Phosphoprotein networking

Mapping of the phosphoproteins interactions was performed using Search Tool for the Retrieval of Interacting Genes/Proteins (STRING) database (version 7.1, 1,513,782 proteins in 373 species, http://string.emble.de/) and visualized with Cytoscape software (version 2.5.1) [121, 122]. At first, non-redundant phosphopeptides with Mascot score < 25 from replicates of all three conditions (0, 5 & 30 min) were converted to *Ensembl* peptide ID. Then the network was created with STRING software using mouse and human database to determine the functional partners of each protein. The active prediction methods selected for STRING search were Experiments and Databases. The confidence level was set to medium (0.4) and no more than 10 interactors were shown. Additional nodes, network depth and edge scaling factor parameters were set to 0, 2 and 80%, respectively.

3.4 Results

3.4.1 Phosphorylation dynamics of IFN-γ treated J774 phosphopeptides

Upon IFN-γ priming, macrophages undergo several morphological and phenotypical changes. Several studies already reported the importance of protein phosphorylation in IFN-γ activating signaling pathways [3, 9]. Yet no extensive kinetic study was ever performed on the phosphoproteome of cytokine stimulated macrophage cells. Here, we present the first study on early changes in protein phosphorylation following IFN-γ administration to J774 mouse macrophage cells.

The experimental method consisted of initially extracting cytosolic proteins from J774 cells treated with IFN-γ at different time-points (0, 5, 10, 30, 60 & 180 min). The digested cytosolic protein extract was enriched with TiO_2 micro-columns proving a high enrichment and recovery of phosphopeptides [53, 123]. The outline of the sample work flow is shown in Figure 3.1.

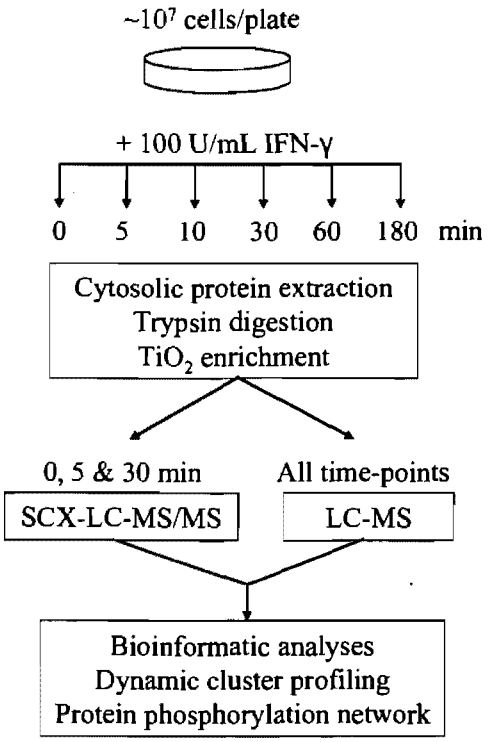

Figure 3.1: **Overview of the analytical strategy and data mining approaches for time-resolved phosphoproteomics.** J774 mouse macrophage cells were incubated with IFN-γ for 0, 5, 10, 30, 60 & 180 min. Cytosolic protein digest was enriched with TiO_2 micro-tips and analyzed on a LTQ-Orbitrap mass spectrometer. Also, a SCX-LC-MS/MS analysis was performed on TiO_2-enriched 0, 5, & 30 min IFN-γ treated macrophages. In-house bioinformatic software processed the data for subsequent FMC clustering and network protein mapping.

The first part of the experiment consisted of determining the IFN-γ incubation times that displayed the most significant changes in phosphorylation of the cytosolic proteins. According to Zheng *et al.* [84] kinetic assay, phosphorylation events were mediated rather quickly upon IFN-α cellular priming. Hence, shorter time-points (5, 10 & 30 min) were selected accordingly to detect early onset of phosphorylation events. In addition, longer time-points (60 & 180 min) were chosen to identify much later signaling events before the synthesis of new proteins. J774 cytosolic protein digest treated for 0, 5, 10, 30, 60 & 180 min with IFN-γ were enriched with TiO_2 micro-columns and detected by LC-MS/MS. To search for patterns in time profiles of identified phosphopeptides (Mascot score >25), 416 phosphopeptide clusters having at least an intensity value for two of three replicates for each condition were further clustered using a c-fuzzy means (FMC) algorithm [80]. For optimal partitioning of the time profiles, the cluster sizes (c-value) and the fuzzification parameter (m-value) were optimized to 6 and 1.5, respectively. Each phosphopeptide profile is denoted by a color to determine the level of membership to its cluster. Pink-red, green-blue and yellow-orange colors suggest high, medium and low association to the trend, respectively. As a result, four different clusters displayed interesting temporal changes of phosphorylation (Fig. 3.2). The first trend consisted of a general dephosphorylation (93 phosphopeptides) taking place upon IFN-γ administration where a 2-fold decrease in phosphorylation change occurred after 180 min (Fig. 3.2a). Also 80 peptide clusters showed a maximum in phosphorylation upon 30 min of macrophage activation (Fig. 3.2b). Lastly, phosphorylation (57) and dephosphorylation (42) upon 5 min of cytokine stimulation were also noted as important clusters from the computed kinetic profiles (Fig. 3.2c-d).

The kinetic analysis of J774 cytosol extracts stimulated by IFN-γ demonstrated that most phosphorylation changes took place upon 5 and 30 min of macrophage stimulation. Hence more extensive study was performed on these two kinetic time-points to understand the implication of protein phosphorylation in different IFN-γ activated signaling pathways.

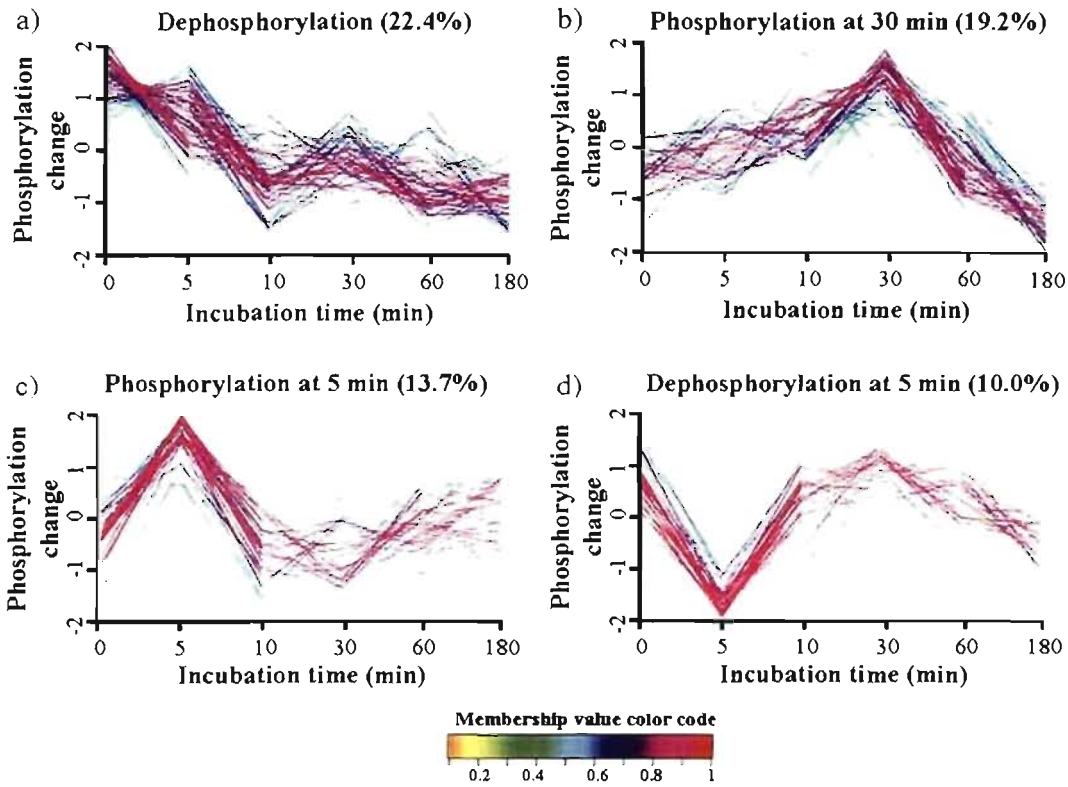

Figure 3.2: **Clustered profiles of dynamic phosphorylation.** Kinetic profiles showing (a) dephosphorylation, phosphorylation abundance increase at (b) 30 min and (c) 5 min, and (d) decrease at 5 min upon IFN-γ stimulation. Each trace colour is coded according to the membership value colour code bar where 1 corresponds to the best fit in the profile.

3.4.2 Statistical analysis of macrophage phosphoproteome

The second set of experiment consisted of combining TiO_2 enrichment and SCX separation with C_{18} analytical chromatography to enhance the number of phosphopeptides identification for 0, 5 and 30 min IFN-γ stimulated J774 cells. This SCX-based strategy was already proven to efficiently retain hydrophilic peptides and significantly enhance phosphopeptide identification [115]. In all, 2831 phosphopeptides with a Mascot score >25 were identified across fractions and replicates of all three conditions, indicating a false positive rate of less than 1%. Interestingly, 3201 phosphorylation sites were determined where 1673 (52%) sites have never been documented in the Swiss-Prot and Phospho ELM database. Also, a high number of singly (2481) and doubly (334) phosphorylated peptides were detected further supporting the TiO_2 specificity towards mono-phosphopeptides compared to IMAC

enrichment [54, 116]. The serine, threonine and tyrosine proportion from the total amount of isolated phosphopeptides was 85, 13 and 2%, respectively (Table 3.1).

Table 3.1: **Statistics on overall distribution of phosphopeptides from IFN-γ stimulated J774 kinetic study**

Category	No. of examples
# Assignment	5420
# Phosphoproteins	1084
# Phosphopeptides	2831
# Phosphorylation sites	3201
# Novel phosphorylation sites identified	1673 (52%)
# Phosphopeptides with 1, 2, 3 or 4 phospho sites	2481, 334, 14, 1
Phosphorylated residues (Ser:Thr:Tyr)	85%, 13%, 2%

Following phosphopeptide detection and clustering, volcano plots representing the change in abundance and p-values distribution of peptide clusters across control and 5 & 30 min IFN-γ treated samples were obtained (Fig. 3.3). The x-axis represents the fold change between the two conditions and the y-axis indicates the p-value for a t-test of differences between both samples. From the spiked α-casein phosphopeptides, an average CV < 23% was obtained for the change in intensity throughout all replicates of every condition. Phosphopeptides are considered up or down-regulated if they represent clusters with change in abundance > 2-fold with p-values < 0.05 (*dotted* regions Fig. 3.3). In all, 1841 phosphopeptide clusters (80.6 %) had similar intensities in the control and 5 min IFN-γ-treated sample whereas 145 (6.3 %) and 299 peptide clusters (13.1 %) were 2-fold down and up-regulated, respectively (Fig. 3.3a). Similarly, 1722 phosphopeptide clusters (75 %) were within 2-fold change for the control sample compared to 30 min IFN-γ treated sample and 164 (7.1 %) and 411 peptide clusters (17.9 %) were down and up-regulated, respectively (Fig. 3.3b).

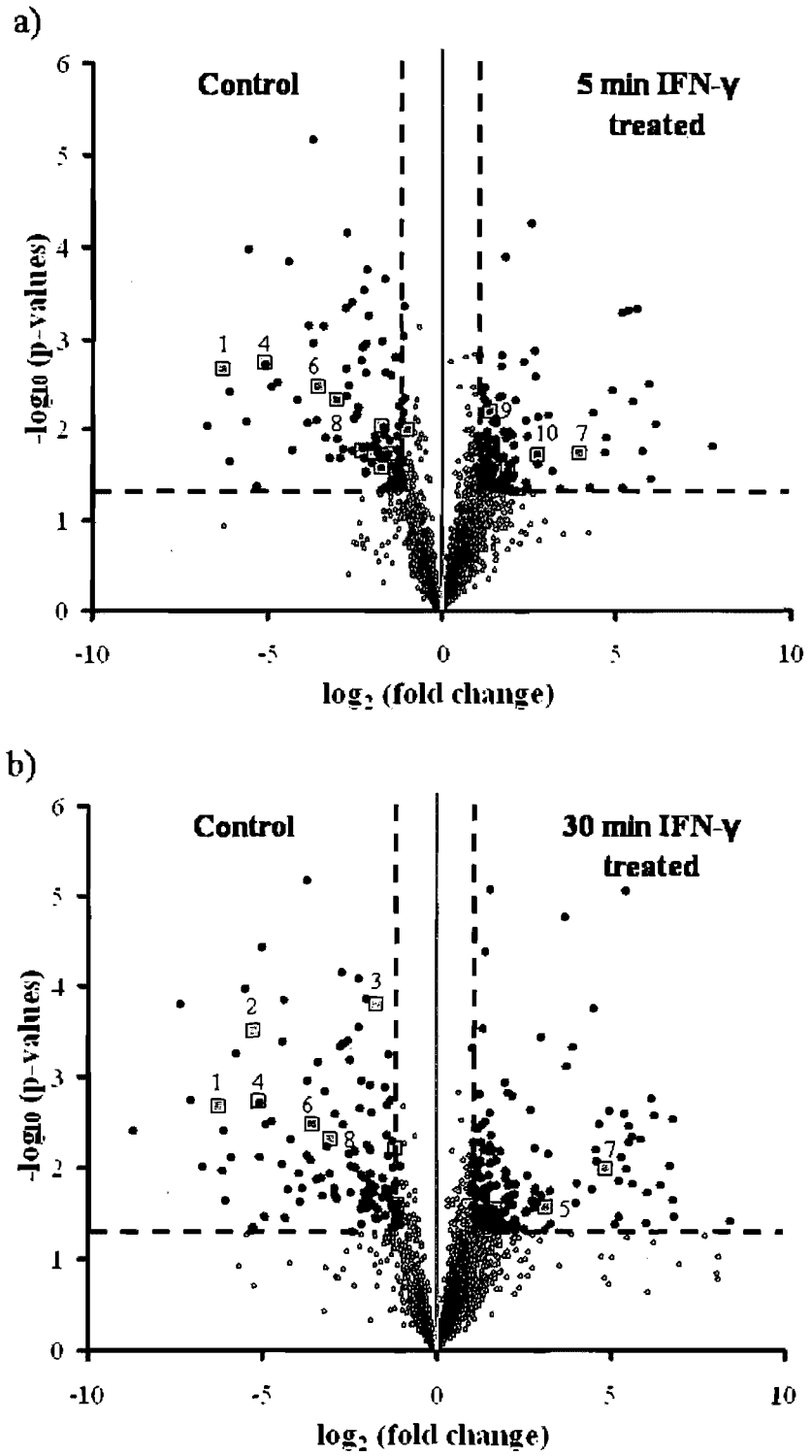

Figure 3.3: **Volcano plot distribution of (a) 5 and (b) 30 min IFN-γ treated cytosolic extracts of J774 cells.** Only phosphopeptides with a Mascot score >25 and intensity values found in all or none of the three replicates were considered. *Solid* line divides peptide clusters more abundant in control and IFN-γ samples. *Dashed* lines delimit peptide populations showing 2-fold change in abundance with p-values <0.05. Numbered squares identify all up- and down-regulated phosphopeptides listed in Table 3.2.

From the large number of phosphopeptides obtained, bioinformatic tools were required to determine which pathways were activated during IFN-γ priming. Data were first analyzed with kinase prediction and motif-x softwares to indicate what type of kinases might be inhibited or activated upon IFN-γ signaling. NetworKIN software specifically determined the kinases responsible for the phosphorylation on serine, threonine and tyrosine residues. NetworKIN holds more meaningful statistical level than other kinase prediction tools since it considers the consensus motif and the protein association between the kinase and substrate [120]. The five most significant kinases (>80 phosphopeptides) for the 5 and 30 min time-points were Cell division protein kinase 2 (CDK2), Casein kinase 2 (CK2), TGF-beta receptor type-2 (TGFBR2), Serine/threonine-protein kinase Pim-2 (PIM2) and Mitogen-activated protein kinase 14 (MAPK14, p38). Figure 3.4 shows all kinases that were matched to at least 45 phosphopeptides with their proportion (%) of substrate that have at least 2-fold change in phosphorylation with p-values < 0.1 upon macrophage activation. As a result, no kinase seemed to significantly phosphorylate less upon IFN-γ administration. On the other hand, CDK2, MAPK14 and CK2 were notably more active upon 5 and 30 min IFN-γ stimulation. Also, PPSP prediction further confirmed the induction of CK2 motifs. Interestingly, these kinases have different consensus motifs where CDK2 and MAPK14 have a proline-directed phosphorylation site (S/T-P) whereas CK2 is an acidic-residue directed kinase (X-pS-X-X-E/D) [124-126]. Kinases potentially associated with these changes in phosphorylation are involved in a multitude of important cellular function such as protein synthesis, cell cycle regulation and gene transcription [126-128].

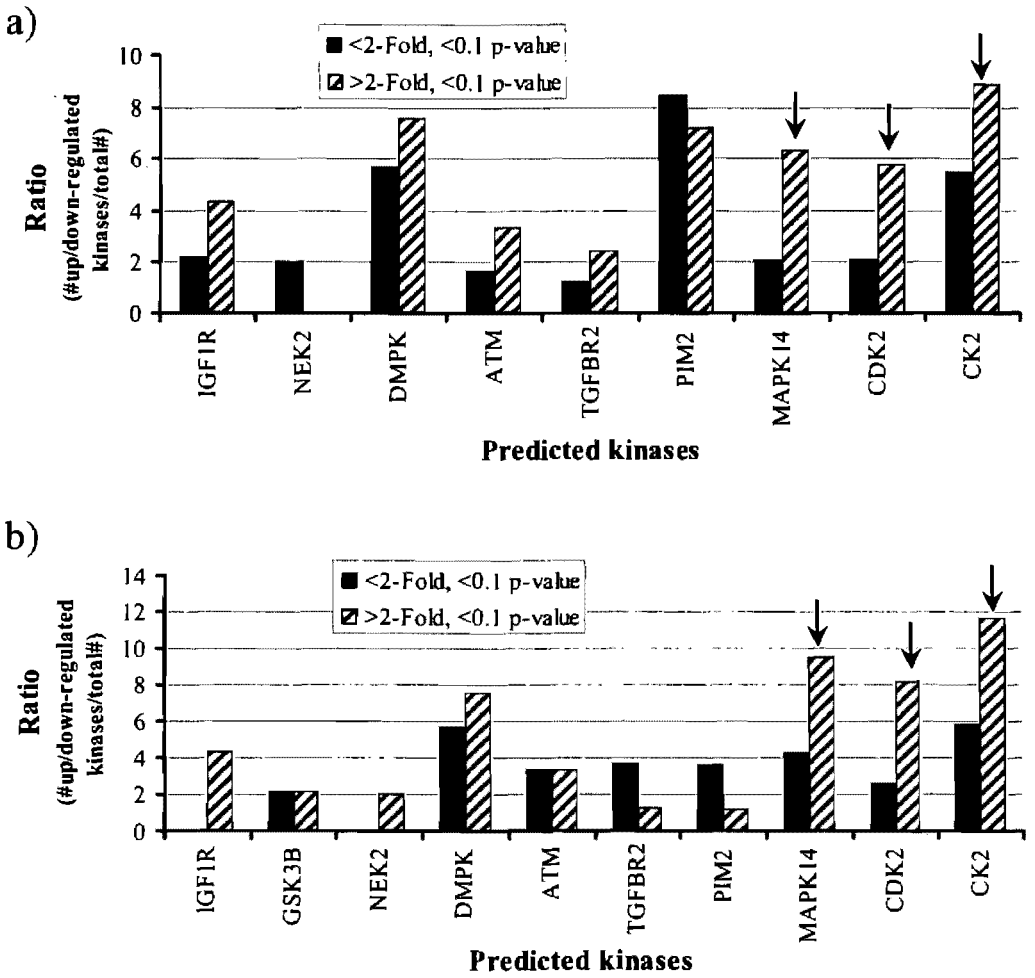

Figure 3.4: **NetworKIN kinase prediction of identified phosphopeptides.** Upon (a) 5 and (b) 30 min IFN-γ stimulation, the kinases which phosphorylated peptides up- and down-regulated upon macrophage activation with p-values < 0.1 were shown as *black* and *striped* bars, respectively. Only kinases matched to at least 45 substrates were represented on the graph.

Furthermore, not only different types of kinases were characterized through NetworKIN but also, a more detailed analysis of the substrate motif was generated using motif-x software. A list of 29 different over-represented patterns for serine and threonine phosphorylation was computed across the non-redundant phosphopeptide list (3134 phosphopeptides with Mascot score >25). The motifs were subsequently divided into 5 categories of proline, acidic residue, arginine, bipolar and serine-directed (Fig. 3.5). The most frequently observed category for J774 phosphopeptides was the proline-directed motifs comprising 51.6% of all phosphopeptides. Yet, the highest number of different patterns (15) was obtained for the acidic residue-directed motifs.

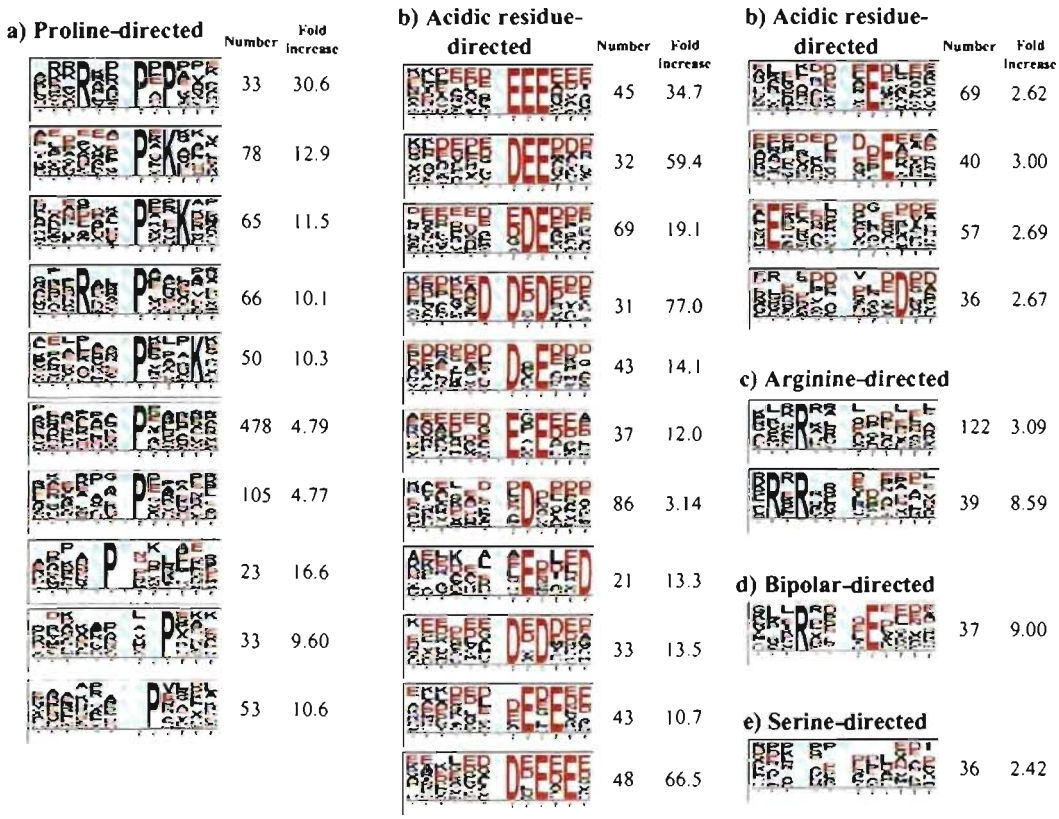

Figure 3.5: **Over-represented motif-x patterns of all identified phosphopeptides.** Five different kinds of motifs were identified: (a) proline-directed, (b) acidic residue-directed, (c) arginine-directed, (d) bipolar-directed and (e) serine-directed.

Also, motif-x computed the over-represented patterns for all phosphopeptides showing 2-fold change in abundance with p-value < 0.1 upon IFN-γ treatment. As a result, acidic residues and proline directed motifs were the frequently observed patterns showing changes in abundance (Fig. 3.6).

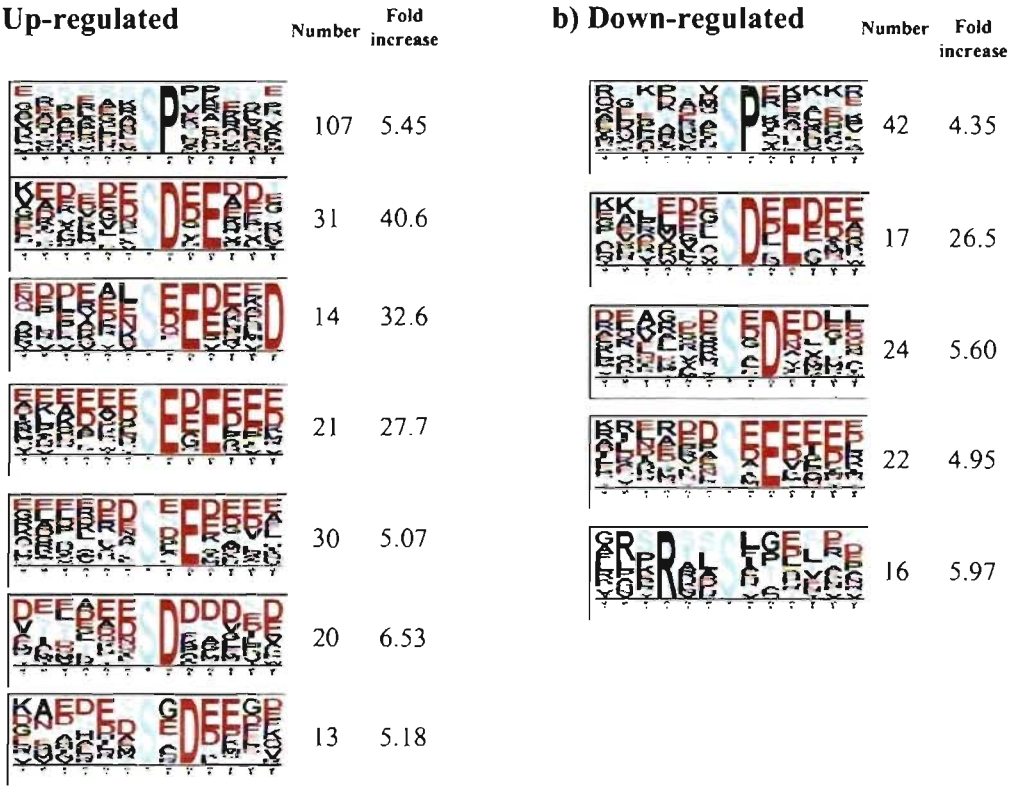

Figure 3.6: **Over-represented motif-x patterns of differentially expressed phosphopeptides.** Mainly proline and acidic residue-directed motifs were identified for up and down-regulated phosphopeptides with a p-value < 0.1.

3.4.3 Network analysis in signaling pathways of activated macrophages

Strategies were implemented to provide a more comprehensive analysis of this large-scale experiment. All non-redundant phosphopeptides detected in 0, 5 and 30 min IFN-γ treated samples (Mascot scores >25) with known *Ensembl* identification were processed through STRING database. Cytoscape software was used to visualize maps illustrating the interactions between different phosphoproteins. As a result, 715 phosphoproteins were integrated in the network with known interacting partners in the literature. Interestingly, several known IFN-γ stimulated pathways such as NAPDH oxidase, apoptosis, mRNA translation, and phospholipid signaling pathways were identified (Fig. 3.7). Even though, these pathways were already known to play important functions during IFN-γ induction, many novel phosphorylated proteins were identified from this kinetic study.

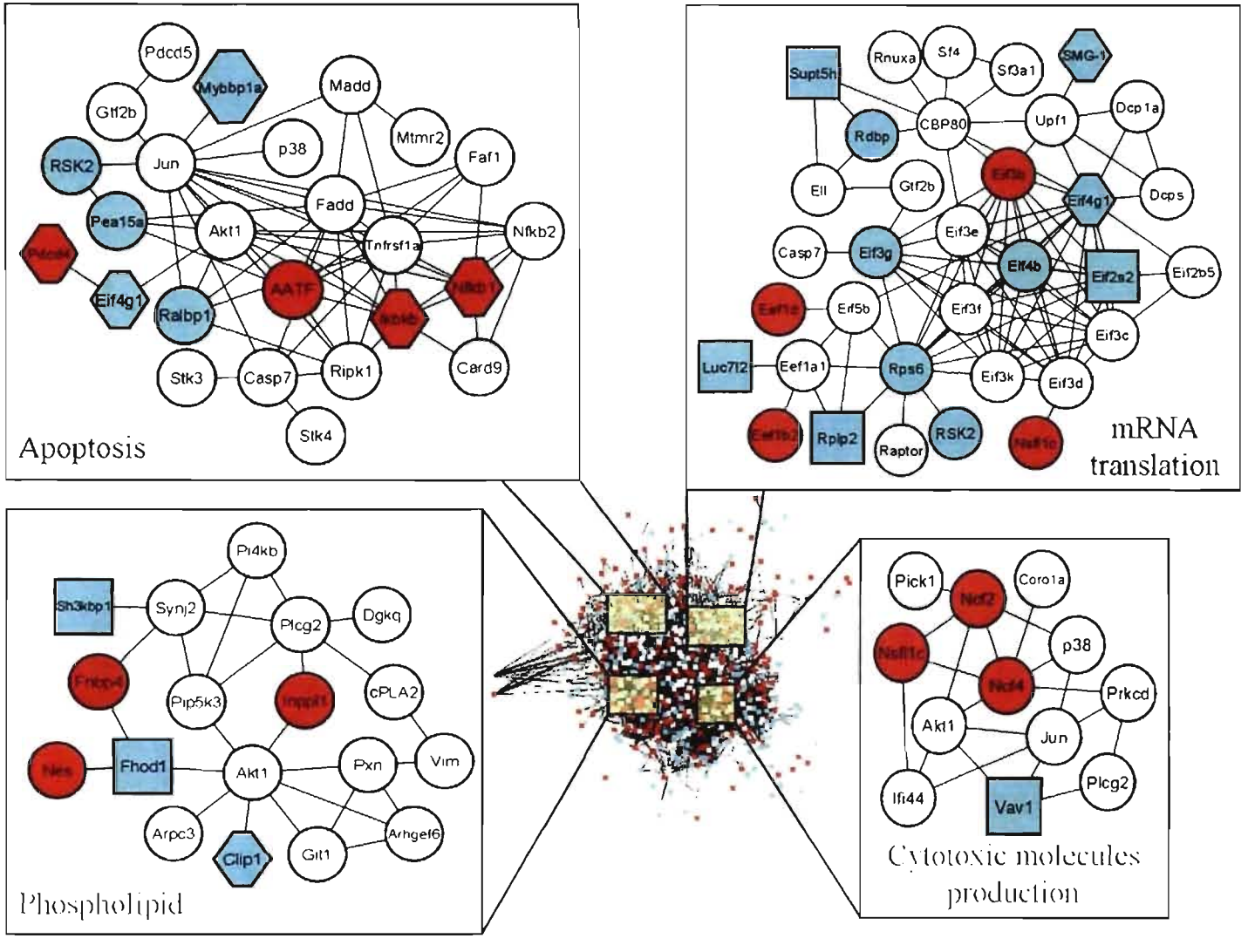

Figure 3.7:
Phosphoprotein interaction networks of J774 macrophages.
A network showing the interaction between unique phosphoproteins (715) present in 0, 5 & 30 min IFN-γ treated cells. Most populated and activated signaling pathways were apoptosis, mRNA translation phospholipids and cytotoxic molecules production. The boxes have a *circular, rectangular and hexagonal shape* depending if the phosphoproteins are under- or over- expressed in both conditions, after 5 or 30 min of IFN-γ exposure, respectively. Also the boxes are coloured in *white, red and blue* when the phosphoprotein does not change significantly, is under or over-expressed, respectively. All phosphoproteins differentially expressed had a p-value < 0.1.

To obtain the complete biological representation of phosphoproteins role and changes, the identified phosphoproteins from STRING network were correlated with their expression data. Accordingly, phosphoproteins showing 2-fold up-, down-regulation or no change upon IFN-γ treatment were colored in *red, blue* and *white*, respectively. Also, for each sub-network examined a *rectangle*, a *hexagon* or an *oval* represent changes occurring after 5 and 30 min IFN-γ incubation or in both conditions, respectively (Fig. 3.7). All macrophage phosphopeptides showing significant changes in intensity changes (at least 2-fold) with p-values <0.1 are listed in Table 3.2. Some of these phosphopeptides are represented by numbered squares on the volcano plots (Fig. 3.3). For example, ribosomal protein S6 kinase alpha-3, eukaryotic translation initiation factor 4B and proto-oncogene vav phosphoproteins were dephosphorylated upon cytokine stimulation. In contrast, $p67^{phox}$, inositol polyphosphate phosphatase-like 1 and inhibitor of nuclear factor kappa B kinase subunit beta were phosphorylated upon macrophage activation.

In addition, this analysis enabled to determine the IFN-γ exposure time required for phosphorylation changes and signaling activation to occur in specific pathways. For instance, most phosphoproteins involved in the mRNA translation pathway significantly changed phosphorylation state after 5 min of IFN-γ treatment. On the other hand, later signaling events took place 30 min upon IFN-γ stimulation and were mainly illustrated in the apoptotic network. Interestingly, many phosphoproteins identified in the cell death network were part of the classical apoptotic pathway. Figure 3.8 illustrates the apoptotic signal transduction including most identified phosphoproteins from the STRING analysis. Key molecules such as NF-κB, 26S proteasome and PEA-15, had considerable phosphorylation changes upon cytokine priming.

In summary, 2D-LC-MS/MS analysis of TiO_2-enriched J774 cell extract combined with protein network predictions identified many important pathways suggesting novel phosphorylation regulation for the mediation of IFN-γ biological effects.

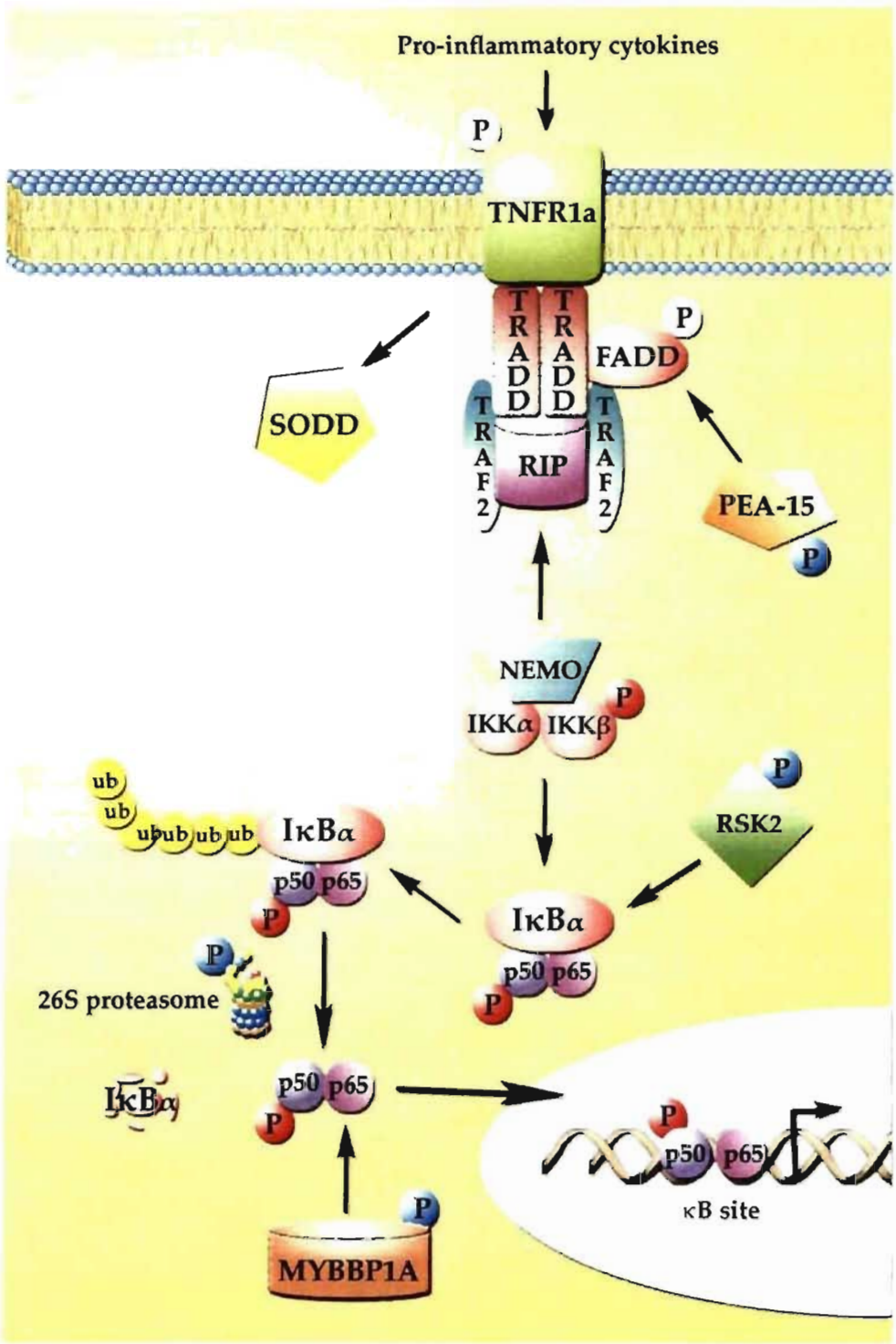

Figure 3.8: **Classical apoptotic signaling pathways highlighting phosphoproteins identified upon 5 and 30 min IFN-γ.** Phosphorylated proteins are represented with a *white, red* and *blue* phosphate group corresponding to no changes, up- and down- regulation upon IFN-γ stimulation, respectively.

Table 3.2: **Phosphopeptides showing differential abundance in 5 and 30 min IFN-γ stimulated J774 cytosol extracts**

Phosphopeptides	Proteins	Function	Fold change	
			5min (p-values)	30 min (p-values)
AY**pS**FCGTVEYMAPEVVNR	Ribosomal protein S6 kinase alpha-3	Apoptosis/ mRNA translation	-77.5 (0.0021)	-77.5 (0.0021)
GLVAAYSGD**pS**DNEEELVER	RNA-binding protein 5	Apoptosis	-2.2 (0.0138)	-1.6 (0.1306)
pSPPEGDTTLFLSR	Death inducer-obliterator 1 isoform 3	Apoptosis	2.5 (0.0145)	2.9 (0.0453)
TSEDTSSG**pS**PPKK	Apoptosis inhibitor 5	Apoptosis	2.0 (0.0169)	2.1 (0.0160)
TPATTAS**pS**PVTTAQVHCLPL SSSSTR	Nuclear factor NF-kappa-B p105 subunit	Apoptosis	1.8 (0.0495)	2.2 (0.0502)
GPVSG**pS**PDSMNVSR	Inhibitor of nuclear factor kappa B kinase subunit beta	Apoptosis	1.6 (0.0197)	2.3 (0.0436)
DIIRQP**pS**EEEIIK	Astrocytic phosphoprotein PEA-15	Apoptosis	-3.4 (0.0056)	-38.0 (0.0003)
HIVNGAKPNTESEEI**pS**p**S**ED DELVGEK	Apoptosis-antagonizing transcription factor	Apoptosis	3.5 (0.0722)	3.5 (0.0354)
SGVAVPT**pS**PK	Programmed cell death protein 4	Apoptosis	1.9 (0.1245)	3.3 (0.0289)
KEVQ**pS**PEQVK	Bcl-2-associated transcription factor 1	Apoptosis	1.8 (0.0772)	49.2 (0.0310)
KG**pS**ITEYTATEEK	BCL2/adenovirus E1B 19 kDa protein-interacting protein 2	Apoptosis	3.1 (0.0463)	3.7 (0.0060)
LSQVNGA**pT**PV**pS**PIEPESK	Myb-binding protein 1A	Apoptosis	-1.7 (0.0344)	-3.34 (0.0002)
TVG**pT**PIASVPGSTNTGTVPG SEKDSDPMETEEK	26S proteasome non-ATPase regulatory subunit 1	Apoptosis/ Proteasome	-33.8 (0.0019)	-33.8 (0.0019)

A**pS**GEMASAQYITAALR	Ubiquitin specific protease 14 isoform 2	Proteasome	8.0 (0.1036)	8.9 (0.0277)
DMPGGFLFDGL**pS**DDEDDFH PSTR	Ubiquitin-like protein 7	Proteasome	2.1 (0.0326)	1.8 (0.2083)
pSSDIVSSVR	GTPase activating protein and VPS9 domains 1	Endocytosis	-3.4 (0.0095)	-1.2 (0.3620)
SR**pS**SDIVSSVR	GTPase activating protein and VPS9 domains 1	Endocytosis	-2.5 (0.0428)	-1.0 (0.8853)
EFE**pS**GDFQDFTR	AP-1 subunit gamma-binding protein 1	Endocytosis	2.6 (0.0242)	1.9 (0.3529)
TP**pS**SEEISPTKFPGLYR	RalA-binding protein 1	Endocytosis	-1.9 (0.0440)	-2.1 (0.0421)
TASESISNLSEAG**pS**VK	Restin	Endocytosis	-1.5 (0.0509)	-3.2 (0.0006)
HSSLPTE**pS**DEDIAPAQR	AP-3 complex subunit delta-1	Vesicle	2.1 (0.0374)	2.3 (0.0306)
VP**pS**MESLFR	Golgin subfamily A member 4	Vesicle	-2.7 (0.0192)	1.2 (0.6733)
pSPEEDQQAFRPLEK	nestin	Cytoskeleton	2.0 (0.0124)	1.9 (0.0073)
VSQVSLESLEKENVQ**pS**PR	nestin	Cytoskeleton	-3.4 (0.0197)	-4.3 (0.0121)
pSLEGENHDPLSSVVK	nestin	Cytoskeleton	2.2 (0.0728)	2.4 (0.0015)
M**pS**GFIYQGK	BetaPix-bL	Cytoskeleton	-11.6 (0.0034)	-11.6 (0.0034)
IDEI**pS**DKETEVEESSEK	Formin binding protein 30	Cytoskeleton	2.5 (0.0306)	4.4 (0.1651)
ARLTHFLAQC**pT**R	FH1/FH2 domain-containing protein	Cytoskeleton	-2.5 (0.0381)	-1.7 (0.0769)

AMLDQLMGT**pS**R	Putative RNA-binding protein Luc7-like 2	mRNA translation	-4.9 (0.0175)	-1.0 (0.9982)
DSGNWDTSGSEL**pS**EGELEK R	Pre-mRNA-processing factor 40 homolog A	mRNA translation	15.4 (0.0190)	29.8 (0.0103)
SM**pS**ADEDLQEPSR	Negative elongation factor E	mRNA translation	-1.9 (0.0286)	-2.2 (0.0061)
SL**pS**EQPVVDTATATEQAK	Negative elongation factor E	mRNA translation	-8.1 (0.0049)	-8.1 (0.0049)
NLATSAD**pT**PPS**pT**IPGTGK	Serine/threonine-protein kinase SMG1	mRNA translation	-1.4 (0.0962)	-2.1 (0.0259)
DVTNLTVGGFTPM**pS**PR	Transcription elongation factor SPT5	mRNA translation	-3.8 (0.0184)	-1.1 (0.8322)
pSPSQEPSAPGK	Eukaryotic translation initiation factor 3 S9 (eta)	mRNA translation	2.8 (0.0219)	2.3 (0.0325)
KEESEE**pS**DDDMGFGLFD	60S acidic ribosomal protein P2	mRNA translation	-3.3 (0.0274)	-1.8 (0.1596)
GATPAEDDEDKDIDLFG**pS**D EEEEDK	Elongation factor 1-delta	mRNA translation	3.7 (0.0276)	3.5 (0.1119)
IE**pS**DAQEPAEPEDDLDIMLG NK	Eukaryotic translation initiation factor 2 subunit 2 (eIF-2-beta)	mRNA translation	-2.4 (0.0287)	-1.2 (0.6228)
DDDDIDLFG**pS**DDEEESEEA K	Elongation factor 1-beta	mRNA translation	2.9 (0.0418)	2.4 (0.0150)
YAALSVDGEDEDEGDDC**pT** E	Eukaryotic translation initiation factor 4B	mRNA translation	-2.0 (0.0466)	-2.3 (0.0532)
SAS**pS**GAEGDVSSEREP	Histidyl tRNA synthetase 2	mRNA translation	-1.1 (0.4411)	3. 9 (0.0078)
EGVILTNENAA**pS**PEQPGDE DAK	tRNA (cytosine-5-)-methyltransferase NSUN2	mRNA translation	2.0 (0.0398)	1.9 (0.0116)
pSPVCSLR	Exosome complex exonuclease RRP46	mRNA translation	2.3 (0.0628)	2.9 (0.0280)

pTPEIFR	$p67^{phox}$	ROS production	2.6 (0.0066)	2.9 (0.0079)
IGWFPSNYVEEDYSE**pY**C	Proto-oncogene vav	ROS production	-2.0 (0.0104)	-1.2 (0.2194)
FSEMMDHMGGDEDVDLPEV DGADDD**pS**QD**pS**DDEK	Prostaglandin E synthase 3	PGE2 production	-6.2 (0.0007)	-6.2 (0.0007)
VFDQQS**pS**PMVTR	Inositol polyphosphate phosphatase-like 1 (SHIP-2)	Phospholipid	6.7 (0.0200)	4.7 (0.1259)
pSIEVENDFLPVEK	SH3-domain kinase-binding protein 1 (RUK)	Phospholipid	-2.0 (0.0310)	-1.0 (0.9388)
GVDLLLEGVQGESpSPTR	Ribosomal protein S6 kinase delta-1 (Rps6kc1)	Phospholipid	2.1 (0.1123)	2.9 (0.0402)
FFHHAEEEEEEEDE**pS**PPER	Inositol hexakisphosphate and diphosphoinositol-pentakisphosphate kinase 2	Phospholipid	2.1 (0.0363)	2.0 (0.0383)
FSGEEGEIEDDE**pS**GTENR	Thyroid hormone receptor-associated protein 3	Transcription	2.1 (0.0088)	2.2 (0.1337)
pSPLQSVVVR	Thyroid hormone receptor-associated protein 3	Transcription	2.3 (0.0451)	2.7 (0.0485)
WAHDKF**pS**GEEGEIEDDESG TENR	Thyroid hormone receptor-associated protein 3	Transcription	2.3 (0.0596)	3.0 (0.0406)
EVIEIEDA**pS**PTK	Transcriptional regulator ATRX	Transcription	2.0 (0.0764)	2.0 (0.0266)
EVIEIEDA**pS**PTKCPITTK	Transcriptional regulator ATRX	Transcription	1.4 (0.2542)	2.5 (0.0446)
VFIDQNL**pS**PGK	Transcription factor Dp-1	Transcription	2.0 (0.0022)	2.1 (0.0001)

3.5 Discussion

In this study, MS-based strategy provided evidence that several cell signaling pathways are directed by phosphorylation events upon IFN-γ stimulation. Tracking changes in phosphorylation at different time-points was not performed by Western blot since general antibodies against phosphoserine and threonine are not specific enough to detect accurate phosphorylation dynamics [37]. Serine and threonine residues hold chemical structures very similar to other acidic residues which decrease their specificity [37]. Even though tyrosine residues hold a distinct ring structure, antibodies directed against a specific phosphorylation site are still more sensitive than general anti-pTyr antibodies. For instance, Zheng *et al.* [84] evaluated the optimal IFN-α treatment conditions by Western blot using pTyr701 STAT1 and a mixture of two anti-pTyr (1:1) antibodies. As a result, the change in tyrosine phosphorylation was only assessed by pTyr701 STAT1 antibody since the general anti-pTyr antibody detected no differences between control and treated samples [84]. For this reason, phosphopeptide enrichment procedure combined with mass spectrometry analysis and label-free quantification consisted as one of the best options for the evaluation of serine, threonine and tyrosine phosphorylation temporal profiles.

Similarly to kinetic studies performed with other cell stimulating agents, the first most important trend of phosphorylation changes immediately took place after 5 min of IFN-γ stimulation [84, 129, and 130]. Zheng *et al.* [84] showed that activation of macrophages induced important changes in phosphotyrosine levels upon 5 and 10 min IFN-α treatment. In general, tyrosine phosphorylation is known to be attributed to earlier signaling events. Since a higher proportion of phosphorylated serine and threonine residues were detected in our samples, activation of later signaling events was observed following 30 min of cytokine stimulation. On the whole, 60 and 180 min IFN-γ stimulation always held a phosphoprotein level similar to the resting cells [131]. One trend depicted the decrease in phosphorylation upon macrophage priming during the entire time profile. These proteins dephosphorylated throughout the whole time course probably function as important modulators of macrophage activation. Overall, the phosphoproteomic dynamics of stimulated macrophages portray early signaling events occurring in the cytosol that subsequently reach the nucleus and activate transcription factors of IFN-γ regulated genes.

In the second part of the study, the experiment was repeated with control, 5 and 30 min IFN-γ stimulated cells. A total of 2831 non-redundant phosphopeptides was identified and correlated with other high-throughput phosphoproteomic studies [80, 115]. Since only the cytosolic part of macrophages was analyzed, a higher proportion (85% & 13%) of peptides was found to be phosphorylated on serine and threonine residues [115].

In addition, label-free quantitative phosphoproteomics enabled reproducible detection and identification of phosphopeptides. These results are consistent with those reported earlier by our group showing that ~70% of all phosphopeptide population does not change following IFN-γ stimulation [116]. The remarkable duty cycle and sensitivity of the LTQ-Orbitrap enabled the identification of a large number of phosphopeptides. As shown on the volcano plots, few down-regulated phosphoproteins such as RSK-2 and 26S proteasome, had similar fold changes during early and late signaling events. In contrast, other phosphoproteins such as Myb-binding protein 1A, were differentially phosphorylated only after 5 or 30 min IFN-γ stimulation.

High-throughput tandem MS generated an exhaustive list of phosphoproteins, which necessitated bioinformatics analysis to gain more insight on the possible groups of kinases involved. From the NetworKIN software, three different kinases, CDK2, CK2 and MAPK14 played important roles during IFN-γ signaling. Interestingly, motif-x analyses were consistent with those obtained from NetworKIN indicating that phosphopeptides showing higher abundance changes comprised proline and acidic amino acids in their consensus motif. Identification of key kinases indicated which pathways are stimulated upon cytokine priming. For instance, CK2 is a serine/threonine kinase involved in numerous cellular functions including the maintenance of cell viability and protein synthesis [127]. From the kinetic study, CK2 substrates were phosphorylated after 5 and 30 min IFN-γ administration with 9 & 11-fold increase, respectively. Interestingly, previous reports indicated that CK2 coordinates cell signaling events by phosphorylating IRF-1 upon IFN-γ treatment [132]. Also, CK2 phosphorylates NF-κB (p65 subunit) for its activation and possible translocation to the nucleus [133]. Finally, the identified elongation factor 1-beta phosphopeptide (GATPAEDDEDKDIDLFG**pS**DEEEEDK, Ser 106) was reported to be phosphorylated by CK2 [134]. Our study showed that phosphorylation on elongation factor 1-beta (Ser

106) increased 2.9 and 2.4-fold upon 5 & 30 min cytokine activation. The kinase motif and prediction analysis suggested that IFN-γ stimulation of macrophages led to the regulation of mRNA translation and apoptotic pathways. Yet, further data analysis was performed to strengthened this observation and discover other possible primed protein networks.

Characterization of the molecular partners of all phosphoproteins using STRING software gave further insights on plausible transduction pathways and their biological functions. Since this analysis was only based upon a sub-population of the cell, interaction maps lacked the presence and inter-connection of many non-phosphorylated partners. Also, major phosphoproteins from the popular JAK-STAT pathway were not identified probably since this signaling network occurs very rapidly within the first minute of IFN-γ activation [9]. Still, several other important networks were identified to provide an overview of the IFN-γ activated signaling pathways.

One interesting network was composed of phosphoproteins involved in PI3'K signaling pathway known to be activated by IFN type I and II [11]. Upon extracellular stimuli, phosphoinositide concentration is regulated through activated phospholipases C (PLCs), phosphoinositide kinases and phosphatases. For instance, SH2 domain containing inositol 5-phosphatase 2 (SHIP-2) and phosphatase and tensin homologue deleted on chromosome ten (PTEN) dephosphorylate $PI(3,4,5)P_3$ into $PI(3,4)P_2$ and $PI(4,5)P_2$, respectively. These phosphoinositide such as $PI(4,5)P_2$ are required for the cytoskeleton rearrangement which ultimately leads to cell movement to reach the area of infection [33]. Interestingly, SHIP-2 was ~7 times more phosphorylated upon IFN-γ stimulation on Ser241 (VFDQQS**p**SPMVTR). Upon phosphorylation, SHIP-2 is translocated to the cytosol suggesting that IFN-γ stimulation may favour dephosphorylation of $PI(3,4,5)P_2$ into $PI(4,5)P_2$ by PTEN for the remodelling of actin filaments [135].

The second phosphoprotein map portrayed some key molecules involved in the formation of NAPDH oxidase and ROS production. IFN-γ induces the formation of NADPH oxidase complex through the phosphorylation and membrane recruitment of cytosolic proteins, $p47^{phox}$, $p40^{phox}$ and $p67^{phox}$ [101, 136]. In this study, we observed the increase in phosphorylation of the $p67^{phox}$ (**p**TPEIFR, Thr 233) protein upon 5 and 30 min of cytokine stimulation indicating an active recruitment of NADPH complex for the production of cytotoxic molecules.

From the STRING network, it was also observed that important phosphoproteins part of the mRNA translation initiation pathway underwent major phosphorylation changes. Our study showed that protein synthesis phosphorylation mainly occurred 5 min upon IFN-γ treatment since the initiation step is tightly regulated and must occur quickly to ensure proper control of mRNA translation [22]. Inflammatory signals activate many transduction pathways such as Ras-MAPK and PI3K/Akt/mTOR, which in turn regulate the specific activity of key translation factors [22, 29, 30]. For instance, PI3K signaling network modulates eukaryotic translation initiation factor 2 beta (eIF2B) phosphorylation [107]. Welsh *et al.* [137] demonstrated that phosphorylation of Ser540 by glycogen synthase kinase-3 (GSK-3) inactivates eIF2B complex hence translation initiation. From our IFN-γ analysis, eIF2B was found to be dephosphorylated (IE**pS**DAQEPAEPEDDLDIMLGNK, Ser105) after 5 min of IFN-γ stimulation. The phosphorylation effect on its activity during translation is still unknown. Depending on the cellular context, PI3K/Akt/mTOR pathway might activate or inhibit mRNA translation to respond to IFN-γ stimulation [138].

The last major protein network which displayed key phosphorylated molecules involved in cell defensive mechanism against infection was the apoptotic pathway. Commonly, IFN-γ signaling pathways inhibit cell death in order to produce necessary proteins to fight against inflammation [3]. On the other hand, apoptosis may also be promoted by IFN-γ to kill tumour cells [25]. Our data suggest that IFN-γ potentially activates the apoptotic pathway. Interestingly, most phosphoproteins were differentially regulated upon 30 min of IFN-γ in order to prioritize the stimulation of other more important pathways such as mRNA translation.

The phosphoproteins identified from the network are part of the classical death receptor pathway which is triggered by pro-inflammatory cytokines such as TNF-α [139]. The signaling cascade is initially activated by the recruitment of TNF-R-associated death domain protein (TRADD), receptor-interacting protein (RIP), TNF-receptor-associated factor 2 (TRAF2) and Fas-associated death domain protein (FADD) to the tumor necrosis factor receptor superfamily member 1A (TNF-R1a) [135, 140, 141]. No changes in abundances were detected on the identified phosphoproteins FADD (Ser 191, already documented) and TNF-R1a (Ser70, unknown) [142]. Site-directed mutagenesis of PEA-15 (Ser116) suggested that its phosphorylation promotes binding to FADD and blocks apoptosis [143]. From our analysis, a decrease (-3.37 and -38.0 fold change upon 5 and 30 min) in phosphorylation takes place upon IFN-γ for the

phosphopeptide DIIRQP**pS**EEEIIK (Ser 116) indicating most probably that apoptosis is activated.

These membrane proteins further recruits the NEMO complex and activates MEKK which is responsible for IKKβ phosphorylation [144]. IKKβ activation is important and essential for nuclear factor-kappa B (NF-κB) activation by inflammatory responses since it phosphorylates IκBα [145]. Ribosomal protein S6 kinase alpha-3 (RSK-2) is also responsible for the phosphorylation of IκBα [146]. Interestingly, both phosphoproteins, IKKβ (Ser 672, GPVSG**pS**PDSMNVSR) and RSK-2 (Ser 227, AY**pS**FCGTVEYMAPEVVNR), were detected as differentially regulated upon IFN-γ activation. The exact role of these phosphorylation sites is still not documented in the literature.

Usually NF-κB is found in the cytoplasm in the inactive form bound to the inhibitory IκB. Upon phosphorylation, IκBα liberates its lysine residues and becomes a target to 26S proteasome [146]. Upon IFN-γ treatment, phosphorylation of 26S proteasome is significantly decreased [147]. Similar observations were noted where TVG**pT**PIASVPGSTNTGTVPGSEKDSDPMETEEK (Thr 273) had a decrease of phosphorylation of ~34 fold upon 5 and 30 min IFN-γ stimulation. Regrettably, phosphorylated IκB was not identified in our study probably due to its relatively low abundance in cytosol extracts upon its rapid degradation by 26S proteasome. After IκB degradation, NF-κB is liberated and can freely enter the nucleus to activate gene transcription of specific IFN-γ mediated genes [140]. Interestingly, NF-κB (p105/p50) phosphopeptide (TPATTAS**pS**PVTTAQVHCLPLSSSSTR, Ser 895) was also identified with a 2.2 fold increase in intensity upon 30 min IFN-γ priming. Yet, the exact function of this phosphorylation site still not clearly defined.

In addition, all phosphoproteins found in these functional networks were linked with their corresponding kinase using NetworKIN software. As a result, CK2 and CDK2 were responsible for the phosphorylation of most proteins in all clusters. No specific kinase activated one of the functional networks except for p38, which was found to only phosphorylate Ser 672 of I-kappa-B-kinase beta in the apoptotic pathway. Even thought the phosphorylation site is known, no proof has been documented in the literature regarding a possible connection between p38 and the I-kappa-B-kinase beta pathway.

In summary, LC-MS approaches combined with protein network analysis led to a more comprehensive characterization of many pathways affected by IFN-γ. We identified known and novel phosphorylation sites from proteins involved in the apoptotic and mRNA translation pathways, NAPDH complex formation and phospholipids signaling network providing new insights on the cellular response to IFN-γ activation. Quantitative phosphoproteomics revealed an unsurpassed level of molecular details on cytokine activation and cell signaling towards a better understanding of IFN-γ as a therapeutic agent against viral and microbial infections.

3.6 References

1. Muhl, H. and J. Pfeilschifter, *Anti-inflammatory properties of pro-inflammatory interferon-gamma.* Int Immunopharmacol, 2003. **3**(9): p. 1247-55.

3. Platanias, L.C., *Mechanisms of type-I- and type-II-interferon-mediated signalling.* Nat Rev Immunol, 2005. **5**(5): p. 375-86.

5. Mann, M., et al., *Analysis of protein phosphorylation using mass spectrometry: deciphering the phosphoproteome.* Trends Biotechnol, 2002. **20**(6): p. 261-8.

9. Schroder, K., et al., *Interferon-gamma: an overview of signals, mechanisms and functions.* J Leukoc Biol, 2004. **75**(2): p. 163-89.

11. Kaur, S., S. Uddin, and L.C. Platanias, *The PI3' kinase pathway in interferon signaling.* J Interferon Cytokine Res, 2005. **25**(12): p. 780-7.

12. Mosser, D.M., *The many faces of macrophage activation.* J Leukoc Biol, 2003. **73**(2): p. 209-12.

22. Shahbazian, D., et al., *The mTOR/PI3K and MAPK pathways converge on eIF4B to control its phosphorylation and activity.* EMBO J, 2006. **25**(12): p. 2781-91.

24. Xu, X., et al., *IFN-gamma induces cell growth inhibition by Fas-mediated apoptosis: requirement of STAT1 protein for up-regulation of Fas and FasL expression.* Cancer Res, 1998. **58**(13): p. 2832-7.

27. Holland, E.C., et al., *Signaling control of mRNA translation in cancer pathogenesis.* Oncogene, 2004. **23**(18): p. 3138-44.

28. Rajasekhar, V.K., et al., *Oncogenic Ras and Akt signaling contribute to glioblastoma formation by differential recruitment of existing mRNAs to polysomes.* Mol Cell, 2003. **12**(4): p. 889-901.

31. Takenawa, T. and T. Itoh, *Phosphoinositides, key molecules for regulation of actin cytoskeletal organization and membrane traffic from the plasma membrane.* Biochim Biophys Acta, 2001. **1533**(3): p. 190-206.

35. Kaufmann, H., J.E. Bailey, and M. Fussenegger, *Use of antibodies for detection of phosphorylated proteins separated by two-dimensional gel electrophoresis.* Proteomics, 2001. **1**(2): p. 194-9.

37. Cohen, P., *The origins of protein phosphorylation.* Nat Cell Biol, 2002. **4**(5): p. E127-30.

50. Larsen, M.R., et al., *Highly selective enrichment of phosphorylated peptides from peptide mixtures using titanium dioxide microcolumns.* Mol Cell Proteomics, 2005. **4**(7): p. 873-86.

51. Thingholm, T.E., et al., *SIMAC - A phosphoproteomic strategy for the rapid separation of mono-phosphorylated from multiply phosphorylated peptides.* Mol Cell Proteomics, 2007.

75. G. Jaitly, E.B., N. Jaitly, K. Eng, C. Pomiès and P. Thibault, *Comprehensive profiling of unlabeled peptide ions from large-scale proteomics experiments using one and two dimensional nanoLC-MS/MS.* 2007(Submitted).

76. McLachlin, D.T. and B.T. Chait, *Analysis of phosphorylated proteins and peptides by mass spectrometry.* Curr Opin Chem Biol, 2001. **5**(5): p. 591-602.

77. Olsen, J.V., et al., *Global, in vivo, and site-specific phosphorylation dynamics in signaling networks.* Cell, 2006. **127**(3): p. 635-48.

81. Zheng, H., et al., *Phosphotyrosine proteomic study of interferon alpha signaling pathway using a combination of immunoprecipitation and immobilized metal affinity chromatography.* Mol Cell Proteomics, 2005. **4**(6): p. 721-30.

85. Elias, J.E. and S.P. Gygi, *Target-decoy search strategy for increased confidence in large-scale protein identifications by mass spectrometry.* Nat Methods, 2007. **4**(3): p. 207-14.

98. Park, J.B., *Phagocytosis induces superoxide formation and apoptosis in macrophages.* Exp Mol Med, 2003. **35**(5): p. 325-35.

104. Proud, C.G., *Signalling to translation: how signal transduction pathways control the protein synthetic machinery.* Biochem J, 2007. **403**(2): p. 217-34.

106. Underhill, D.M. and A. Ozinsky, *Phagocytosis of microbes: complexity in action.* Annu Rev Immunol, 2002. **20**: p. 825-52.

107. Dash, S., et al., *Interferons alpha, beta, gamma each inhibit hepatitis C virus replication at the level of internal ribosome entry site-mediated translation.* Liver Int, 2005. **25**(3): p. 580-94.

108. Reich, N.C. and L. Liu, *Tracking STAT nuclear traffic.* Nat Rev Immunol, 2006. **6**(8): p. 602-12.

109. Samuel, C.E., et al., *Mechanism of interferon action. Increased phosphorylation of protein synthesis initiation factor eIF-2 alpha in interferon-treated, reovirus-infected mouse L929 fibroblasts in vitro and in vivo.* J Biol Chem, 1984. **259**(21): p. 13451-7.

110. Ptacek, J., et al., *Global analysis of protein phosphorylation in yeast.* Nature, 2005. **438**(7068): p. 679-84.

111. Schmelzle, K. and F.M. White, *Phosphoproteomic approaches to elucidate cellular signaling networks.* Curr Opin Biotechnol, 2006. **17**(4): p. 406-14.

112. Beausoleil, S.A., et al., *Large-scale characterization of HeLa cell nuclear phosphoproteins.* Proc Natl Acad Sci U S A, 2004. **101**(33): p. 12130-5.

113. Marcantonio, M., et al., *Combined enzymatic and data mining approaches for comprehensive phosphoproteome analyses; application to cell signaling events of interferon- stimulated macrophages.* Mol Cell Proteomics, 2007.

114. Zhu, X., M. Gerstein, and M. Snyder, *Getting connected: analysis and principles of biological networks.* Genes Dev, 2007. **21**(9): p. 1010-24.

115. Schwartz, D. and S.P. Gygi, *An iterative statistical approach to the identification of protein phosphorylation motifs from large-scale data sets.* Nat Biotechnol, 2005. **23**(11): p. 1391-8.

116. Xue, Y., et al., *PPSP: prediction of PK-specific phosphorylation site with Bayesian decision theory.* BMC Bioinformatics, 2006. **7**: p. 163.

117. Linding, R., et al., *Systematic discovery of in vivo phosphorylation networks.* Cell, 2007. **129**(7): p. 1415-26.

118. Shannon, P., et al., *Cytoscape: a software environment for integrated models of biomolecular interaction networks.* Genome Res, 2003. **13**(11): p. 2498-504.

119. von Mering, C., et al., *Quantitative phylogenetic assessment of microbial communities in diverse environments.* Science, 2007. **315**(5815): p. 1126-30.

120. Pinkse, M.W., et al., *Highly robust, automated, and sensitive online TiO2-based phosphoproteomics applied to study endogenous phosphorylation in Drosophila melanogaster.* J Proteome Res, 2008. **7**(2): p. 687-97.

121. Torrecilla, I., et al., *Phosphorylation and regulation of a G protein-coupled receptor by protein kinase CK2.* J Cell Biol, 2007. **177**(1): p. 127-37.

122. Kaur, R., et al., *Activation of p21-activated kinase 6 by MAP kinase kinase 6 and p38 MAP kinase.* J Biol Chem, 2005. **280**(5): p. 3323-30.

123. Brown, N.R., et al., *Cyclin B and cyclin A confer different substrate recognition properties on CDK2.* Cell Cycle, 2007. **6**(11): p. 1350-9.

124. Llorens, F., et al., *Eukaryotic translation-initiation factor eIF2beta binds to protein kinase CK2: effects on CK2alpha activity.* Biochem J, 2003. **375**(Pt 3): p. 623-31.

125. Platanias, L.C., *The p38 mitogen-activated protein kinase pathway and its role in interferon signaling.* Pharmacol Ther, 2003. **98**(2): p. 129-42.

126. Schmelzle, K., et al., *Temporal dynamics of tyrosine phosphorylation in insulin signaling.* Diabetes, 2006. **55**(8): p. 2171-9.

127. Blagoev, B., et al., *Temporal analysis of phosphotyrosine-dependent signaling networks by quantitative proteomics.* Nat Biotechnol, 2004. **22**(9): p. 1139-45.

128. Valledor, A.F., et al., *Selective Roles of MAPKs during the Macrophage Response to IFN-gamma.* J Immunol, 2008. **180**(7): p. 4523-9.

129. Lin, R. and J. Hiscott, *A role for casein kinase II phosphorylation in the regulation of IRF-1 transcriptional activity.* Mol Cell Biochem, 1999. **191**(1-2): p. 169-80.

130. Bird, T.A., et al., *Activation of nuclear transcription factor NF-kappaB by interleukin-1 is accompanied by casein kinase II-mediated phosphorylation of the p65 subunit.* J Biol Chem, 1997. **272**(51): p. 32606-12.

131. Chen, C.J. and J.A. Traugh, *Expression of recombinant elongation factor 1 beta from rabbit in Escherichia coli. Phosphorylation by casein kinase II.* Biochim Biophys Acta, 1995. **1264**(3): p. 303-11.

132. Pengal, R.A., et al., *SHIP-2 inositol phosphatase is inducibly expressed in human monocytes and serves to regulate Fcgamma receptor-mediated signaling.* J Biol Chem, 2003. **278**(25): p. 22657-63.

133. Lapouge, K., et al., *Architecture of the p40-p47-p67phox complex in the resting state of the NADPH oxidase. A central role for p67phox.* J Biol Chem, 2002. **277**(12): p. 10121-8.

134. Welsh, G.I., et al., *Regulation of eukaryotic initiation factor eIF2B: glycogen synthase kinase-3 phosphorylates a conserved serine which undergoes dephosphorylation in response to insulin.* FEBS Lett, 1998. **421**(2): p. 125-30.

135. Kaur, S., et al., *Role of the Akt pathway in mRNA translation of interferon-stimulated genes.* Proc Natl Acad Sci U S A, 2008. **105**(12): p. 4808-13.

136. Thomas D. Pollard, W.C.E., *Cell Biology.* 1st ed, ed. Saunders. 2004, Philadelphia. 772-782.

137. Hayden, M.S., A.P. West, and S. Ghosh, *NF-kappaB and the immune response.* Oncogene, 2006. **25**(51): p. 6758-80.

138. Stanger, B.Z., et al., *RIP: a novel protein containing a death domain that interacts with Fas/APO-1 (CD95) in yeast and causes cell death.* Cell, 1995. **81**(4): p. 513-23.

139. Chen, G., et al., *Phosphorylated FADD induces NF-kappaB, perturbs cell cycle, and is associated with poor outcome in lung adenocarcinomas.* Proc Natl Acad Sci U S A, 2005. **102**(35): p. 12507-12.

140. Renganathan, H., et al., *Phosphorylation of PEA-15 switches its binding specificity from ERK/MAPK to FADD.* Biochem J, 2005. **390**(Pt 3): p. 729-35.

141. Nemoto, S., J.A. DiDonato, and A. Lin, *Coordinate regulation of IkappaB kinases by mitogen-activated protein kinase kinase kinase 1 and NF-kappaB-inducing kinase.* Mol Cell Biol, 1998. **18**(12): p. 7336-43.

142. Li, X., et al., *IKKalpha, IKKbeta, and NEMO/IKKgamma are each required for the NF-kappa B-mediated inflammatory response program.* J Biol Chem, 2002. **277**(47): p. 45129-40.

143. Schouten, G.J., et al., *IkappaB alpha is a target for the mitogen-activated 90 kDa ribosomal S6 kinase.* EMBO J, 1997. **16**(11): p. 3133-44.

144. Bose, S., et al., *gamma-Interferon decreases the level of 26 S proteasomes and changes the pattern of phosphorylation.* Biochem J, 2001. **353**(Pt 2): p. 291-7.

4. General Conclusion

In signal transduction pathways, protein phosphorylation is the most abundant and studied PTM. Recent advancement in mass spectrometry and affinity chromatography enabled the detection of phosphopeptides of very low abundance leading to a better understanding of phosphoprotein function in cell signaling. Yet, phosphopeptides do not efficiently ionize in positive ion mode due to the presence of the phosphate group, making their detection difficult. Hence, the first part of my report described the application of AP treatment for the enhanced detection of TiO_2-enriched J774 phosphopeptides.

Initially, the novel TiO_2 enrichment procedure was evaluated for large-scale phosphoproteomic studies. To ensure maximal phosphopeptide enrichment of J774 cell extract, the loading capacity, sensitivity and linear dynamic range of TiO_2 micro-columns was assessed. The TiO_2 technique demonstrated a greater enrichment (~77%) and recovery level of phosphopeptides than the traditional IMAC extraction method. Interestingly, it was also noted that TiO_2 micro-columns had higher affinity for singly phosphorylated peptides whereas IMAC micro-columns enriched more efficiently multi-phosphorylated peptides. The optimal amount of cell extract loaded on 1.25 mg TiO_2 micro-column was 250 µg. The LTQ-Orbitrap detected as low as 25 fmol of spiked α-casein in TiO_2-enriched cell extract. Also, the linear recovery of spiked α-casein digest showed that even phosphopeptides present in the complex sample would yield a linear response across different abundance level. Overall, TiO_2 enrichment method was proven to be reproducible and highly selective for phosphopeptide detection.

Next, the alkaline phosphatase strategy was evaluated with a positive (α-casein) and negative (non-phosphorylated protein mixture) control. No significant changes in abundance were observed upon dephosphorylation of the non-phosphorylated protein mixture. On the other hand, alkaline phosphatase treatment on α-casein notably enhanced phosphopeptide detection especially of highly phosphorylated peptides. The incubation conditions of the alkaline phosphatase treatment were optimal since known α-casein phosphopeptides were not detected by mass spectrometry upon dephosphorylation. Yet, if ever incomplete dephosphorylation occurred to multiply phosphorylated peptides, the intensity of the dephosphorylated cognate might be lower and new doubly or triply phosphorylated peptides might appear upon alkaline

phosphatase treatment. To avoid such cases, correlation of the phospho- and dephosphorylated partners was only done with unique peptides detected in non-treated and AP-treated samples.

The enzymatic approach was further validated with a complex mixture of J774 cell extract. The intensity and retention time of phosphopeptides and their dephosphorylated counterpart were compared using in-house bioinformatic tools. Interestingly, the overall abundance of dephosphorylated peptides was ~2 fold more intense than their corresponding phosphopeptide. Also, 716 new putative phosphopeptides were identified only upon AP treatment. Since the peptide's hydrophobicity should increase upon phosphate group removal, an overall higher retention time was expected after enzymatic dephosphorylation. However, dephosphorylated peptides displayed variation of retention time as high as 5 min making them either more or less hydrophobic. The loss of hydrophobicity upon dephosphorylation was partially explained by the formation of salt bridges between the phosphate group and nearby acidic residue. α-Casein N-acetylated phosphopeptides showed a consistent increase in retention time upon dephosphorylation unlike the non-derivatized phosphopeptides, further supporting the salt bridge model. In brief, the AP treatment led to not only a higher phosphopeptide detection but also provided new insight of phosphopeptide behaviour in MS.

Lastly, the analytical potentials of the AP approach were applied on J774 macrophage cells treated with IFN-γ for 5 min. TiO_2 enrichment enabled the identification of 1143 phosphopeptides from 432 proteins of which 125 phosphopeptides showed at least 2-fold change upon IFN-γ stimulation. Key phosphoproteins in the NADPH oxidase complex formation and mRNA translation were detected to be differentially expressed upon IFN-γ exposure. Upon AP treatment on TiO_2-enriched samples, the number of putative phosphopeptides nearly doubled and led to the identification of several other differentially phosphorylated proteins in IFN-γ activated pathways. For instance, the putative phosphopeptide of AP-3 complex was found more abundant upon cytokine stimulation where this phosphorylation was already reported to participate in vesicle formation.

The IFN-γ activation of macrophages showed that phosphorylated protein played major roles in signal transduction. Up to now, the JAK-STAT pathway is the only well characterized cellular event triggered by IFN-γ [19]. Many other signal transductions are recognized to be primed upon cytokine stimulation, but their signaling pathway is still not completely defined. Hence, the second part of the study reported for the first time a phosphoproteome dynamics of IFN-γ primed macrophages. According to the phosphoproteome kinetic profiles, most significant phosphorylation changes occurred 5 and 30 min upon IFN-γ administration. Also a dephosphorylation pattern was observed throughout the whole time profile.

Determination of important IFN-γ triggered signaling pathways was achieved by SCX-LC-MS analysis of TiO_2-enriched phosphopeptides incubated for 5 and 30 min with IFN-γ. This high-throughput procedure enabled the identification of 2831 phosphopeptides with a Ser/Thr/Tyr proportion of 85:13:2. For the 5 and 30 min treated samples, ~20 and 25% of phosphopeptide clusters had at least a 2-fold change in abundance, respectively. In total, this sensitive MS-based strategy detected 1673 novel phosphorylation sites, providing new insights on IFN-γ activated pathways.

Different strategies were applied to determine the key cellular events that were affected by phosphoproteomic changes upon IFN-γ treatment. Initially, a kinase prediction using NetworKIN software showed that most up-regulated phosphopeptides upon 5 and 30 min IFN-γ treatment were phosphorylated by MAPK14, CK2 and CDK2. Also, the motif-x analysis demonstrated that most overrepresented patterns in differentially expressed phosphopeptides were acidic amino acid and proline-directed. Interestingly, the NetworKIN prediction was in concordance with motif-x results since MAPK14 and CDK2 have a Ser-Pro consensus motif and CK2 phosphorylates sites near acidic residues. These kinases play important roles in a multitude of cellular events. For instance, CK2 phosphorylates proteins involved in the apoptotic and mRNA translation pathway. The elongation factor 1-beta phosphopeptide was up-regulated upon cytokine stimulation and was already documented to be phosphorylated by CK2 [134]. Also, CK2 activates NF-κB by phosphorylation, which is implicated in cell death, initiation of inflammatory responses, immunity and cell proliferation [133].

The last part of the analysis consisted of characterizing the molecular partners of all phosphoproteins using STRING software. Four different phosphoproteins network maps were identified and corresponded to the activation of transduction pathways in apoptosis, protein synthesis, cytotoxic molecules formation and phospholipids.

Differential phosphorylation in mRNA translation pathway occurred very quickly (5 min) to tightly regulate translation factors in the initiation step. In contrast, apoptosis signal transduction primarily took place during the late signaling events (30 min). Most phosphoproteins detected in the cell death network were associated with the classical apoptotic pathway. For instance, important kinases, RSK-2 and IKKβ known to phosphorylate IκBα were detected as differentially regulated upon cytokine stimulation. Also, the abundance of phosphoprotein PEA-15 was significantly lowered upon IFN-γ suggesting that cell death was activated since dephosphorylation of PEA-15 was shown to promote apoptosis [143].

To conclude, highly sensitive MS combined with SCX and TiO_2 chromatography enabled the characterization of macrophage inflammation resulting in a cascade of signaling events in apoptosis, protein synthesis, NADPH oxidase formation and phospholipids signaling. In addition, the AP treatment led to the detection of several phosphoproteins necessary to respond to the IFN-γ biological effects. Yet, the AP strategy had some limitations. For instance, the location of the exact phosphosite of new putative phosphopeptides containing multiple hydroxyamino acids could have not been identified. As an alternative, new phosphatases can be engineered to remove the phosphate group and also leave behind a marker with a different mass, which can pinpoint the phosphorylation site. Also, the experiments for the alkaline phosphatase treatment could have only been performed in 1D-LC mode, which restricted the starting material to ~250 μg of peptides. On the other hand, the 2D-LC analysis used a much larger amount (1.25 mg) of digested proteins, which was initially enriched using TiO_2 micro-columns and then injected onto the LC/MS. As a result, this study offered a much higher level of phosphopeptide detection and enabled assessing the importance of NF-κB in inflammatory responses, which can be further investigated by site-directed mutagenesis of the protein's new phosphorylation site followed by protein's structure and function studies. Identification of novel IFN-γ targets will help understanding macrophage activation pathways and provide knowledge for a fundamental immunological response important for many diseases.

5. General References

1. Muhl, H. and J. Pfeilschifter, *Anti-inflammatory properties of pro-inflammatory interferon-gamma.* Int Immunopharmacol, 2003. **3**(9): p. 1247-55.

2. Darnell, J.E., Jr., I.M. Kerr, and G.R. Stark, *Jak-STAT pathways and transcriptional activation in response to IFNs and other extracellular signaling proteins.* Science, 1994. **264**(5164): p. 1415-21.

3. Platanias, L.C., *Mechanisms of type-I- and type-II-interferon-mediated signalling.* Nat Rev Immunol, 2005. **5**(5): p. 375-86.

4. Sickmann, A. and H.E. Meyer, *Phosphoamino acid analysis.* Proteomics, 2001. **1**(2): p. 200-6.

5. Mann, M., et al., *Analysis of protein phosphorylation using mass spectrometry: deciphering the phosphoproteome.* Trends Biotechnol, 2002. **20**(6): p. 261-8.

6. Ahmed, R., M.B. Oldstone, and P. Palese, *Protective immunity and susceptibility to infectious diseases: lessons from the 1918 influenza pandemic.* Nat Immunol, 2007. **8**(11): p. 1188-93.

7. Bruce Alberts, A.J., Julian Lewis, Martin Raff, Keith Roberts, Peter Walter, *Molecular Biology of the Cell.* 4th ed. 2002, New York: Garland Science. 1434-1453

8. Nishiya, T. and A.L. DeFranco, *Ligand-regulated chimeric receptor approach reveals distinctive subcellular localization and signaling properties of the Toll-like receptors.* J Biol Chem, 2004. **279**(18): p. 19008-17.

9. Schroder, K., et al., *Interferon-gamma: an overview of signals, mechanisms and functions.* J Leukoc Biol, 2004. **75**(2): p. 163-89.

10. Hanada, T. and A. Yoshimura, *Regulation of cytokine signaling and inflammation.* Cytokine Growth Factor Rev, 2002. **13**(4-5): p. 413-21.

11. Kaur, S., S. Uddin, and L.C. Platanias, *The PI3' kinase pathway in interferon signaling.* J Interferon Cytokine Res, 2005. **25**(12): p. 780-7.

12. Mosser, D.M., *The many faces of macrophage activation.* J Leukoc Biol, 2003. **73**(2): p. 209-12.

13. Yoshimura, A., *Signal transduction of inflammatory cytokines and tumor development.* Cancer Sci, 2006. **97**(6): p. 439-47.

14. Klimp, A.H., et al., *A potential role of macrophage activation in the treatment of cancer.* Crit Rev Oncol Hematol, 2002. **44**(2): p. 143-61.

15. Bukrinsky, M. and D. Sviridov, *HIV and cardiovascular disease: contribution of HIV-infected macrophages to development of atherosclerosis.* PLoS Med, 2007. **4**(1): p. e43.

16. Reljic, R., *IFN-gamma therapy of tuberculosis and related infections.* J Interferon Cytokine Res, 2007. **27**(5): p. 353-64.

17. Aoki, N. and Z. Xing, *Use of cytokines in infection.* Expert Opin Emerg Drugs, 2004. **9**(2): p. 223-36.

18. Katsoulidis, E., et al., *The p38 mitogen-activated protein kinase pathway in interferon signal transduction.* J Interferon Cytokine Res, 2005. **25**(12): p. 749-56.

19. Aaronson, D.S. and C.M. Horvath, *A road map for those who don't know JAK-STAT.* Science, 2002. **296**(5573): p. 1653-5.

20. Samuel, C.E., *Antiviral actions of interferons.* Clin Microbiol Rev, 2001. **14**(4): p. 778-809, table of contents.

21. Viatour, P., et al., *Phosphorylation of NF-kappaB and IkappaB proteins: implications in cancer and inflammation.* Trends Biochem Sci, 2005. **30**(1): p. 43-52.

22. Shahbazian, D., et al., *The mTOR/PI3K and MAPK pathways converge on eIF4B to control its phosphorylation and activity.* EMBO J, 2006. **25**(12): p. 2781-91.

23. Ghosh, S. and M. Karin, *Missing pieces in the NF-kappaB puzzle.* Cell, 2002. **109 Suppl**: p. S81-96.

24. Fang, P., V. Hwa, and R.G. Rosenfeld, *Interferon-gamma-induced dephosphorylation of STAT3 and apoptosis are dependent on the mTOR pathway.* Exp Cell Res, 2006. **312**(8): p. 1229-39.

25. Xu, X., et al., *IFN-gamma induces cell growth inhibition by Fas-mediated apoptosis: requirement of STAT1 protein for up-regulation of Fas and FasL expression.* Cancer Res, 1998. **58**(13): p. 2832-7.

26. Karin, M. and A. Lin, *NF-kappaB at the crossroads of life and death.* Nat Immunol, 2002. **3**(3): p. 221-7.

27. Kaempfer, R., *RNA sensors: novel regulators of gene expression.* EMBO Rep, 2003. **4**(11): p. 1043-7.

28. Ben-Asouli, Y., et al., *Human interferon-gamma mRNA autoregulates its translation through a pseudoknot that activates the interferon-inducible protein kinase PKR.* Cell, 2002. **108**(2): p. 221-32.

29. Holland, E.C., et al., *Signaling control of mRNA translation in cancer pathogenesis.* Oncogene, 2004. **23**(18): p. 3138-44.

30. Rajasekhar, V.K., et al., *Oncogenic Ras and Akt signaling contribute to glioblastoma formation by differential recruitment of existing mRNAs to polysomes.* Mol Cell, 2003. **12**(4): p. 889-901.

31. Lekmine, F., et al., *Interferon-gamma engages the p70 S6 kinase to regulate phosphorylation of the 40S S6 ribosomal protein.* Exp Cell Res, 2004. **295**(1): p. 173-82.

32. Sly, L.M., et al., *The role of SHIP in macrophages.* Front Biosci, 2007. **12**: p. 2836-48.

33. Takenawa, T. and T. Itoh, *Phosphoinositides, key molecules for regulation of actin cytoskeletal organization and membrane traffic from the plasma membrane.* Biochim Biophys Acta, 2001. **1533**(3): p. 190-206.

34. Lee, I.H., et al., *AHNAK-mediated activation of phospholipase C-gamma1 through protein kinase C.* J Biol Chem, 2004. **279**(25): p. 26645-53.

35. Leusen, J.H., A.J. Verhoeven, and D. Roos, *Interactions between the components of the human NADPH oxidase: a review about the intrigues in the phox family.* Front Biosci, 1996. **1**: p. d72-90.

36. Shiose, A. and H. Sumimoto, *Arachidonic acid and phosphorylation synergistically induce a conformational change of p47phox to activate the phagocyte NADPH oxidase.* J Biol Chem, 2000. **275**(18): p. 13793-801.

37. Kaufmann, H., J.E. Bailey, and M. Fussenegger, *Use of antibodies for detection of phosphorylated proteins separated by two-dimensional gel electrophoresis.* Proteomics, 2001. **1**(2): p. 194-9.

38. Nalivaeva, N.N. and A.J. Turner, *Post-translational modifications of proteins: acetylcholinesterase as a model system.* Proteomics, 2001. **1**(6): p. 735-47.

39. Cohen, P., *The origins of protein phosphorylation.* Nat Cell Biol, 2002. **4**(5): p. E127-30.

40. Raggiaschi, R., S. Gotta, and G.C. Terstappen, *Phosphoproteome analysis.* Biosci Rep, 2005. **25**(1-2): p. 33-44.

41. Yan, J.X., et al., *Protein phosphorylation: technologies for the identification of phosphoamino acids.* J Chromatogr A, 1998. **808**(1-2): p. 23-41.

42. Reinders, J. and A. Sickmann, *State-of-the-art in phosphoproteomics.* Proteomics, 2005. **5**(16): p. 4052-61.

43. Fey, S.J. and P.M. Larsen, *2D or not 2D. Two-dimensional gel electrophoresis.* Curr Opin Chem Biol, 2001. **5**(1): p. 26-33.

44. Greenberg, R., M.L. Groves, and H.J. Dower, *Human beta-casein. Amino acid sequence and identification of phosphorylation sites.* J Biol Chem, 1984. **259**(8): p. 5132-8.

45. Loyet, K.M., J.T. Stults, and D. Arnott, *Mass spectrometric contributions to the practice of phosphorylation site mapping through 2003: a literature review.* Mol Cell Proteomics, 2005. **4**(3): p. 235-45.

46. Gronborg, M., et al., *A mass spectrometry-based proteomic approach for identification of serine/threonine-phosphorylated proteins by enrichment with phospho-specific antibodies: identification of a novel protein, Frigg, as a protein kinase A substrate.* Mol Cell Proteomics, 2002. **1**(7): p. 517-27.

47. Sun, T., et al., *Preparation and application of antibodies to phosphoamino acid sequences.* Biopolymers, 2001. **60**(1): p. 61-75.

48. Kalo, M.S. and E.B. Pasquale, *Multiple in vivo tyrosine phosphorylation sites in EphB receptors.* Biochemistry, 1999. **38**(43): p. 14396-408.

49. Thingholm, T.E., et al., *Highly selective enrichment of phosphorylated peptides using titanium dioxide.* Nat Protoc, 2006. **1**(4): p. 1929-35.

50. Posewitz, M.C. and P. Tempst, *Immobilized gallium(III) affinity chromatography of phosphopeptides.* Anal Chem, 1999. **71**(14): p. 2883-92.

51. Kokubu, M., et al., *Specificity of immobilized metal affinity-based IMAC/C18 tip enrichment of phosphopeptides for protein phosphorylation analysis.* Anal Chem, 2005. **77**(16): p. 5144-54.

52. Ficarro, S.B., et al., *Phosphoproteome analysis by mass spectrometry and its application to Saccharomyces cerevisiae.* Nat Biotechnol, 2002. **20**(3): p. 301-5.

53. Larsen, M.R., et al., *Highly selective enrichment of phosphorylated peptides from peptide mixtures using titanium dioxide microcolumns.* Mol Cell Proteomics, 2005. **4**(7): p. 873-86.

54. Thingholm, T.E., et al., *SIMAC - A phosphoproteomic strategy for the rapid separation of mono-phosphorylated from multiply phosphorylated peptides.* Mol Cell Proteomics, 2007.

55. Hsieh, H.C., et al., *Development of a titanium dioxide nanoparticle pipette-tip for the selective enrichment of phosphorylated peptides.* J Chromatogr A, 2007. **1165**(1-2): p. 128-35.

56. Wang, J., et al., *Phosphopeptide detection using automated online IMAC-capillary LC-ESI-MS/MS.* Proteomics, 2006. **6**(2): p. 404-11.

57. Pinkse, M.W., et al., *Selective isolation at the femtomole level of phosphopeptides from proteolytic digests using 2D-NanoLC-ESI-MS/MS and titanium oxide precolumns.* Anal Chem, 2004. **76**(14): p. 3935-43.

58. Corthals, G.L., R. Aebersold, and D.R. Goodlett, *Identification of phosphorylation sites using microimmobilized metal affinity chromatography.* Methods Enzymol, 2005. **405**: p. 66-81.

59. Thompson, A.J., et al., *Characterization of protein phosphorylation by mass spectrometry using immobilized metal ion affinity chromatography with on-resin beta-elimination and Michael addition.* Anal Chem, 2003. **75**(13): p. 3232-43.

60. McLachlin, D.T. and B.T. Chait, *Improved beta-elimination-based affinity purification strategy for enrichment of phosphopeptides.* Anal Chem, 2003. **75**(24): p. 6826-36.

61. Liao, P.C., et al., *An approach to locate phosphorylation sites in a phosphoprotein: mass mapping by combining specific enzymatic degradation with matrix-assisted laser desorption/ionization mass spectrometry.* Anal Biochem, 1994. **219**(1): p. 9-20.

62. Aebersold, R. and D.R. Goodlett, *Mass spectrometry in proteomics.* Chem Rev, 2001. **101**(2): p. 269-95.

63. Torres, M.P., et al., *Phosphatase-directed phosphorylation-site determination: a synthesis of methods for the detection and identification of phosphopeptides.* J Proteome Res, 2005. **4**(5): p. 1628-35.

64. Wilm, M. and M. Mann, *Analytical properties of the nanoelectrospray ion source.* Anal Chem, 1996. **68**(1): p. 1-8.

65. Kocher, T., et al., *PhosTShunter: a fast and reliable tool to detect phosphorylated peptides in liquid chromatography Fourier transform tandem mass spectrometry data sets.* J Proteome Res, 2006. **5**(3): p. 659-68.

66. Li, X., et al., *Large-scale phosphorylation analysis of alpha-factor-arrested Saccharomyces cerevisiae.* J Proteome Res, 2007. **6**(3): p. 1190-7.

67. Gross, J.H., *Mass Spectrometry.* 2004, New York: Springer.

68. Aebersold, R. and M. Mann, *Mass spectrometry-based proteomics.* Nature, 2003. **422**(6928): p. 198-207.

69. Steen, H. and M. Mann, *The ABC's (and XYZ's) of peptide sequencing.* Nat Rev Mol Cell Biol, 2004. **5**(9): p. 699-711.

70. Cech, N.B. and C.G. Enke, *Practical implications of some recent studies in electrospray ionization fundamentals.* Mass Spectrom Rev, 2001. **20**(6): p. 362-87.

71. Snyder, A.P., *Interpreting Protein Mass Spectra; A Comprehensive Resource*, ed. A.C. Society. 2000, Washington, D.C.: OXFORD University Press.

72. Makarov, A., et al., *Performance evaluation of a hybrid linear ion trap/orbitrap mass spectrometer.* Anal Chem, 2006. **78**(7): p. 2113-20.

73. Scigelova, M. and A. Makarov, *Orbitrap mass analyzer--overview and applications in proteomics.* Proteomics, 2006. **6 Suppl 2**: p. 16-21.

74. Makarov, A., et al., *Dynamic range of mass accuracy in LTQ Orbitrap hybrid mass spectrometer.* J Am Soc Mass Spectrom, 2006. **17**(7): p. 977-82.

75. Liebler, D.C., *Introduction to Proteomics; Tools for the New Biology.* 2002, New Jersey: Humana Press.

76. Salih, E., *Phosphoproteomics by mass spectrometry and classical protein chemistry approaches.* Mass Spectrom Rev, 2005. **24**(6): p. 828-46.

77. Salek, M., et al., *Analysis of protein tyrosine phosphorylation by nanoelectrospray ionization high-resolution tandem mass spectrometry and tyrosine-targeted product ion scanning.* Anal Chem, 2003. **75**(11): p. 2724-9.

78. G. Jaitly, E.B., N. Jaitly, K. Eng, C. Pomiès and P. Thibault, *Comprehensive profiling of unlabeled peptide ions from large-scale proteomics experiments using one and two dimensional nanoLC-MS/MS.* 2007(Submitted).

79. McLachlin, D.T. and B.T. Chait, *Analysis of phosphorylated proteins and peptides by mass spectrometry.* Curr Opin Chem Biol, 2001. **5**(5): p. 591-602.

80. Olsen, J.V., et al., *Global, in vivo, and site-specific phosphorylation dynamics in signaling networks.* Cell, 2006. **127**(3): p. 635-48.

81. Steen, H., et al., *Phosphorylation analysis by mass spectrometry: myths, facts, and the consequences for qualitative and quantitative measurements.* Mol Cell Proteomics, 2006. **5**(1): p. 172-81.

82. Bodenmiller, B., et al., *Reproducible isolation of distinct, overlapping segments of the phosphoproteome.* Nat Methods, 2007. **4**(3): p. 231-7.

83. Zhou, H., J.D. Watts, and R. Aebersold, *A systematic approach to the analysis of protein phosphorylation.* Nat Biotechnol, 2001. **19**(4): p. 375-8.

84. Zheng, H., et al., *Phosphotyrosine proteomic study of interferon alpha signaling pathway using a combination of immunoprecipitation and immobilized metal affinity chromatography.* Mol Cell Proteomics, 2005. **4**(6): p. 721-30.

85. Ishihama, Y., et al., *Enhancement of the efficiency of phosphoproteomic identification by removing phosphates after phosphopeptide enrichment.* J Proteome Res, 2007. **6**(3): p. 1139-44.

86. Wu, H.Y., V.S. Tseng, and P.C. Liao, *Mining Phosphopeptide Signals in Liquid Chromatography-Mass Spectrometry Data for Protein Phosphorylation Analysis.* J Proteome Res, 2007.

87. Kersey, P.J., et al., *The International Protein Index: an integrated database for proteomics experiments.* Proteomics, 2004. **4**(7): p. 1985-8.

88. Elias, J.E. and S.P. Gygi, *Target-decoy search strategy for increased confidence in large-scale protein identifications by mass spectrometry.* Nat Methods, 2007. **4**(3): p. 207-14.

89. Makrantoni, V., et al., *Rapid enrichment and analysis of yeast phosphoproteins using affinity chromatography, 2D-PAGE and peptide mass fingerprinting.* Yeast, 2005. **22**(5): p. 401-14.

90. Feng, S., et al., *Fe3+ immobilized metal affinity chromatography with silica monolithic capillary column for phosphoproteome analysis.* Proteomics, 2007. **7**(3): p. 351-60.

91. Gautier, T., et al., *Nucleolar KKE/D repeat proteins Nop56p and Nop58p interact with Nop1p and are required for ribosome biogenesis.* Mol Cell Biol, 1997. **17**(12): p. 7088-98.

92. Wen, X., et al., *Structural organization and cellular localization of tuftelin-interacting protein 11 (TFIP11).* Cell Mol Life Sci, 2005. **62**(9): p. 1038-46.

93. Flati, V., S.J. Haque, and B.R. Williams, *Interferon-alpha-induced phosphorylation and activation of cytosolic phospholipase A2 is required for the formation of interferon-stimulated gene factor three.* Embo J, 1996. **15**(7): p. 1566-71.

94. Trinidad, J.C., et al., *Comprehensive identification of phosphorylation sites in postsynaptic density preparations.* Mol Cell Proteomics, 2006. **5**(5): p. 914-22.

95. Thingholm, T.E., et al., *SIMAC - A phosphoproteomic strategy for the rapid separation of mono-phosphorylated from multiply phosphorylated peptides.* Mol. Cell. Proteomics, in press.

96. Marcantonio M., M.T., M. Desjardins, and P. Thibault. *Combined enzymatic and data mining approaches for comprehensive phosphoproteome analyses in sub-cellular protein extracts of macrophages.* in *Proc. of 54th ASMS conference on Mass Spectrometry and allied topics.* 2006. Seatlle, WA.

97. Nielsen, M.L., et al., *Physicochemical properties determining the detection probability of tryptic peptides in Fourier transform mass spectrometry. A correlation study.* Anal Chem, 2004. **76**(19): p. 5872-7.

98. Errington, N. and A.J. Doig, *A phosphoserine-lysine salt bridge within an alpha-helical peptide, the strongest alpha-helix side-chain interaction measured to date.* Biochemistry, 2005. **44**(20): p. 7553-8.

99. Mayne, L., et al., *Stabilizing Effect of a Multiple Salt Bridge in a Prenucleated Peptide.* J. Am. Chem. Soc., 1998. **120**(41): p. 10643-10645.

100. Ferret, P.J., et al., *Auto-protective redox buffering systems in stimulated macrophages.* BMC Immunol, 2002. **3**: p. 3.

101. Park, J.B., *Phagocytosis induces superoxide formation and apoptosis in macrophages.* Exp Mol Med, 2003. **35**(5): p. 325-35.

102. Hefner, Y., et al., *Serine 727 phosphorylation and activation of cytosolic phospholipase A2 by MNK1-related protein kinases.* J Biol Chem, 2000. **275**(48): p. 37542-51.

103. Sellmayer, A., et al., *Arachidonic acid increases activation of NADPH oxidase in monocytic U937 cells by accelerated translocation of p47-phox and co-stimulation of protein kinase C.* Cell Signal, 1996. **8**(5): p. 397-402.

104. Faundez, V., J.T. Horng, and R.B. Kelly, *A function for the AP3 coat complex in synaptic vesicle formation from endosomes.* Cell, 1998. **93**(3): p. 423-32.

105. Salem, N., et al., *A v-SNARE participates in synaptic vesicle formation mediated by the AP3 adaptor complex.* Nat Neurosci, 1998. **1**(7): p. 551-6.

106. Faundez, V.V. and R.B. Kelly, *The AP-3 complex required for endosomal synaptic vesicle biogenesis is associated with a casein kinase Ialpha-like isoform.* Mol Biol Cell, 2000. **11**(8): p. 2591-604.

107. Proud, C.G., *Signalling to translation: how signal transduction pathways control the protein synthetic machinery.* Biochem J, 2007. **403**(2): p. 217-34.

108. Scheper, G.C., et al., *Phosphorylation of eukaryotic initiation factor 4E markedly reduces its affinity for capped mRNA.* J Biol Chem, 2002. **277**(5): p. 3303-9.

109. Underhill, D.M. and A. Ozinsky, *Phagocytosis of microbes: complexity in action.* Annu Rev Immunol, 2002. **20**: p. 825-52.

110. Dash, S., et al., *Interferons alpha, beta, gamma each inhibit hepatitis C virus replication at the level of internal ribosome entry site-mediated translation.* Liver Int, 2005. **25**(3): p. 580-94.

111. Reich, N.C. and L. Liu, *Tracking STAT nuclear traffic.* Nat Rev Immunol, 2006. **6**(8): p. 602-12.

112. Samuel, C.E., et al., *Mechanism of interferon action. Increased phosphorylation of protein synthesis initiation factor eIF-2 alpha in interferon-treated, reovirus-infected mouse L929 fibroblasts in vitro and in vivo.* J Biol Chem, 1984. **259**(21): p. 13451-7.

113. Ptacek, J., et al., *Global analysis of protein phosphorylation in yeast.* Nature, 2005. **438**(7068): p. 679-84.

114. Schmelzle, K. and F.M. White, *Phosphoproteomic approaches to elucidate cellular signaling networks.* Curr Opin Biotechnol, 2006. **17**(4): p. 406-14.

115. Beausoleil, S.A., et al., *Large-scale characterization of HeLa cell nuclear phosphoproteins.* Proc Natl Acad Sci U S A, 2004. **101**(33): p. 12130-5.

116. Marcantonio, M., et al., *Combined enzymatic and data mining approaches for comprehensive phosphoproteome analyses; application to cell signaling events of interferon- stimulated macrophages.* Mol Cell Proteomics, 2007.

117. Zhu, X., M. Gerstein, and M. Snyder, *Getting connected: analysis and principles of biological networks.* Genes Dev, 2007. **21**(9): p. 1010-24.

118. Schwartz, D. and S.P. Gygi, *An iterative statistical approach to the identification of protein phosphorylation motifs from large-scale data sets.* Nat Biotechnol, 2005. **23**(11): p. 1391-8.

119. Xue, Y., et al., *PPSP: prediction of PK-specific phosphorylation site with Bayesian decision theory.* BMC Bioinformatics, 2006. **7**: p. 163.

120. Linding, R., et al., *Systematic discovery of in vivo phosphorylation networks.* Cell, 2007. **129**(7): p. 1415-26.

121. Shannon, P., et al., *Cytoscape: a software environment for integrated models of biomolecular interaction networks.* Genome Res, 2003. **13**(11): p. 2498-504.

122. von Mering, C., et al., *Quantitative phylogenetic assessment of microbial communities in diverse environments.* Science, 2007. **315**(5815): p. 1126-30.

123. Pinkse, M.W., et al., *Highly robust, automated, and sensitive online TiO2-based phosphoproteomics applied to study endogenous phosphorylation in Drosophila melanogaster.* J Proteome Res, 2008. **7**(2): p. 687-97.

124. Torrecilla, I., et al., *Phosphorylation and regulation of a G protein-coupled receptor by protein kinase CK2.* J Cell Biol, 2007. **177**(1): p. 127-37.

125. Kaur, R., et al., *Activation of p21-activated kinase 6 by MAP kinase kinase 6 and p38 MAP kinase.* J Biol Chem, 2005. **280**(5): p. 3323-30.

126. Brown, N.R., et al., *Cyclin B and cyclin A confer different substrate recognition properties on CDK2.* Cell Cycle, 2007. **6**(11): p. 1350-9.

127. Llorens, F., et al., *Eukaryotic translation-initiation factor eIF2beta binds to protein kinase CK2: effects on CK2alpha activity.* Biochem J, 2003. **375**(Pt 3): p. 623-31.

128. Platanias, L.C., *The p38 mitogen-activated protein kinase pathway and its role in interferon signaling.* Pharmacol Ther, 2003. **98**(2): p. 129-42.

129. Schmelzle, K., et al., *Temporal dynamics of tyrosine phosphorylation in insulin signaling.* Diabetes, 2006. **55**(8): p. 2171-9.

130. Blagoev, B., et al., *Temporal analysis of phosphotyrosine-dependent signaling networks by quantitative proteomics.* Nat Biotechnol, 2004. **22**(9): p. 1139-45.

131. Valledor, A.F., et al., *Selective Roles of MAPKs during the Macrophage Response to IFN-{gamma}.* J Immunol, 2008. **180**(7): p. 4523-9.

132. Lin, R. and J. Hiscott, *A role for casein kinase II phosphorylation in the regulation of IRF-1 transcriptional activity.* Mol Cell Biochem, 1999. **191**(1-2): p. 169-80.

133. Bird, T.A., et al., *Activation of nuclear transcription factor NF-kappaB by interleukin-1 is accompanied by casein kinase II-mediated phosphorylation of the p65 subunit.* J Biol Chem, 1997. **272**(51): p. 32606-12.

134. Chen, C.J. and J.A. Traugh, *Expression of recombinant elongation factor 1 beta from rabbit in Escherichia coli. Phosphorylation by casein kinase II.* Biochim Biophys Acta, 1995. **1264**(3): p. 303-11.

135. Pengal, R.A., et al., *SHIP-2 inositol phosphatase is inducibly expressed in human monocytes and serves to regulate Fcgamma receptor-mediated signaling.* J Biol Chem, 2003. **278**(25): p. 22657-63.

136. Lapouge, K., et al., *Architecture of the p40-p47-p67phox complex in the resting state of the NADPH oxidase. A central role for p67phox.* J Biol Chem, 2002. **277**(12): p. 10121-8.

137. Welsh, G.I., et al., *Regulation of eukaryotic initiation factor eIF2B: glycogen synthase kinase-3 phosphorylates a conserved serine which undergoes dephosphorylation in response to insulin.* FEBS Lett, 1998. **421**(2): p. 125-30.

138. Kaur, S., et al., *Role of the Akt pathway in mRNA translation of interferon-stimulated genes.* Proc Natl Acad Sci U S A, 2008. **105**(12): p. 4808-13.

139. Thomas D. Pollard, W.C.E., *Cell Biology.* 1st ed, ed. Saunders. 2004, Philadelphia. 772-782.

140. Hayden, M.S., A.P. West, and S. Ghosh, *NF-kappaB and the immune response.* Oncogene, 2006. **25**(51): p. 6758-80.

141. Stanger, B.Z., et al., *RIP: a novel protein containing a death domain that interacts with Fas/APO-1 (CD95) in yeast and causes cell death.* Cell, 1995. **81**(4): p. 513-23.

142. Chen, G., et al., *Phosphorylated FADD induces NF-kappaB, perturbs cell cycle, and is associated with poor outcome in lung adenocarcinomas.* Proc Natl Acad Sci U S A, 2005. **102**(35): p. 12507-12.

143. Renganathan, H., et al., *Phosphorylation of PEA-15 switches its binding specificity from ERK/MAPK to FADD.* Biochem J, 2005. **390**(Pt 3): p. 729-35.

144. Nemoto, S., J.A. DiDonato, and A. Lin, *Coordinate regulation of IkappaB kinases by mitogen-activated protein kinase kinase kinase 1 and NF-kappaB-inducing kinase.* Mol Cell Biol, 1998. **18**(12): p. 7336-43.

145. Li, X., et al., *IKKalpha, IKKbeta, and NEMO/IKKgamma are each required for the NF-kappa B-mediated inflammatory response program.* J Biol Chem, 2002. **277**(47): p. 45129-40.

146. Schouten, G.J., et al., *IkappaB alpha is a target for the mitogen-activated 90 kDa ribosomal S6 kinase.* EMBO J, 1997. **16**(11): p. 3133-44.

147. Bose, S., et al., *gamma-Interferon decreases the level of 26 S proteasomes and changes the pattern of phosphorylation.* Biochem J, 2001. **353**(Pt 2): p. 291-7.